

Inaugural dissertation
for
obtaining the doctoral degree
of the
Combined Faculty of Mathematics, Engineering and Natural Sciences
of the
Ruprecht - Karls - University
Heidelberg

Presented by
M.Sc. Michael Hertwig

Born in Worms, Germany

Oral examination on 27th of March 2025

Immune Complex-Induced Migration of Slan⁺ Non-Classical Monocytes

Referees

Prof. Dr. Nina Papavasiliou

Prof. Dr. med Knut Schäkel

Table of Contents

SUMMARY	5
ZUSAMMENFASSUNG	6
LIST OF ABBREVIATIONS	7
LIST OF FIGURES	8
1. INTRODUCTION	9
1.1 The Immune System: Components and Functions	9
1.1.1 Innate vs. Adaptive Immune System	9
1.1.2 Cellular vs. Humoral Immune Response	10
1.1.3 Cell Migration	10
1.2 Monocytes: Central Players in Immunity	12
1.2.1 Monocyte Subsets	13
1.2.2 Non-Classical Monocyte Patrolling	13
1.2.3 Non-Classical Monocytes in Disease	15
1.3 Immune Complexes and Fcγ Receptors	16
1.3.1 Immune Complexes	16
1.3.2 Fcγ Receptors	18
1.4 Aims of this Work	20
2. MATERIALS AND METHODS	21
2.1 Materials	21
2.1.1 Animals	21
2.1.2 Antibodies	21
2.1.3 Cell Media, Supplements, Buffers and Solutions	22
2.1.4 Chemicals and Reagents	23
2.1.5 Consumables and Equipment	23
2.1.6 Software and Analysis Tools	24
2.2 Methods	24
2.2.1 Animal Experiments	24
2.2.2 Immune Complexes	25
2.2.3 Cell Isolation and Preparation	26
2.2.4 Molecular and Cellular Assays	28
2.2.5 Sequencing and Transcriptomic Analysis	31
3. RESULTS	32
3.1 Characterization of ICs and their Binding to Leukocyte Subsets	32
3.2 The Role of Non-Classical Monocytes in IC-induced Inflammation in Mice	38
3.3 Non-Classical Monocyte-specific Responses to IC-Binding	46
3.4 Transcriptomic Analysis of IC-induced Migration in SlanMo	61

4. DISCUSSION	68
4.1 NCMs in Intravascular Immunity	68
4.2 NCMs in SLE	71
4.3 Challenges and Advances in Usage of Human IgG ICs	72
4.4 IC-induced Migration of S1a1Mo	73
4.5 Transcriptomic Analysis	75
5. REFERENCES	78
6. ACKNOWLEDGEMENTS	89

Summary

Immune complexes (ICs) are antibody-antigen complexes, which are constantly formed as part of the humoral immune response against pathogens, facilitating their recognition and clearance. However, when ICs are formed in large excess they can accumulate in the vasculature, tissues and organs and lead to severe pathology including inflammation, tissue damage and organ failure. The formation of ICs is a hallmark of the autoimmune disease systemic lupus erythematosus (SLE), in which the persistent formation of ICs from autoantibodies binding to self-antigen leads to severe chronic inflammation and organ dysfunction. The inflammatory cascade is initiated by immune cells recognizing the deposited ICs via Fc γ -receptors, triggering additional immune cell recruitment, cellular activation and pro-inflammatory cytokine release, whereby the mechanisms leading to initial IC recognition and the involved cell types remain unclear.

This dissertation examines the mechanisms underlying the process of IC-induced migration of slan⁺ non-classical monocytes (SlanMo). SlanMo, a subset of non-classical monocytes, are known as intravascular, patrolling cells, which protect blood vessels. They exhibit a high Fc γ receptor diversity and expression, enabling them to uniquely respond to IC-mediated activation. The results in this work demonstrate that SlanMo show strong, Fc γ RIII-dependent binding affinity toward ICs and migrate in a very distinct migration pattern on immobilized ICs. During this unique process, SlanMo internalize and digest ICs. Additionally, SlanMo are attracted by and migrate toward ICs in a concentration-dependent and gradient-dependent manner, resembling chemotaxis. This finding is G protein-coupled receptor independent and solely observed in SlanMo, but not in other Fc γ R-expressing immune cells. It represents a novel mechanism of immune cell recruitment and enables SlanMo to potentially act as first responders in IC-mediated disease, such as SLE.

Transcriptomic profiling of SlanMo revealed that migration on immobilized ICs triggers a distinct gene expression program in SlanMo, characterized by the upregulation of gene sets associated with SLE and protein digestion. These results suggest an important role in immune responses, with a focus on SLE and the clearance of ICs.

This work integrates into the broader understanding of non-classical monocyte biology by highlighting their unique capability and response to ICs. Previous studies have identified mostly anti-inflammatory functions of NCMs, and this work emphasizes their potential role as early responders to ICs and potential scavengers who remove deposited ICs. The notion of IC-induced chemotaxis resembles a completely new principle in cell recruitment to inflammatory sites, bridging gaps in the current literature. By linking SlanMo behavior to SLE pathogenesis, this dissertation provides new insights into potential therapeutic strategies targeting Fc γ receptors to modulate NCM activity in IC-mediated diseases.

Zusammenfassung

Immunkomplexe (IKs) sind Antikörper-Antigen Komplexe, die stetig während der humoralen Immunantwort gebildet werden, um Pathogene zu erkennen und zu eliminieren. Kommt es jedoch zu vermehrter Bildung solcher Protein Aggregate, können sich diese in Blutgefäßen, Gewebe und Organen ablagern und zu schweren Entzündungen und Gewebeschäden führen. Die Entstehung von IKs ist ein Hauptmerkmal der Autoimmunkrankheit Systemischer Lupus erythematoses (SLE), bei welcher die kontinuierliche Bildung von IKs durch die Bindung von Autoantikörpern an körpereigene Proteine zu schweren chronischen Entzündungen führt. Diese Inflammation wird von Immunzellen eingeleitet, die mittels ihrer Fc γ -Rezeptoren durch IKs aktiviert werden, dadurch weitere Immunzellen rekrutieren und pro-inflammatorische Zytokine ausschütten. Die Mechanismen und Zelltypen, die zur Erkennung der IKs führen sind dabei noch nicht ausreichend erforscht.

Diese Arbeit untersucht das Phänomen der IK-vermittelten Migration von slan+ nicht-klassischen Monozyten (SlanMo). SlanMo sind am Endothel patrouillierende Leukozyten, die für ihre protektiven Eigenschaften von Blutgefäßen bekannt sind. Sie exprimieren eine hohe Anzahl und Vielfalt von Fc γ -Rezeptoren, was es ihnen ermöglicht auf besondere Weise mit IKs zu interagieren. Die Ergebnisse dieser Thesis zeigen, dass SlanMo IKs sehr stark im Vergleich zu anderen Zellen binden und immobilisierte IKs ein einzigartiges Migrationsverhalten in SlanMo induzieren. Während dieser Migration werden die IKs internalisiert und verdaut. Außerdem konnte gezeigt werden, dass SlanMo durch IKs angelockt werden und dadurch zu einer höheren Konzentration von IKs migrieren. Dieser Prozess ist konzentrationsabhängig und findet, sehr ähnlich zur Chemotaxis, nur statt, wenn ein Gradient von IKs vorliegt. Er verläuft unabhängig von G-Protein-gekoppelten Rezeptoren und stellt eine völlig neue Art der Rekrutierung von Immunzellen dar, die möglicherweise eine große Rolle in IK-vermittelten Krankheiten wie SLE spielt.

Transkriptom Analysen von SlanMo konnten zeigen, dass durch die Migration auf IKs vor allem Gene, die mit SLE und dem Verdau von Proteinen assoziiert sind, hochreguliert werden. Diese Ergebnisse lassen auf eine wichtige Rolle bei der Pathogenese von SLE und der Beseitigung von IKs schließen.

Die Resultate dieser Arbeit tragen zum besseren Verständnis der Rolle von nicht-klassischen Monozyten bei SLE bei. Frühere Studien ergaben, dass sie überwiegend anti-inflammatorische Funktionen haben. Diese Arbeit deutet auf eine Beteiligung bei SLE durch frühe Erkennung von und gerichteter Migration zu IKs hin. Die Idee der Chemotaxis zu Immunkomplexen stellt ein völlig neues Prinzip der Zellrekrutierung zu Entzündungsherden dar. Außerdem wird auf einen potenziellen Mechanismus zur Beseitigung von Immunkomplexen hingewiesen. Durch die Untersuchung von SlanMo-IK Interaktionen liefert diese Dissertation neue Ansatzpunkte für therapeutische Strategien, um die Aktivität von nicht-klassischen Monozyten in IK-vermittelten Krankheiten wie SLE zu beeinflussen.

List of Abbreviations

ab	Antibody
ag	Antigen
Amyloid beta	A β
APC	Antigen presenting cell
BSA	Bovine serum albumin
CSF1	colony-stimulating factor-1
DEG	Differentially expressed gene
DGE	Differential gene expression
Fab	Fragment antigen-binding
FACS	fluorescence-activated cell sorting
Fc	Fragment crystallizable
FcyR	Fc-gamma receptor
FDR	False discovery rate
GPCR	G protein-coupled receptor
GSEA	Gene set enrichment analysis
hIgG1	Human IgG1
hIgG2	Human IgG2
hIgG3	Human IgG3
hIgG4	Human IgG4
IBF	interfaculty biomedical research department
IC	immune complexes
IgG	Immunoglobulin G
ITAM	immunoreceptor tyrosine-based activating motif
ITIM	immunoreceptor tyrosine-based inhibiting motif
i.v.	Intravenously
KEGG	Kyoto Encyclopedia of Genes and Genomes
LPS	lipopolysaccharide
mIgG2b	Murine IgG2b
MFI	Mean fluorescent intensity
NCM	Non-classical monocytes
NES	Normalised enrichment score
NP	4-hydroxy-3-nitrophenyl acetyl
PBMC	Peripheral blood mononuclear cell
PFA	Paraformaldehyde
PLPP	Photoinitiator (PhotoLabile Protecting Polymer)
PenStrep	Penicillin / Streptomycin
PRR	Pattern-recognition receptor
Ptx	Pertussis toxin
RPA	Reverse passive arthus reaction
RT	Room temperature
Slan	6-sulfo LacNAc
SlanMo	Slan+ non-classical monocytes
SLE	Systemic lupus erythematosus
s.c.	subcutaneous
SPF	Specific pathogen-free
t-SNE	t-distributed stochastic neighbour embedding

List of Figures

Figure 1. Migration mechanisms in leukocytes.	11
Figure 2. Monocytes belong to the myeloid lineage.	12
Figure 3. Clearance of antigen bound in an IC via complement fixation, erythrocyte binding and FcγR-mediated tissue-resident macrophage phagocytosis.	17
Figure 4. IC-induced FcγR signalling of activating FcγRs.	19
Figure 5. Deletion of Nr4a1 super enhancer subdomain depletes Ly6clow monocytes.	21
Figure 6. Mass photometry of antibodies, antigens and immune complexes.	33
Figure 7. Binding affinity of murine-, and human IgG immune complexes to mouse and human peripheral blood leukocytes.	34
Figure 8. IC binding to peripheral blood leukocytes.	36
Figure 9: t-SNE visualization of all FcγR-expressing leukocytes from peripheral whole blood and their IC binding capacity.	37
Figure 10. Nr4a1 ^{se-/-} mice show loss of NCMs in peripheral blood.	39
Figure 11. Nr4a1 ^{se-/-} mice show loss of non-classical monocytes in spleen.	40
Figure 12. Comparison of FcγRIV expression on neutrophils, classical monocytes and non-classical monocytes in mouse peripheral blood and spleen.	41
Figure 13. RPA reaction model in Nr4a1 ^{se-/-} mice does not show different course of inflammation compared to WT mice.	42
Figure 14. Adoptive transfer of WT non-classical monocytes into FcγR ^{-/-} mice could not rescue WT RPA reaction phenotype.	44
Figure 15. Peritoneal RPA reaction does not show differences between WT and Nr4a1 ^{se-/-} mice.	46
Figure 16. SlanMo change into very distinct migratory morphology.	47
Figure 17. SlanMo migrate on immobilized IC.	48
Figure 18 : Immobilized ICs are crucial for adhesion, initiation and maintaining migration.	50
Figure 19. UV-based photo micropatterning system allows generation of immobilized IC gradients.	52
Figure 20. SlanMo internalize immobilised ICs during IC-induced migration.	54
Figure 21. SlanMo transmigrate towards ICs.	55
Figure 22. SlanMo transmigrate toward ICs in a gradient-dependent manner.	58
Figure 23. IC-induced transmigration of SlanMo is CD16-dependent, GPCR-independent and occurs only in SlanMo but not in classical monocytes, neutrophils or NK cells.	60
Figure 24. Transcriptomic analysis of IC-induced migration of Slan+ non-classical monocytes.	62
Figure 25. Systemic lupus erythematosus gene set is enriched by IC-induced migration in SlanMo.	65

1. Introduction

1.1 The Immune System: Components and Functions

The immune system is a complex network of organs, specialized cells, and proteins that acts as a defense against foreign bacteria or viruses, as well as against the body's own malignant cells. It was already mentioned as early as 430 BC, when Thucydides, an Athenian historian, unknowingly observed immunological memory in plague victims as he mentioned "Yet it was with those who had recovered from the disease that the sick and the dying found most compassion. [...] for the same man was never attacked twice- never at least fatally." in his writings, *The History of the Peloponnesian War*². In the past ~2400 years since, we have gained a strong understanding about the functions and components of the immune system. One of the most important functions of the immune system is the discrimination between self and non-self, meaning the ability to distinguish foreign pathogens from an organism's own cells. Furthermore, it must differentiate between healthy cells, infected cells, and malignant cells to effectively eliminate the latter. This fine discrimination is crucial for maintaining immune tolerance while preventing autoimmune diseases, in which self-tissue is mistakenly targeted. The immune system further has to be able to launch a response to an infection but at the same time must not cause excessive damage to the host. These inherent restrictions highlight the immune system's incredible ability to modulate and adapt its response. This fine-tuning is possible due to the many specialized players involved in the immune reaction, which are divided into the innate and adaptive arms of the immune response.

1.1.1 Innate vs. Adaptive Immune System

In vertebrates, the immune system is classified into two subsystems: the innate and the adaptive immune system. The innate immune system is the first line of defense and confers a nonspecific, immediate immune response. It recognizes a broad variety of microbes and pathogens by detecting shared surface antigens through pattern recognition receptors (PRR), enabling it to identify them as foreign and to initiate an immune response. The term "innate" reflects the fact that this branch of the immune system is present from birth and, unlike the adaptive immune system, does not require prior exposure to pathogens to mount an immune response. It is comprised of physical barriers (i.a. skin, mucosal surfaces), leukocytes (i.a. monocytes, macrophages, NK cells) and soluble macromolecules (i.a. complement proteins, cytokines), with this work primarily focusing on monocytes.

The adaptive immune system provides a highly specific immune response to pathogens, that the body has already encountered. Compared to the innate immune system, it confers a less immediate immunological reaction and includes specialized cells (i.a. T cells, B cells), organs (i.a. lymph node), and highly specific proteins, mainly antibodies. It forms an immunological memory which leads to enhanced responses to future encounters with that pathogen and therefore provides long-lasting protection.

Both described branches of the immune system contain cellular and humoral components. Understanding the interplay between cellular and humoral immune responses is essential for exploring how soluble factors like antigen-antibody complexes (immune complexes) can trigger specific cellular responses.

1.1.2 Cellular vs. Humoral Immune Response

As the name suggests, the cellular immune response involves activation of cells, i.a. T cells, NK cells and monocytes. It relies on immune cells directly engaging and eliminating infected or abnormal cells. Next to NK cells and cytotoxic T cells, which directly kill target cells by inducing apoptosis, a main component of this multi-faceted response is the mononuclear phagocytic system, consisting of phagocytic cells³. These cells are primarily monocytes and macrophages, removing infected cells, antibody-opsonized bacteria or potentially harmful immune complexes (ICs) from the circulation via phagocytosis.

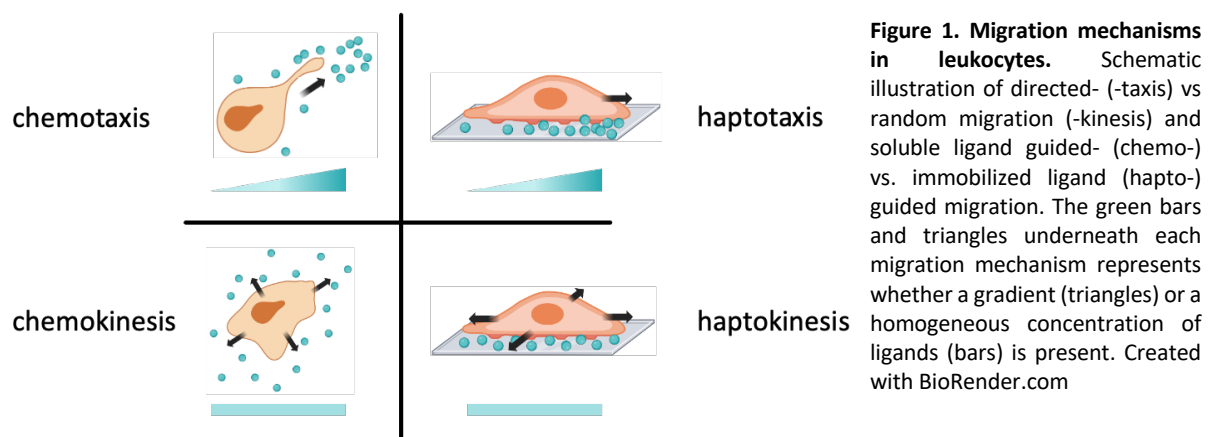
Since many harmful bacteria causing infectious disease multiply in extracellular fluids, these extracellular spaces must be protected by soluble proteins, mainly antibodies and complement proteins. The humoral immunity is the aspect of immunity that is mediated by these macromolecules and is particularly effective against extracellular pathogens such as bacteria and viruses in the bloodstream or mucosal surfaces. Antibodies are highly specific proteins secreted by B cells and can bind to virtually any antigen. Their main function includes neutralization, opsonization, and complement activation. During neutralization, antibodies protect the host from pathogens or toxins by directly binding to them and thereby blocking access to target cells or receptors. Since antibody binding to bacteria does not prevent their replication, antibodies also “mark” bacteria for phagocytes. Monocytes e.g. then recognize antibodies bound to the pathogen via Fc receptors (FcRs) and remove the pathogen from circulation. This coating process of pathogens is termed opsonization. Antibodies bound to the bacterial surface can also be recognized by and activate complement proteins. These proteins can directly lyse and kill some bacteria^{4,5}. However, their main function is to recruit granulocytes and monocytes to the site of infection⁶. This recruitment, alongside with the delicate interplay of all mentioned aspects of immunity relies heavily on the tightly regulated migration of immune cells to sites of infection or inflammation.

1.1.3 Cell Migration

The mobilization and recruitment of immune cells is a major pillar of the immune system enabling effective immune surveillance, tolerance, and rapid response to infection or tissue damage⁷⁻⁹. It enables dynamic interactions between immune cells and their environment, and its impairment leads to severe pathology¹⁰⁻¹².

Cell migration can be broadly categorized into random migration process termed kinesis (from ancient Greek (*kinēsis*) meaning “movement”) and a directed migration towards a stimulus, namely taxis (from ancient greek (*taxis*) meaning “order”)¹³. Kinesis, the random locomotory behaviour, is often associated with functions like immune surveillance and scouting or patrolling behaviours^{12,14}. An immune cell type well-known for their patrolling behaviour are

NCMs, a monocyte subset. Their distinct migration behaviour, characterized by patrolling along the endothelium, was a crucial observation leading to their discovery and classification as separate monocyte subset¹⁵ and coined the generally accepted term “patrolling monocytes”^{16,17}. In contrast to kinesis, taxis describes directed migration towards a specific stimulus, such as chemical gradients or cytokine cues. Cytokines that can induce a directed migration in leukocytes are called chemokines. They act through binding to chemokine receptors on a cell’s surface to induce chemotaxis, the directed migration along a chemokine gradient. Prerequisite for any gradient-dependent directed migration is the cell’s ability to sense a change in chemokine concentration alongside its surface, meaning across a cell’s diameter in the micrometer range¹⁸⁻²⁰. While chemotaxis is extensively studied in a variety of leukocyte subsets, it is not well described in NCMs. Neutrophils and dendritic cells are the most well-studied cells regarding chemotaxis, with neutrophil responses to chemokines, like IL-8 (CXCL8)²¹⁻²³, and bacterial peptides like fMLP^{24,25} being equally intensively studied as the fundamental dendritic cell migration to the lymph nodes driven by chemokines CCL19 and CCL21²⁶⁻²⁸.



Directed cell migration does not only occur via sensing of soluble factors like chemokines but also occurs as response to surface bound stimuli in the form of haptotaxis. Other directed cell migration mechanisms such as durotaxis (cells are guided by rigidity gradients)²⁹, topotaxis (sensing of differences in topographical surface features such as grooves, fibres, etc.)³⁰, and galvanotaxis (sensing differences in electrical fields)³¹ exist but are not within the scope of this thesis.

To migrate through their complex three-dimensional environment filled with cells and extracellular matrix, leukocytes must actively generate forces that propel them in the wanted direction. This is either done via pulling on adhesive ligands and interactions between the cell membrane and its surroundings³² or by intracellular force generation and propulsion through active polymerization and simultaneous depolymerization of the actin cytoskeleton³³. Coordinated actin polymerization at one site within the cell, generates protrusive forces that drive the extension of the cell membrane at this site, generating the leading edge³⁴. Similarly, actin depolymerization generates contractile forces, resulting in retraction of the cell membrane at the trailing edge³⁵. Through the propulsive forces of intracellular actin polymerization at the leading edge, a membrane sheet-like structure called lamellipodium is

formed³⁶. As an almost two-dimensional cell membrane protrusion the lamellipodium forms an extension of the cell, actively involved in sensing its environment and guiding the cell³⁷ (see Figure 16).

Cell migration is a well-established field of interest, with extensive studies throughout the years emphasizing its importance in a plethora of pathways and diseases, i.a. embryonic development, wound healing and cancer metastasis³⁸⁻⁴⁰. Despite the long history of cell migration studies, great advancements in microscopy still enable the emergence of important and fundamental principles, such as e.g. “nuclear probing”⁴¹. It describes the process of how cells sample their dense environment for pores large enough to squeeze through by using their largest compartment, the nucleus, as a sensor and is essential in the understanding of how cells navigate through complex tissues.

As cell migration continues to be a pivotal focus of research, it is crucial to explore how the migration of specific immune cell subsets, such as the distinct patrolling behaviour of NCMs, is linked to their poorly understood function in the immune system. Studying their migration may provide valuable insights into their roles within immune responses.

1.2 Monocytes: Central Players in Immunity

Monocytes are large leukocytes (~12µm ø) and comprise about 10% of total leukocytes in humans. Derived from bone marrow progenitors, they circulate in the bloodstream before migrating into tissues, where they differentiate into macrophages or dendritic cells⁴² (Figure 2).

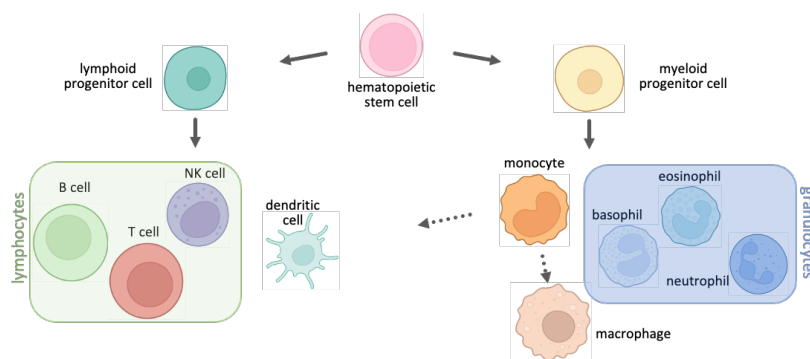


Figure 2. Monocytes belong to the myeloid lineage. Monocytes and granulocytes are both derived from the common myeloid progenitor cell. Sharing the same progenitor, monocytes and neutrophils are both efficient phagocytes but only monocytes have the potential to further differentiate to macrophages or dendritic cells. Created with BioRender.com

Historically, monocytes were regarded as a mere reservoir of motile progenitor cells destined to differentiate into dendritic cells or macrophages upon inflammatory stimulus or tissue damage^{43,44}. However, this perspective has shifted since studies have uncovered their direct, independent roles in immune responses, i.a. initial inflammatory response via pro-inflammatory cytokines⁹, antigen presentation^{45,46}, removal of apoptotic cells via phagocytosis⁴⁷, tissue repair⁴⁷, and vascular homeostasis^{17,48}. This makes them central to both homeostatic and inflammatory processes. Especially NCMs are now recognized for their active roles in vascular surveillance or inflammatory features in systemic lupus erythematosus⁴⁹.

1.2.1 Monocyte Subsets

Monocytes are traditionally divided into three subsets based on their phenotypic characteristics, specifically the expression of CD14 (LPS co-receptor) and CD16 (FcγRIII). In humans, these subsets are classified as classical (CD14⁺CD16⁻), intermediate (CD14⁺CD16⁺), and NCM (CD14⁻CD16⁺). Similarly, in mice, monocyte subsets are distinguished by their expression of Ly6C (undefined function) and CX3CR1 (fractalkine receptor): classical monocytes are Ly6C⁺CX3CR1^{low}, while NCM are Ly6C⁻CX3CR1^{high}. Intermediate monocytes are thought to be a transitional stage in cell development and share characteristics with both classical and non-classical subsets. Modern studies using mass cytometry or RNA sequencing techniques have defined even more subsets and shown a large heterogeneity within monocytes⁵⁰.

Classical monocytes are the most abundant subset, comprising approximately 80-90% of circulating monocytes, and are heavily involved in acute inflammatory responses. NCM, even though less studied, have gained increasing attention in recent years due to their unique patrolling behaviour and role in vascular surveillance. Their low abundance (comprising about 5-10% of circulating monocytes) makes them challenging to investigate compared to classical monocytes. In our group, we are using 6-sulfo LacNAc (slan) as single marker to identify and isolate NCM for our studies. Slan is a carbohydrate modification on the PSGL-1 protein on the surface of NCMs⁵¹ and 50-60% of NCMs are slan⁺^{36,52}. Recently, it was shown that slan⁺ NCMs (SlanMo) are suitable representatives of the prototypical NCM, making slan an excellent marker for their identification and isolation⁵².

Monocyte development begins in the bone marrow, where hematopoietic stem cells give rise to monocyte progenitors (Figure 2), followed by differentiation to classical monocytes. They are then released into the bloodstream, where they have a half-life of ~1d and differentiate into intermediate and non-classical monocytes through a process of sequential maturation⁵³. NCMs have longer half-lives with ~2d in mice and 5-7d in humans⁵⁴. This maturation is regulated by various transcription factors and cytokines, including NR4A1 in mice, which is critical for the development of non-classical monocytes¹. Beyond their development and subset-specific characteristics, NCMs are distinct from not only other monocyte subsets but all leukocytes by their hallmark vascular patrolling behaviour. This unique observation has been described many times, yet its precise biological role remains incompletely understood.

1.2.2 Non-Classical Monocyte Patrolling

The recruitment of leukocytes to sites of infection is one of the most important functions of the immune system. It is mediated by cell-adhesion molecules expressed on leukocytes and on endothelial cells, the cells lining the inner side of blood and lymphatic vessels. Under normal conditions, leukocytes such as classical monocytes and neutrophils flow in the center of small blood vessels due to the blood flow. Upon inflammatory responses, blood vessels dilate, and the therefore slower blood flow allows for leukocyte-endothelial interactions and adhesion. P-selectin and E-selectin e.g., are induced on activated endothelium as response to

a local infection and facilitate initial leukocyte adhesion⁵⁵, termed tethering or rolling adhesion. Inflammatory mediators, i.a., secreted by macrophages during an infection, and chemokines i.a. CXCL8 (interleukin-8) and CX3CL1 (fractalkine) lead to expression of more adhesion molecules such as the leukocyte integrin LFA-1 and its ligand ICAM-1 on endothelial cells^{56,57}. These allow for increased, tight adhesion of leukocytes to endothelial cells and ultimately for transendothelial migration, called diapedesis, along a chemokine gradient to the site of infection⁵⁸.

In strong contrast to this, NCMs constantly adhere to and patrol the endothelium, irrespective of inflammatory or homeostatic conditions^{17,59}. In fact, at least 50-60% of non-classical monocytes in mice are attached to and crawl on the vessel wall in uninflamed conditions^{15,60}. Interestingly, this patrolling is 100 to 1000-fold slower than rolling of other leukocytes and independent of blood flow¹⁵. Under homeostatic conditions, it is LFA-1 dependent, since blocking of either one of the two integrin chains, CD18 and $\alpha_L\beta_2$, making up this protein, leads to detachment of NCMs of the vessel wall¹⁵. The CX₃CR1 – CX3CL1 axis is also involved in the patrolling of NCM in mice, shown by a reduction of crawling monocyte numbers in CX₃CR1-deficient mice by two-thirds¹⁵. However, LFA-1 blocking antibody mediated release of crawling monocytes on the vessels wall of CX₃CR1-competent mice indicates that this due to fractalkine-induced upregulation of integrins. Strikingly, an LFA-1 dependent patrolling was also observed in human NCMs after adoptive transfer of labeled human NCM into recipient mice⁶¹, strongly supporting that this is a conserved mechanism across species crucial to NCM function. Recently, the whole vascular bed was identified to be the nurturing niche for NCMs, as scavenging the growth factor colony-stimulating factor-1 (CSF1) present on endothelial cells is needed for NCM survival⁶². The underlying work nicely ties together LFA-1 and fractalkine involvement in NCM patrolling, by showing that integrin α_L - (a subunit of LFA-1) or CX₃CR1-deficient monocytes have impaired CSF1 uptake and decreased patrolling behaviour. This directly links NCM patrolling on the endothelium to their own survival and defines the whole vascular branch as NCMs' niche.

Patrolling NCMs were shown to be immediate responders to bacterial infection of the peritoneum¹⁵, which was associated with their slow movement and therefore increased presence during patrolling. It allowed for an early tissue invasion, several hours before invasion of neutrophils or classical monocytes. Patrolling NCMs were shown to be the fast responders as they were the only source of proinflammatory cytokines, i.a. TNF- α and genes coding for IL-1, PRRs, complement and Fc γ R were upregulated as early as 2h after infection. Supporting the role of NCMs as early responders, are findings in inflamed kidney glomeruli of rats. NCMs were patrolling in the uninflamed glomerular endothelium in an LFA-1 dependent manner but during IC-mediated nephrotoxic nephritis, NCMs were infiltrating inflamed glomeruli as first responders⁶³. Subsequent classical monocyte infiltration occurred several days later and was accompanied by tissue destruction. Interestingly, next to the glomerular endothelium, NCMs also patrol and protect the lung endothelium. They are crucial for protection against seeding of metastatic tumor cells in the lung vasculature⁶⁴ as Nr4a1-deficient mice (mice depleted of NCMs) show increased lung metastasis. Conclusively,

adoptive transfer of NCMs into Nr4a1-deficient mice prevented tumor invasion. Patrolling NCMs interacted early with tumor cells in the lung microvasculature, phagocytosing metastatic cells and preserving lung homeostasis. In a different model it could be shown that NCMs scavenge microparticles (0,2 μm – 2 μm) and high-molecular-weight dextran from the endothelium⁴⁸. Thereby, they do not stop their patrolling motion or detach, but instead persist in patrolling while carrying their cargo.

While these findings underscore the vital role of NCM in maintaining vascular homeostasis and integrity, dysregulation or altered functions of NCM have been increasingly implicated in the pathogenesis of a wide range of diseases, including immune complex-mediated disorders such as rheumatoid arthritis (RA) and systemic lupus erythematosus (SLE).

1.2.3 Non-Classical Monocytes in Disease

The general notion that patrolling NCMs are responsible for preserving vascular homeostasis is widely accepted. However, several studies have shown that this monocyte subset can also promote the resolution of inflammation and contribute to the pathogenesis of disease.

NCMs are involved in resolving inflammation or tissue repair during many pathologies, e.g. soft tissue injury⁶⁵, myocardial infarction⁴⁷, mucosal wounds in the large intestine⁶⁶ and reperfusion injury in kidney vasculature⁶⁷. The mechanisms behind these anti-inflammatory properties are numerous and diverse, i.a. promotion of angiogenesis⁴⁷, scavenging of apoptotic cells⁴⁸ and differentiation to wound healing macrophages⁶⁵, highlighting the plasticity and adaptability of these cells. Contrary, proinflammatory roles have been described for NCMs in different diseases and pathologies. In a RA mouse model e.g., NCMs are required for the initiation of joint inflammation and furthermore differentiate into M1 macrophages, which continue to drive disease pathogenesis⁶⁸. Supporting observations have been made in RA patients, where monocytes in the synovial fluid showed strongly increased CD16 expression, a key marker of NCMs, compared to peripheral blood monocytes⁶⁹. Beyond that, numbers of NCMs in blood of patients with active RA were increased⁷⁰. Similarly, NCM levels are significantly enriched in the blood of HIV patients, correlating with the viral load of these patients⁷¹. In another viral infection, as in severe cases of COVID-19, these cells are reduced in peripheral blood^{72,73} but increased in pulmonary mucus⁷³, supporting a migration of NCMs to the corona virus infected lung. Single cell RNA sequencing data of CD16⁺ monocytes from people with COVID-19 shows that they also express a transcriptional signature of cell migration, cell activation and inflammatory response⁷⁴, further hinting towards NCM migration as response to inflammation.

Most studies investigating the proinflammatory roles of NCM have focused on their involvement in SLE. SLE is an autoimmune disease, characterized by local and systemic inflammation caused by autoantibodies recognizing nuclear autoantigens. In SLE mouse models, myeloid cell-specific deficiency of Fc γ RIIb decreased SLE development in lupus prone mice, suggesting a disease-supporting role of Fc γ RIIb-expressing monocytes⁷⁵. In lupus nephritis, an inflammation caused by SLE, patrolling NCMs were found to be significantly

increased in the glomeruli of diseased mice whereas NCM-deficient Nr4a1^{-/-} mice were completely protected from disease pathology⁷⁶. Additionally, ICs (a hallmark pathologic feature of SLE) have been shown to recruit and capture human NCMs to kidneys of an SLE mouse model and induce the secretion of the pro-inflammatory molecules TNF- α , IL-6 and CXCL2 in NCM⁷⁷.

Similar findings were made in human SLE patients, describing significantly increased numbers of patrolling NCMs in kidneys of patients with SLE⁷⁶ and TNF- α production of NCMs in lupus nephritis glomeruli⁷⁷. SlanMo, a subset of NCMs, were found to be enriched in skin lesions of systemic and cutaneous lupus erythematosus patients and highly pro-inflammatory due to TNF- α production⁷⁸. Moreover, NCMs are enriched and show a proinflammatory phenotype in peripheral blood of SLE patients⁷⁹.

Interestingly, the diseases in which NCM have been reported to play a pro-inflammatory role - RA, SLE, and COVID-19 - are all either immune complex-mediated or exhibit pathology significantly driven by immune complexes. In RA, the rheumatoid factor is an autoimmune antibody recognizing self IgG and leading to the formation of ICs. In SLE, these antigen-antibody complexes are a main driver of the disease. ICs have also been shown to contribute to immunopathology in COVID-19, as their abundance correlates with disease severity and reaches levels of IC concentrations found in SLE patients⁸⁰. Since NCM express a broad pattern and high level of Fc γ Rs⁸¹, they are most likely specialized in recognizing and responding to ICs. Indeed, Fc γ RIII was recently identified to enable a subset of NCMs to uniquely bind and respond to ICs⁸².

1.3 Immune Complexes and Fc γ Receptors

Immune complexes and their recognition via Fc γ Rs play crucial roles in both, the immune system's protective function and the development of various diseases.

1.3.1 Immune Complexes

ICs form in every humoral immune response when antibodies bind their cognate antigen. In healthy individuals, under homeostatic conditions these antigen-antibody complexes are responsible for pathogen clearance. However, when this clearance mechanism is perturbed or the built up of new ICs surpasses the capacity of the IC removal machinery, ICs can accumulate and deposit in blood vessels, skin, and organs such as the kidneys, leading to severe inflammation and tissue damage.

The clearance of potentially harmful pathogens via formation of ICs and their subsequent disposal begins with the binding of pathogen-specific antibodies to the pathogen's surface (see section 1.1.2 Cellular vs. Humoral Immune Response). C1q, a multivalent protein of the complement system with high avidity towards IgG, binds to antigen-bound antibodies and initiates the complement cascade⁸³. The deposition of the downstream complement proteins C4b and C3b on the IC is recognized by the complement receptor 1 (CR1) on erythrocytes⁸⁴. After binding, erythrocytes then transport the IC through the blood stream to liver and spleen,

where tissue-resident macrophages remove the complexes from the erythrocytes by binding them via CR1 and Fcγ receptors. This leads to an internalization and destruction of the antibody- and complement opsonized antigen by the macrophages. Noteworthy, only splenic but not hepatic uptake of ICs was significantly reduced in C1q-deficient mice⁸⁵, hinting towards several redundant pathways for IC removal. Correspondingly, defects in early complement components, i.a. C1, C2 and C4 are associated with the accumulation of immune complexes and susceptibility to SLE⁸⁶.

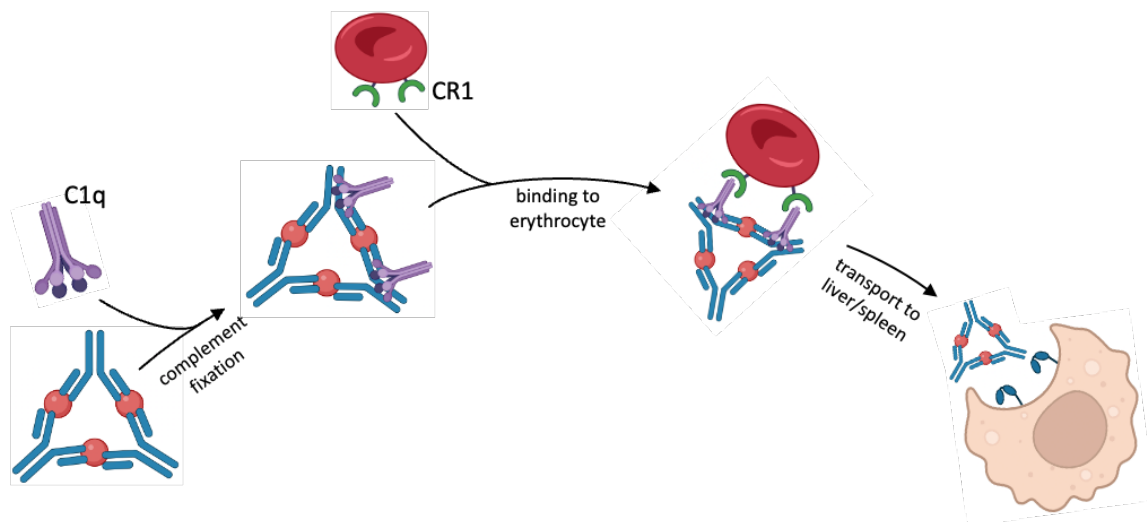


Figure 3. Clearance of antigen bound in an IC via complement fixation, erythrocyte binding and FcγR-mediated tissue-resident macrophage phagocytosis. C1q binds to antigen-bound IgG and starts the complement cascade, leading to deposition of C3b and C4b on the IC. These complement proteins opsonizing the IC, are recognized by erythrocyte CR1 and transported further through the bloodstream to liver and spleen. Here, tissue resident macrophages, such as Kupffer-cells, phagocytose the IC and digest the antigen. Created with BioRender.com

ICs play dual roles in immune regulation, not only facilitating the clearance of antigens but also enhancing antigen presentation. Through their interactions and uptake via FcγRs on antigen-presenting cells such as monocytes, dendritic cells and macrophages, the bound antigen is internally processed and loaded onto MHC molecules for presentation to T cells⁸⁷. Follicular dendritic cells are specialized in capturing intact ICs and using them for antigen presentation, as they store undegraded ICs for long periods of time on their surface and in intracellular nondegradative cycling compartments⁸⁸. This enables prolonged, constant antigen presentation and FcγR-activation of B cells in the germinal center, promoting B cell differentiation, -somatic hypermutation and -survival⁸⁹.

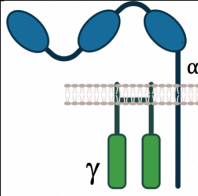
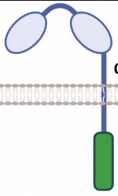
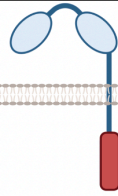
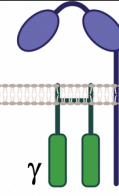
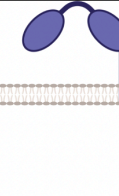
One example of excess formation of ICs leading to inflammation, is the Arthus reaction. This type III hypersensitivity reaction occurs, when circulating antibodies recognize locally injected antigen, e.g. after repeated injection of an antigen or vaccine, and form ICs. This IC-triggered inflammation is initiated by FcRs and most likely driven by mast cell degranulation^{90,91}. The phenomenon is used as a model reaction in IC-induced inflammation and initiated by i.v. injection of large amounts of antigen, immediately followed by intradermal injection of correspondent antibody and termed reverse passive arthus (RPA) reaction. IC formation at the site of antibody injection leads to inflammatory responses, such as edema and haemorrhage.

IC-mediated inflammation and -antigen removal heavily rely on FcγRs. The next section will explore the distribution, classification and diverse functions of these Fcγ receptors.

1.3.2 Fcγ Receptors

FcγRs are membrane bound cell surface proteins that recognize the Fc domain of IgG antibodies. They are expressed on a wide range of leukocytes and induce cellular effector functions like phagocytosis and antibody-dependent cytotoxicity⁹². The human FcγR system comprises six distinct members: FcγRI (CD64), FcγRIIa (CD32a), FcγRIIb (CD32b), FcγRIIc (CD32c), FcγRIIIa (CD16a) and FcγRIIIb (CD16b). CD32c only occurs in a fraction of the human population and is therefore not further described in this study^{93,94}. These receptors have different affinities toward different IgG subclasses (see Table 1) and are broadly classified into activating and inhibitory receptors, with FcγRIIb acting as the only inhibitory FcγR.

Table 1. Characterization of human FcγRs on leukocytes. *mono = monomeric IgG, **compl = complexed, aggregated IgG, +++ very high affinity, ++ high affinity, + low affinity, - no affinity. Information taken from ^{50,81,95-98}

Fcγ Receptors									
name		FcγRI (CD64)	FcγRIIa (CD32a)	FcγRIIb (CD32b)	FcγRIIIa (CD16a)	FcγRIIIb (CD16b)			
class		activating	activating	inhibitory	activating	activating			
IgG affinity		<i>*mono</i>	<i>**compl</i>	<i>*mono</i>	<i>**compl</i>	<i>*mono</i>	<i>**compl</i>	<i>*mono</i>	<i>**compl</i>
	IgG1	+	+++	-	+++	-	+	-	+++
	IgG2	-	-	-	+	-	-	-	-
	IgG3	++	+++	-	+++	-	++	-	+++
	IgG4	++	+++	-	++	-	+	-	-
Expression on		<ul style="list-style-type: none">class. MonosmDC2	<ul style="list-style-type: none">neutrophilseosinophilsbasophilsclass. monosnon-class monomDC2pDC	<ul style="list-style-type: none">B cellsnon-class mono	<ul style="list-style-type: none">NK cellsnon-class mono	<ul style="list-style-type: none">neutrophils			
Signaling motif		ITAM (γ-chain)	ITAM (α-chain)	ITIM (α-chain)	ITAM (γ-chain)	-			

All FcγRs act as multimeric protein complexes. In most FcγRs, the ligand binding- (α-chain) and the signalling subunits are two separately encoded proteins that non-covalently interact. The α-chain is the IgG-binding transmembrane protein that contains two extracellular IgG-like domains (three in the case of FcγRI⁹⁹) but only for FcγRII the α-chain also contains the immunoreceptor tyrosine-based signalling domains (see Table 1, top row). As an activating FcγR, FcγRIIa contains an immunoreceptor tyrosine-based activation motif (ITAM), whereas the FcγRIIb α-chain contains the inhibitory ITIM domain. FcγRI and FcγRIIIa on the other hand associate with the FcR common γ-chain, which contains several ITAM domains but is not

involved in ligand binding. Noteworthy, FcγRIIIb is the only Fcγ receptor that is anchored to the cell membrane via a glycosylphosphatidylinositol (GPI) unit and does not contain an intracellular domain. It is solely expressed on neutrophils and generally accepted as a scavenging receptor¹⁰⁰ of ICs, since it has the largest copy number of all FcγRs on all hematopoietic cells⁸¹. The intracellular signal transduction of FcγRIIIb is poorly understood, but it is known to associate with CD32a and use its signalling machinery¹⁰¹.

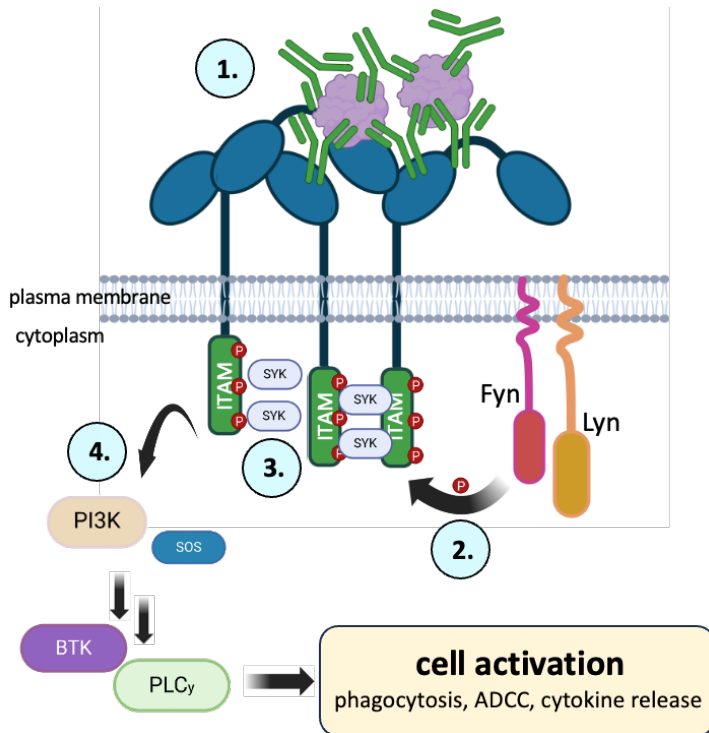


Figure 4. IC-induced FcγR signalling of activating FcγRs. After crosslinking of activating FcγRs by ICs, Lyn and Fyn, members of the Src kinase family, are recruited to and phosphorylate tyrosine residues at the intracellular ITAM domain. This creates membrane docking sites for and activates SYK, which in turn further activates the signalling proteins PI3K and SOS. Further signal transduction via BTK and PLC_γ leads to cell effector functions, such as phagocytosis, ADCC or cytokine release.

Signalling by FcγRs is initiated when the receptor binds to antigen-bound IgG. The multivalency of ICs leads to a clustering of engaging FcγRs, which is the trigger for further intracellular signalling. The activating FcγRs FcγRI, -IIa and -IIIa recruit membrane-bound members of the Src kinase family, *e.g.* Lyn and Fyn, which phosphorylate tyrosine residues at the ITAMs^{92,102}. This in turn leads to a recruitment and activation of the tyrosine kinase SYK, now further activating downstream signal transduction molecules, *i.a.* phosphoinositide 3-kinase (PI3K) and the RAS-GTPase Son of Sevenless (SOS). PI3K phosphorylates phosphoinositides in the plasma membrane, serving as a docking site for the signalling proteins Bruton's tyrosine kinase (BTK) and phospholipase C_γ (PLC_γ). During signalling of inhibitory FcγRIIb on B cells, the ITIM recruits the phosphatase SHIP, which counteracts PI3K action by dephosphorylation of phosphoinositide binding platforms¹⁰³. This inhibits recruitment and activation of BTK and PLC_γ. For activating FcγRs, activation of PLC_γ leads to Ca²⁺ influx-induced triggering of further downstream events. Together, PI3K, SOS, BTK and PLC_γ lead to cell activation and several different effector functions, such as phagocytosis, ADCC and cytokine release. Interestingly, it recently has been shown that FcγRIIIa on NCMs facilitates superior IC binding and uniquely induces cell migration upon activation by immobilized ICs^{82,104}.

1.4 Aims of this Work

The primary aim of my thesis is to unravel the molecular and cellular mechanisms of immune complex-induced migration in slan⁺ non-classical monocytes.

The achievement of the primary aim was approached by pursuing several secondary objectives. First, I aimed at characterizing SlanMo's IC binding capacity in comparison to all other FcγR-expressing leukocytes before investigating underlying IC-induced migration mechanisms with FcγR blocking antibodies. As next secondary objective, I assessed whether IC-induced migration of SlanMo is directional, particularly if it follows a gradient, to elucidate if chemotactic mechanisms are involved. To fully address the primary objective, the focus was put on defining the transcriptional signature associated with IC-induced migration in SlanMo to explore its relevance to specific diseases or cellular functions using transcriptomic approaches. Lastly, I aimed at determining the contribution of SlanMo to IC-mediated inflammation *in vivo* using the RPA reaction model in NCM-deficient mice.

2. Materials and Methods

2.1 Materials

2.1.1 Animals

Housing: All animals were at Heidelberg interfaculty biomedical research department (IBF) under specific pathogen-free conditions (SPF). Mice were housed in conventional cages with semi-open tops, under a light-dark cycle of 12h light – 12h dark at 22°C ± 2°C. Mice were fed *ad libitum* and had constant access to water through either water bottle with ball-valve nozzle or through hydration gel during transport to our laboratory.

FcγR^{-/-} strain: FcγR^{-/-} were kindly provided by Prof. Dr. med. Ralf Ludwig (Lübeck, Institute of Experimental Dermatology, University of Luebeck) and housed and bred under SPF conditions at IBF Heidelberg.

WT mice were purchased from Charles River (C57BL/6 background) and backcrossed into FcγR^{-/-} and used as littermate controls.

Nr4a1^{se-/-} strain: WT mice were backcrossed into Nr4a1^{se-/-} and either homozygous Nr4a1^{se+/+} or heterozygous Nr4a1^{se+/-} littermate mice were used as controls.

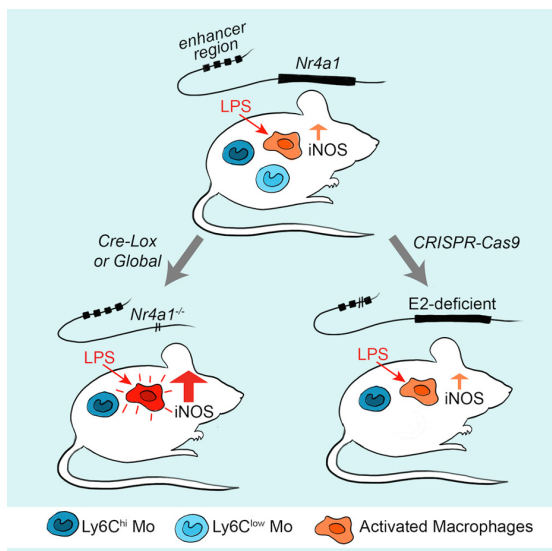


Figure 5. Deletion of Nr4a1 super enhancer subdomain depletes Ly6C^{low} monocytes. Taken from Thomas et. al.¹ The Nr4a1 enhancer domain E2 is essential for NCM development in mice yet dispensable for macrophage inflammatory response.

2.1.2 Antibodies

Target	Conjugate	Clone	Use	Company	Reference #
CD1c	BV605	L161	1:100	BioLegend	331538
CD3	PerCP	UCHT1	1:100	BioLegend	
CD11c	BV510	S-HCL-3	1:100	BioLegend	371514
CD16	A700	DJ130c	1:100	NovusBio	NB100-64346AF700
CD16	PE		BD Biosciences		
CD20	SparkUV387	S18015E	1:100	BioLegend	375527

CD56	PE-Dazzle 594	HCD56	1:80	BioLegend	318348
CD14	APC	63D3		BioLegend	367118
CD123	BV421	6H6	1:100	BioLegend	306018
CD141	PE-Cy7	M80	1:80		
HLA-DR	Pacific Blue	L243	1:80	BioLegend	307633
Siglec-8	BUV395	837535	1:100		
Slan		MDC8			
Mouse IgM	PE	(goat f(ab') ₂)	1:200	Southern Biotech	1022-09
Mouse IgM	FITC				
Immunoglobulin 1 (IgG1), from normal human plasma	-	-		Athens Research & Technology	16-16-090707-1
Immunoglobulin 2 (IgG2), from normal human plasma	-	-		Athens Research & Technology	16-16-090707-2
Immunoglobulin 3 (IgG3), from normal human plasma	-	-		Athens Research & Technology	16-16-090707-3
Immunoglobulin 4 (IgG4), from normal human plasma	-	-		Athens Research & Technology	16-16-090707-4
CD16		3G8	1:100	BioLegend	302050
CD64		10.1	1:100	Invitrogen	305016
CD32		AT10	1:100	BioRad	MCA1075EL
CD115	PE	AFS98	1:100	BioLegend	135506
Ly6C	PerCP/Cy5.5	HK1.4	1:100	BioLegend	128012
CD45	PE/Cy7	S18001F	1:100	BioLegend	157206
CD11c	APC	N418	1:100	BioLegend	117310
CD11b	A700	M1/70	1:100	BioLegend	101222
Ly6G	BV421	1A8	1:100	BioLegend	127628
F4/80	FITC	BM8	1:100	BioLegend	123108
CD19	BV510	6D5	1:100	BioLegend	115546
NK1.1	BV510	PK136	1:100	BioLegend	108738
CD3	BV510	17A2	1:100	BioLegend	100233

2.1.3 Cell Media, Supplements, Buffers and Solutions

Name	Company	Reference #	Composition
FACS buffer	-	-	2% FCS PBS
MACS buffer	-	-	2 mM EDTA

PBS/EDTA	-	-	2,5% HSA PBS 2 mM EDTA PBS 0,5 % BSA 1 % P/S X-Vivo™-15
Transmigration medium			
PBMC Medium	Spin	pluriSelect	60-00092-12
PBS		Gibco™	14190-169
X-Vivo™-15		Lonza	02-060Q
Human serum albumin (albumnorm 20%)		Octapharma GmbH	
Penicillin	-	Gibco™	15240122
Streptomycin			
L-Glutamine		Gibco™	25030081
Natrium Azide		AppliChem	A1430

2.1.4 Chemicals and Reagents

Name	Company	Reference #
BSA-6FITC	Invitrogen	A23015
PLPP Gel	Alvéole	NA
PE / R-Phycoerythrin Conjugation Kit	Abcam	ab102918
Lightning-Link® pHrodo™ Antibody Labeling Kit	Thermo Fisher	P36014
NK Cell Isolation Kit human	Miltenyi Biotec	130-092-657
CD14 MicroBeads human	Miltenyi Biotec	130-050-201
Anti-Mouse IgM MicroBeads	Miltenyi Biotec	130-047-301
Pierce™ DSS, No-Weigh™ Format	Thermo Fisher	A39267
Ketamine/Xylazine	Sigma-Aldrich	K4138
Veet Depilation Creme	dm	1593053

2.1.5 Consumables and Equipment

Name	Company	Reference #
Black bottom OptiPlate 96F HB	Fisher Scientific	50-905-1576
CellTiter Glow® Luminescent Cell Viability Assay	Promega	G7571

AutoMACS columns		130-021-101
Neuroprobe ChemoTx		
micro-Insert 4 Well in μ -Dish 35 mm, high	Ibidi	80406
Cell strainer 40 μ m/70 μ m	Corning	
EDTA blood collection	Sarstedt	
S-Monovette, 9mL		
Axio Observer Z1 inverted microscope	Axio	
Frosted microscope slide	Marienfeld	10 002 00
Pap pen	Kisker Biotech	MKP-1
Omnican®F, 1mL injection syringe	Braun	
MicroBeta Trilux 1450 LSC & Luminescence Counter	PerkinElmer	
Flow Cytometer Gallios 4L	Beckmann Coulter	
Cytek Aurora	Cytek	

2.1.6 Software and Analysis Tools

Software	Version	Supplier
ImageJ	1.54k	
R	4.2.2	R Core Team
RStudio		posit
FlowJo	10.10	
SpectroFlo		Cytek
Celleste	5	ThermoFisher
GraphPad Prism	8	

2.2 Methods

2.2.1 Animal Experiments

2.2.1.1 Ethical statement

All animal procedures were conducted in accordance with ethical guidelines and regulations for animal welfare. They were approved by the regional administrative authority in Karlsruhe, Germany. When performing mouse experiments, all efforts to comply with the 3R principle were made. Approval number: G-186/19.

2.2.1.2 Cutaneous reverse passive Arthus reaction

Female mice of 8-12w of age were anaesthetized with 100 μ L/10 g bodyweight of a 1:6 dilution of 80mg/ml Ketamin + 6mg/ml Xylazin (Sigma-Aldrich) and their back was shaved the day prior the experiment. The shaved area was depilated using Veet® depilation cream, which was completely removed after 2min of incubation.

Mice were anaesthetized with 100 μ L/10 g bodyweight of a 1:6 dilution of 80mg/ml Ketamin + 6mg/ml Xylazin (Sigma-Aldrich) and placed on a heated platform maintained at 37°C to prevent excessive cooling. Eyes were creamed with Bepanthen creme to prevent drying. 60 μ g of α BSA polyclonal rabbit IgG or isotype control in 30 μ L PBS was injected intradermally in back skin of the animal. α BSA antibody was injected on right flank of animal and isotype control on left flank of same animal. Right after, 200 μ L of 20 μ g/g bodyweight BSA in PBS + 0,1% Evans Blue was injected i.v.. Animals were sacrificed after 2h, back skin was removed, pinned on Styrofoam block to take images and 1 - 3 biopsy punches (8 mm diameter) were taken from both intradermal injection sites. Biopsy punches were then weighed and placed in 500 μ L formamide for 48h at 55°C on orbital shaker for Evans Blue extraction. Extracted Evans Blue was quantified by measuring absorbance at 620nm in plate reader.

2.2.1.3 Peritoneal reverse passive Arthus reaction

Female mice of 8-12w of age were anaesthetized with 100 μ L/10 g bodyweight of a 1:6 dilution of 80mg/ml Ketamin + 6mg/ml Xylazin for shaving their back the day prior the experiment.

Mice were anaesthetized with 100 μ L/10 g bodyweight of a 1:6 dilution of 80mg/ml Ketamin + 6mg/ml Xylazin and placed on a heated platform maintained at 37°C to prevent excessive cooling. Eyes were creamed with Bepanthen creme to prevent drying. 800 μ g/mL of α BSA polyclonal rabbit IgG or isotype control in 400 μ L PBS were injected intraperitoneally (i.p.). Right after, 200 μ L of 20 μ g/g bodyweight BSA in PBS was injected i.v. and mice were sacrificed after 2h. Up to 4 mL of intraperitoneal lavage was harvested, centrifuged, washed and stained with F4/80-FITC, CD115-PE, Ly6C-PerCP/Cy5.5, CD45-PE/Cy7, CD11c-APC, CD11b-A700, Ly6G-BV421, CD3-BV510, CD19-BV510, NK1.1-BV510 (1 μ L each) and ZombieAqua (1:1000) in total volume of 50 μ L and acquired via FACS.

2.2.2 Immune Complexes

2.2.2.1 Generation of immune complexes for binding assays (section 3.1, figures 2,3,4)

2 μ L of antigen (1 mg/mL BSA-11NP-FITC) were added to 5 μ L of 1 mg/mL of α NP IgG (either mIgG1, mIgG2a, mIgG2b, mIgG2c, mIgG3, hIgG1, hIgG2, hIgG3, hIgG4 or rabbit IgG) and incubated at 37°C for 15 min.

2.2.2.2 Generation of immune complexes for transmigration assay and haptokinesis

For transmigration experiments, 1 μ L of antigen (1 mg/mL BSA-6FITC) was added to 6,4 μ L of 1 mg/mL α FITC rabbit IgG (BioRad) and incubated for 15min at 37°C. For serial dilutions, IC were then diluted with PBS accordingly. Standard dilution used for experiments (Figure 21 A, Figure 22, Figure 23 A, B) was 0,5 μ g ag/mL and was obtained by adding 1993 μ L of transmigration medium (see section 2.1.3) to preformed IC.

To observe haptokinesis on IC-coated surfaces (Figure 17 A, B, C, Figure 19), also IC generated from 1 μ L of antigen (1 mg/mL BSA-6FITC) added to 6.4 μ L of 1 mg/mL α FITC rabbit IgG (BioRad) were used. IC were incubated at 37°C for 15min. IC antigen was diluted 1:120 with

PBS before coating, meaning that 113 μL of PBS were added to IC after 15 min incubation at 37°C. This corresponds to a final antigen concentration of $C_{\text{antigen, final}} = 8.3 \mu\text{g/mL}$ and final antibody concentration of $C_{\text{antibody, final}} = 53.3 \mu\text{g/mL}$

2.2.2.3 Generation of immune complexes for mass photometry

See Table 2, section 2.2.4.1.

2.2.3 Cell Isolation and Preparation

2.2.3.1 Isolation of peripheral blood mononuclear cells from human buffy coats

Buffy coats of healthy donors were obtained from Blutbank/ Blutspendezentrale of Städtisches Klinikum Karlsruhe and processed to isolate PBMCs on the day of collection. Upon receipt, buffy coats were stored at room temperature and processed within 4 hours to ensure cell viability. PBMC isolation was performed using density gradient centrifugation with PBMC Spin medium, by carefully layering 35 mL of buffy coat over 15 mL of PBMC Spin medium in 50 mL Falcon tubes and centrifuging for 25min, at 3000 rpm (1851xg) without brakes to allow the formation of distinct layers. From now on, cold medium was used throughout the process, to maintain cell viability. After centrifugation, the PBMC layer - a distinct white interface between plasma and PBMC Spin layer - was carefully aspirated using a sterile 10 mL pipette and transferred to a new 50 mL tube. PBMCs were then washed twice with PBS/EDTA, by centrifugation at 1200 rpm (321xg), 4°C for 8 minutes. The cell pellet was resuspended in 20 mL of cold X-VivoTM-15 and stored on ice overnight. PBMCs were counted and viability assessed with a hemocytometer using trypan blue exclusion.

2.2.3.2 Isolation of SlanMo from PBMCs

Isolation of slanMo was performed as previously described¹⁰⁵. Briefly, after PBMC isolation, cells were washed once using cold PBS/EDTA and resuspended in 1 mL cold MACS buffer and 10 μL of M-DC8 α slan mouse IgM hybridoma supernatant per 1×10^8 PBMCs. After incubation at 4°C for 15 min, cells were washed and resuspended in 400 μL cold MACS buffer and 20 μL of Anti-Mouse IgM MicroBeads (Miltenyi Biotec) per 1×10^8 PBMCs and incubated for 15 min at 4°C. After washing, cells were resuspended in 400 μL of MACS buffer per 1×10^8 PBMCs and magnetically labelled SlanMo were positively selected over AutoMACS columns using AutoMACS Pro Separator (Miltenyi). Purity, yield and cell viability of isolated SlanMo were assessed right after isolation using FACS (Gallios 4L, Beckmann Coulter). Purified SlanMo were collected by AutoMACS Pro Separator in 500 μL of MACS buffer, of which 9 μL were transferred into a V-bottom 96 well plate for staining. Staining solution was prepared by adding 1 μL of CD16-PE, 1 μL of CD3-APC, 0,5 μL of IgM-FITC and 1 μL of 1:20 dilution of Fixable Viability Dye eFluorTM 780 to 1,5 μL of FACS buffer. 1 μL of staining solution was added to 9 μL of isolated SlanMo and incubated at 4°C for 15 min. After washing, cells were resuspended in 200 μL of FACS buffer and acquired for purity-, yield- and viability analysis using FACS.

2.2.3.3 Isolation of classical monocytes, NK cells and neutrophils from buffy coats

Classical Monocytes:

50x10⁶ PBMCs, purified from buffy coats were used for CD14⁺ monocyte isolation. PBMCs were washed and cell pellet was resuspended in 400 µL MACS. 100 µL of CD14 MicroBeads were added to cell suspension, mixed well and incubated in fridge for 15 min. Cells were washed by adding MACS buffer up to 15 mL total volume and discarding the supernatant after centrifuging at 1200 rpm (321xg) for 8min at 4°C. Cell pellet was then resuspended in 500 µL MACS buffer and CD14⁺ cells were positively selected using the AutoMACS Pro Separator. Cells were counted using a hemocytometer and trypan blue. 9 µL of purified cells were stained with 1 µL of CD14-APC, 1 µL CD3-PerCP and 1 µL of 1:20 dilution of Fixable Viability Dye eFluor™ 780 to determine cell viability, and cell purity via FACS.

NK cells:

100x10⁶ PBMCs, purified from buffy coats were used for NK cell isolation. PBMCs were washed and cell pellet was resuspended in 400 µL MACS. 100 µL of NK Cell Biotin-Antibody Cocktail were added to cell suspension, mixed well and incubated in fridge for 5 min. 300 µL of MACS buffer and 200 µL of NK Cell MicroBead Cocktail was added. Cell suspension was mixed well and incubated for 10min at 4°C. Cells were negatively selected using the AutoMACS Pro Separator. Cells were counted using a hemocytometer and trypan blue. 9 µL of purified cells were stained with 1 µL of CD56-PE, 1 µL CD3-PerCP and 1 µL of 1:20 dilution of Fixable Viability Dye eFluor™ 780 to determine cell viability, and cell purity via FACS.

Neutrophils:

After density gradient centrifugation of buffy coats during PBMC isolation, 5 mL of bottom fraction containing erythrocytes and granulocytes was transferred into new 50 mL conical tube and stored on ice overnight. Erythrocyte lysis was performed by mixing well with 45 mL of ammonium chloride-potassium (ACK) buffer. Lysis was performed for 8 min at RT and then cell suspension was centrifuged at 1200 rpm (321xg) for 8 min at RT. Lysis step was repeated 2 or 3 times until no more red erythrocytes were visible. Cell pellet was resuspended in 1 mL of MACS buffer and counted using a hemocytometer and trypan blue. 9 µL of cell suspension was stained with 1 µL of CD16-PE, 1 µL CD3-APC and 1 µL of 1:20 dilution of Fixable Viability Dye eFluor™ 780 to determine cell viability, and cell purity via FACS.

2.2.3.4 Isolation of leukocytes from peripheral blood

Depending on the experiment 9 to 36 mL of blood were drawn from volunteers into 9 mL EDTA monovettes. Blood was transferred into 50 mL conical tubes and filled up to 50 mL with ACK buffer (RT). Erythrocyte lysis was performed for 8 min at RT and cell suspension was centrifuged at 1200 rpm (321xg) for 8 min, 21°C. Lysis was repeated 1 or 2 times until no red erythrocytes were visible. Cells were resuspended in 1 mL FACS buffer and counted using a hemocytometer and trypan blue for further use.

2.2.4 Molecular and Cellular Assays

2.2.4.1 Mass photometry

Mass photometry measurements of IC samples, antigen and antibody controls were performed using a TwoMP mass photometer (Refeyn) at EMBL, Heidelberg. Since IC had to be highly diluted for measurement, IC were fixated before dilution to avoid dissociation of antigen and antibodies. For fixation the PierceTM DSS, No-WeighTM Format kit was used according to the product's instructions. The following table shows the composition and fixation of the measured samples.

Table 2. Volumes and concentrations of immune complex reagents investigated via mass photometry.

name Sample	V antigen	V antibody	cStock antigen	cStock antibody	Vadded Buffer	Vadded DSS (4.2mM)	Vadded Quenching	cfinal DSS [μM]	cfinal Protein [μM]
BSA-11NP-FITC	4 μL		1mg/mL		24μL	2	0.75μL	273	1.9
antiBSA hIgG1		10 μL		1mg/mL	18μL	2	0.75μL	273	2.15
BSA NP IC	4 μL	10 μL	1mg/mL	1mg/mL	14μL	2	0.75μL	273	4.05
BSA-6-FITC	2μL		1mg/mL		28μL	2	0.8μL	256	0.88
antiFITC BioRad		13μL		1mg/mL	17μL	2	0,8μL	256	2.6
IC BSA6FITC + antiFITC	2μL	13μL	1mg/mL	1mg/mL	15μL	2	0,8μL	256	3.48

Measurements were taken at a final concentration of 20 nM in PBS. Data analysis was performed using the DiscoverMP software (v.2.5.0; Refeyn). Measurements and analysis were kindly performed by Dr. Karine Lapouge, Scientific Officer – Biophysical Characterisation.

2.2.4.2 IC binding to human leukocytes from peripheral blood

Leukocytes were prepared as described in section 2.2.3.4 and IC according to section 2.2.2.1. 3x9 mL blood was drawn into EDTA monovettes from 3 different donors. After erythrocyte lysis using ACK buffer, cells were washed and resuspended in FACS buffer to obtain 50x10⁶ cells/mL. 200 μL (10x10⁶ cells) were transferred into wells of a 96-well V-bottom plate and washed. Cells were first stained for 15 min at 4°C in 200 μL staining volume, including 50 μL of BD Horizon Brilliant Stain Buffer (BD Biosciences), CD1c-BV605, CD3-PerCP, CD11c-BV510, CD14-APC, CD16-A700, CD20-SparkUV387, CD123-BV421, CD141-PE/Cy7, HLA-DR-Pacific Blue, Siglec-8-BUV395, αslan hybridoma SN (concentrations are listed under 2.1.2) and FACS buffer. After washing, cells were incubated with goat F(ab')₂ αmouse IgM-PE (Southern Biotech) for 15 min at 4°C as secondary staining for slan labelling. After washing, cells were incubated with preformed ICs for 15 min at 4°C, washed once and acquired at the CytexTM Aurora immediately after. At least 5x10⁶ events were acquired per sample.

For experiments including FcγR-blocking, cells were incubated with in 100 μL of 10 μg/mL of respective FcγR blocking antibodies (FcγRI:10.1, FcγRII:AT10, FcγRIII: 3G8) after secondary antibody staining and prior to incubation with ICs.

2.2.4.3 Flow Cytometry

Single cell suspensions were stained at 1×10^6 cells/mL and in 50 μ L – 100 μ L staining volume, if applicable. Staining was performed in 96-well V-bottom plates and incubation occurred at 4°C in a fridge. In between washing and staining steps, plate was kept on ice. Experiments from Figure 7, Figure 10, Figure 11, Figure 12, and Figure 15 were performed on Gallios 4L (Beckmann Coulter) and experiments from Figure 8, Figure 9 were performed on the Cytex Aurora (Cytex).

2.2.4.4 Transmigration assay

To assess transmigration activity, the ChemoTx® Disposable Chemotaxis System (Neuro Probe) with 3 μ m pore size was used. Cells and chemoattractant were suspended in transmigration medium (see section 2.1.3). For all cell types, 29 μ L of chemoattractant or medium control was placed in the receiver well before firmly attaching framed filter on the well plate. Afterwards, 25 μ L of 2×10^6 cells/mL were carefully added on corresponding site on membrane and lid was carefully placed on top. Cells were incubated in humidified incubator at 37°C, 5% CO₂ for 2h. Standard concentrations used in this assay were: for ICs 0,5 μ g Ag/mL, for fractalkine 10 ng/mL, for C5a 10 ng/mL.

To alter the direction and the magnitude of the chemoattractant gradient (see Figure 22) ICs or C5a were either added in the bottom receiver well, directly added to the cell suspension before seeding the 25 μ L cell droplet, or added to both. Concentrations were ensured to remain the exact same by resuspending the cells directly in the medium containing either ICs or C5a, if needed.

Number of transmigrated cells was determined using CellTiter-Glo® Luminescent Cell Viability Assay (Promega). 29 μ L from receiver wells were transferred in black bottom 96 well OptiPlate (PerkinElmer) and mixed well with 30 μ L of CellTiter-Glo® solution (at RT). 96 well plate was incubated in BetaCounter for 10 minutes before measuring bioluminescence using MicroBeta Trilux 1450 LSC & Luminescence Counter. To determine the frequency of transmigrated cells from bioluminescence data, 29 μ L of serial dilutions of initial 2×10^6 cells/mL cell suspension was also mixed with 30 μ L of CellTiter-Glo® and used to generate a standard curve.

2.2.4.5 UV-based micro photopatterning of immobilized IC gradients

To generate immobilized IC patterns including immobilized IC gradients, the UV-based PRIMO contactless photopatterning system by Alvéole was used. Glass coverslips were cleaned and surface activated by oxygen plasma treatment (0.4 mbar, 200 W) in a plasma cleaner (TePla, #100-E) for 2 minutes. Then, coverslips were treated with 0.01% of poly-L-lysine solution (Sigma Aldrich, #P4832) for 30 minutes. Afterward, coverslips were rinsed and incubated with 5 mg of mPEG-SVA (Laysan Bio, #MPEG-SVA-5000) in 0.1 ml of 10 mM HEPES pH 8.5 for 1 hour. Coverslips were then gently rinsed, dried under a stream of nitrogen, and incubated after layering with 3 μ L of PLPP gel (Alveole) diluted in 60 μ L of pure ethanol for 5 minutes. Then, coverslips were patterned with UV-A illumination ($\lambda = 375$ nm, 30 mJ/mm²) using a widefield microscope (Nikon, Nikon Eclipse Ti2E) equipped with a patterning module (Alveole, Primo)

and dedicated software (Alveole, Leonardo). Surface patterns were drawn using the graphic software Inkscape. Finally, patterned coverslips were rinsed and incubated with IC (see section 2.2.2.2) for 1h at RT and washed once with PBS before seeding 0.5×10^6 SlanMo/mL on the coverslip. SlanMo were imaged for at least 4h in incubator at 37°C, 5% CO₂ using an Axio Observer Z1 inverted microscope.

All experiments were kindly guided and supported by Dr. Victoria Levario-Diaz, I Chen and Prof. Dr. Elisabetta Ada Cavalcanti-Adam.

2.2.4.6 Haptokinesis on immobilized IC or monomeric IgG

Channels of Ibidi μ -slide VI 0.4 were coated with either IC (section 2.2.2.2) (for Figure 17 A,B,C) or 10 μ g/mL monomeric human IgG1, IgG2, IgG3 or IgG4 in PBS (for Figure 17 D,E). Slides were incubated over night at 4°C, or at RT for 1h for coating. 50 μ L of 1×10^6 cell/mL were carefully loaded on each channel using a yellow pipette tip after rinsing channel with 100 μ L of PBS at least 2 times. Cells were allowed to attach for 5min in humidified incubator at 37°C, 5%CO₂ before loading the slides into incubation chamber of EVOS™ M7000 Imaging System. Cells were kept at 37°C, 5%CO₂, and imaged for 1h by taking 1 image every minute. Cell migration was analysed by manual tracking using Celleste 5 Cell Analysis software.

2.2.4.7 Phagocytosis of immobilized IC during migration

α FITC rabbit IgG (BioRad) was labeled with pHrodo dye pHrodo™ antibody labeling kit (Thermo Fisher Scientific) according to the product instruction manual. IC were then generated with labeled antibodies according to section 2.2.2.2 and Ibidi slides were coated and cells imaged according to previous section 2.2.4.6. Images were taken using the PE filter of the EVOS™ M7000 Imaging System.

2.2.4.8 Migration on immobilized, fluorescent ICs adjacent to antigen coated surface

To generate the fluorescent IC coating adjacent to immobilized antigen (Figure 18 A), first a rectangle of approximately 30 mm x 30 mm was drawn on a microscope slide using a hydrophobic barrier pen and coated with 200 μ L of 10 μ g/mL BSA-6FITC for 1h at RT. Area was washed with PBS and a sterile 4-well silicone micro insert (Ibidi) was placed on the coated surface. Each well of the insert was filled with 10 μ L of 50 μ g/mL of PE labeled α FITC rabbit IgG antibody that was labeled using the PE Lightning-Link® conjugation kit according to the product manual and incubated for 1h at RT. Antibody was aspirated from wells and wells were washed 2x with 10 μ L PBS. Placement of wells was marked on bottom of glass slide using black marker before removing the silicone insert to find the IC coating under the microscope. 200 μ L of 0.5×10^6 SlanMo/mL were seeded onto coated area and allowed to adhere for 5min in humidified incubator at 37°C, 5%CO₂, before imaging in incubator of EVOS™ M7000 Imaging System.

2.2.5 Sequencing and Transcriptomic Analysis

2.2.5.1 Bioinformatics

Raw list of differentially gene expression was obtained by Schäkel group. Previously, Hao Zhang had performed SlanMo isolation, classical monocyte isolation and incubated each cell type on either HAS-1.5FITC: α FITC rabbit IgG (OriGene) ICs or on untreated plastic for 4h, 37°C, 5%CO₂. Illumina sequencing was performed in correspondence with DKFZ - Genomics and Proteomics Core Facility. Chip 200739030020 and chip 200739030033 were used for raw expression values.

Raw lists of gene expression values were analyzed by the Bioinformatics Team of the Next Generation Sequencing Core Facility of UMM Mannheim. Differentially expressed genes were calculated by using limma1 package. Genes with an adjusted p-value < 0.05 were considered as significant and genes with logFC > |1| were considered dysregulated. Geneset2 package was used to perform Gene Set Enrichment Analysis (GSEA) and to determine whether defined lists (or sets) of genes exhibit a statistically significant bias in their distribution within a ranked gene list. Pathways belonging to various cell functions such as cell cycle or apoptosis were obtained from public external databases (KEGG, <http://www.genome.jp/kegg>; GO, <http://geneontology.org/> and Reactome, <https://reactome.org/>).

All statistical procedures and plots were conducted with the R programming language running under the open-source computer software R v4.4.03.

3. Results

3.1 Characterization of ICs and their Binding to Leukocyte Subsets

To characterize the ICs used in this study, mass photometry was performed to determine their size and abundance, while FACS was employed to analyse their binding affinities to murine and human leukocyte subsets in a whole-cell-based approach. Mass photometry measures molecular mass and quantifies particle concentration by measuring light scattering properties of particles as they adsorb onto a glass surface. ICs were generated by mixing antigen and correspondent antibody solution in the wanted stoichiometric manner. In a pilot experiment, antigen-antibody aggregates could not be detected via mass photometry. It was concluded that the low concentrations ($< 20\text{nM}$) needed for detection via mass photometry resulted in the dissociation of ICs. To prevent dissociation, ICs were fixated using amine-reactive crosslinkers, which covalently linked antigen to antibody. This fixation occurred only if the antigen and antibody were already bound, as the crosslinker was only 8 Å and required close proximity of primary amine groups of both ligands for fixation. Now, aggregates could be detected even though the fraction of antigen-antibody complexes was surprisingly low compared to the antigen- and antibody monomers contained in the sample (Figure 6). In this sample, BSA-6FITC was used as antigen and α FITC rabbit IgG as antibody to generate ICs (Figure 6 A, green sample). 80% of all measured particles were either monomeric BSA-6FITC antigen (62 kDa, 54%) or monomeric α FITC rabbit IgG antibody (145 kDa, 26%). Notably, the antigen solution (yellow sample) shows 9% dimers and the antibody solution partial degradation since heavy- or light chain fragments (65 kDa, blue peak) are detected. 7% of all measured particles in the IC solution had a molecular weight around 217 kDa and accounted for 1:1 ag:ab complexes. Less than 1% of the measured particles of the IC sample represented 2:1 ag:ab complexes (286 kDa). Only the remaining measured particles with a molecular weight of > 286 kDa are larger aggregates containing two or more antibodies and are capable of activating cells via Fc γ R-crosslinking. The 360 kDa peak refers to 1:2 ag:ab complexes, which are the smallest ICs capable of Fc γ R-crosslinking. It is important to mention, that most likely too little of the crosslinking reagents were used and could not crosslink all ICs. Therefore, the fractions of differently sized aggregates probably does not reflect the real composition of ICs. Nevertheless, IC-dependent effects could be observed when these ICs were used for migration experiments on immobilized ICs and for transmigration experiments towards soluble ICs (see section 3.3).

Another set of ICs was used to investigate binding affinities between ICs and murine or human peripheral blood leukocytes. These ICs contained recombinant human, murine, or rabbit IgG, all of which shared the same antigen-binding Fab region but varied in their Fc domains. As an example, the BSA-11NP-FITC: α NP human IgG1 IC was chemically fixated and characterized using mass photometry (Figure 6 B). This IC is representative of the set, as the consistent Fab region ensures similar antigen-binding properties and a comparable IC size across subclasses and species¹⁰⁶. The antigen solution of this sample showed 5% dimers (Figure 6 B, 129 kDa, yellow peak) and the antibody solution 7% (300 kDa, blue peak). No degradation to heavy- or

light chain fragments was observed in the antibody solution. The IC sample contained 34% monomeric antigen (68 kDa, green peak) and 37% monomeric antibody (149 kDa, green peak). 5% and 1% of all measured particles in the IC solution were 1:2 ag:ab complexes (363 kDa) or 1:3 ag:ab complexes (522 kDa), respectively.

To further study and characterize IC-cell interactions, I generated ICs suitable for comparing IgG isotype-dependent binding of different cells by employing the same system of fixed Fab- but varying Fc domains. In this setup, the antigen was a fluorescently labelled, hapten-conjugated BSA (BSA-11NP-FITC) while the antibodies were engineered to have a constant, hapten-specific Fab domain but either human IgG1, IgG2, IgG3, IgG4, murine IgG1, IgG2a, IgG2b, IgG2c, IgG3 or rabbit IgG as their Fc region. With this approach, I ensured that the generated ICs only differed in their Fc regions but not in the ag:ab ratio or size, allowing to compare IgG isotype-dependent IC binding to various cells (Figure 7).

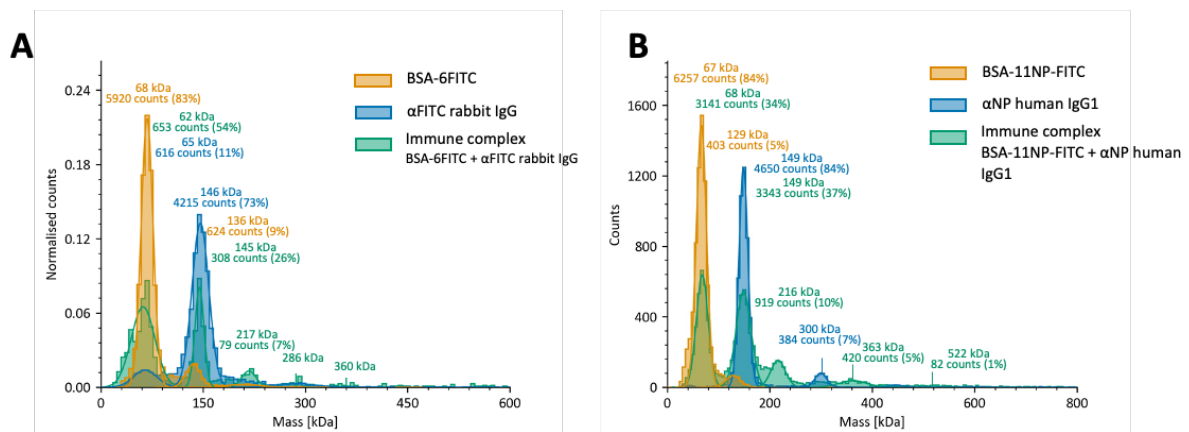


Figure 6. Mass photometry of antibodies, antigens and immune complexes. **A** Histogram showing distribution of monomers, multimers and aggregates in BSA-6FITC antigen (yellow), αFITC rabbit IgG antibody (blue) and immune complex (green) solution. **B** Histogram showing distribution of monomers, multimers and aggregates in BSA-11NP-FITC antigen (yellow), αNP human IgG1 antibody (blue) and immune complex (green) solution.

To investigate Fc-dependent binding capabilities of the generated ICs, I first examined their binding to mouse peripheral blood leukocytes using FACS. According to Kerntke *et al.*⁸¹ mouse NCMs, classical monocytes and neutrophils express the highest levels of FcγRs and were therefore the focus of this analysis. Neutrophils were defined as CD45⁺dump⁻CD11b⁺Ly6G⁺ cells, classical monocytes as CD45⁺dump⁻CD11b⁺CD115⁺Ly6C⁺ and NCMs as CD45⁺dump⁻CD11b⁺CD115⁺Ly6C^{low} (Figure 7 A, thick boxes). Surprisingly, neutrophils and classical monocytes showed only weak binding of ICs (Figure 7 B). Neutrophils, bound human IgG3 (hIgG3) and murine IgG2b (mIgG2b) weakly, while classical monocytes additionally showed weak binding of hIgG1- and mIgG1 ICs. In contrast, NCMs demonstrated strong IC binding, with the highest affinity for hIgG3, followed by hIgG1 and mIgG2b. Weak binding to mIgG1 and mIgG2c ICs was also observed in NCMs.

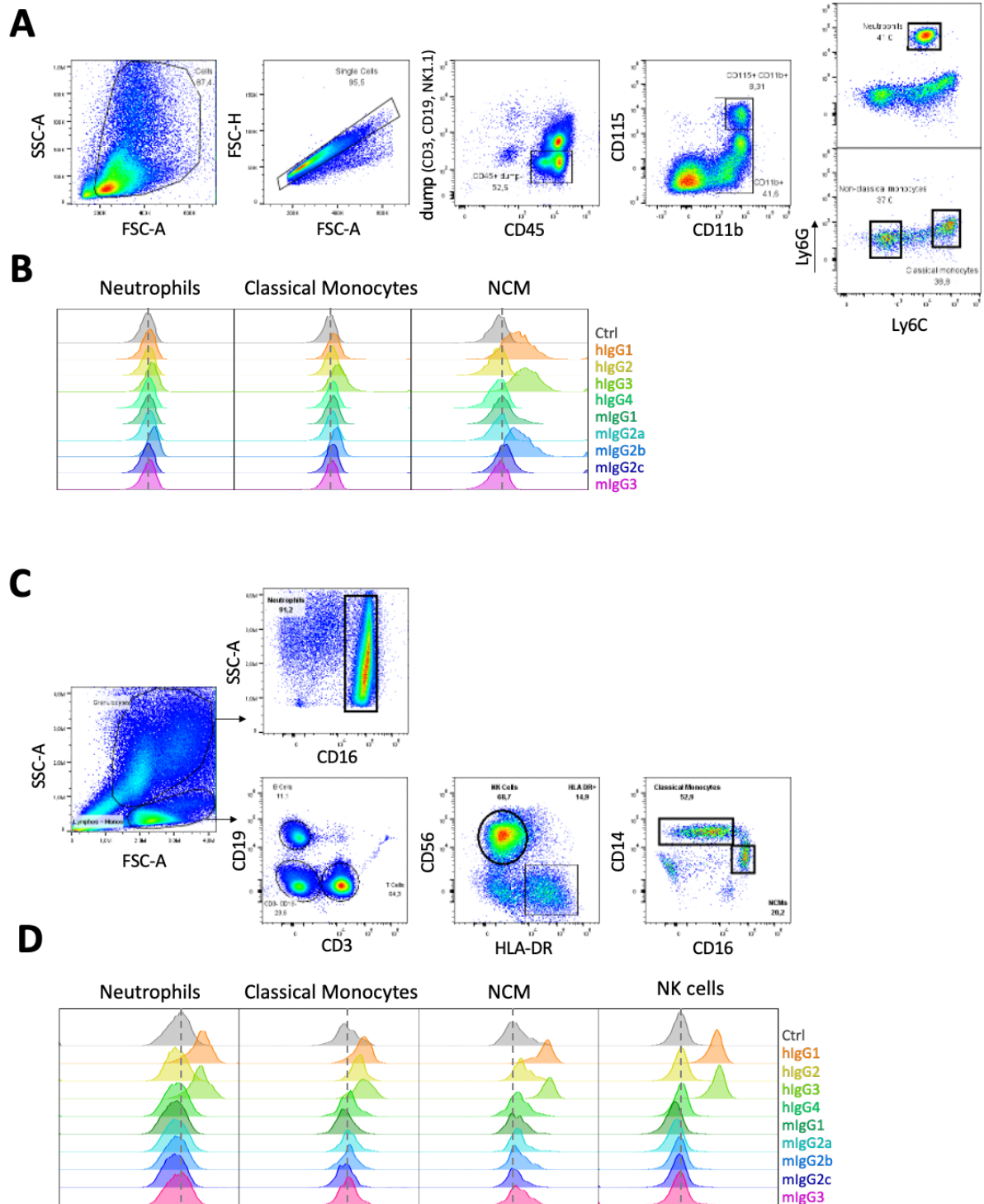


Figure 7. Binding affinity of murine- and human IgG immune complexes to mouse and human peripheral blood leukocytes. 1×10^5 leukocytes from mouse peripheral whole blood or 1×10^6 human leukocytes were stained with FACS antibody cocktail and incubated with fluorescently labelled ICs or antigen (Ctrl). **A** Gating strategy to identify mouse neutrophils, classical monocytes and NCMs (thick boxes). **B, D** Overlay of histograms showing binding affinity of different ICs to respective cell population. Dotted grey line indicates background signal due to unspecific binding of fluorescently labelled antigen. **C** Gating strategy to identify human neutrophils, classical monocytes, NCMs and NK cells.

Next, I analysed IC binding to human peripheral blood leukocytes, including NK cells due to their high FcγRIII expression as reported by Kerntke *et al.*⁸¹. The gating strategy for identifying neutrophils, NK cells, classical monocytes and NCMs was based on forward and sideward scatter properties, as well as expression of the lineage-specific markers CD16, CD56, HLA-DR

and CD14 (Figure 7 C). In contrast to the previous findings in mouse leukocytes, human neutrophils and classical monocytes exhibited strong binding to ICs containing hIgG1 and hIgG3 (Figure 7 D). Interestingly, classical monocytes showed an additional moderate binding of hIgG2 ICs. NK cells and NCMs displayed strong binding of ICs containing hIgG1 and hIgG3 ICs.

Given the interesting findings of these experiments, I increased the scope to not only investigate IC-binding to specific cell types but instead to all FcγR-expressing cells of human peripheral whole blood, including T cells as FcγR⁻ control. Therefore, I established a 15 colour FACS panel to distinguish all FcγR-expressing cells (Figure 8 B), namely basophils, B cells, classical monocytes, intermediate monocytes, NCMs, eosinophils, myeloid dendritic cells 1 (mDC1), myeloid dendritic cells 2 (mDC2), plasmacytoid dendritic cells (pDC), neutrophils, T cells and NK cells, including the NK cell subset CD56^{bright}CD16^{dim} and NKT-like cells. Furthermore, the carbohydrate slan was included as a marker to identify prototypical NCMs⁵².

To include mDC1, a rare DC subtype that only occurs with a frequency of 0.05% among PBMCs¹⁰⁷, I acquired 10x10⁶ cells per sample. mDCs were then further subdivided into mDC1 and mDC2, as these subpopulations express different FcγRs¹⁰⁸ and should not be combined to mDCs when investigating FcγR-mediated binding. T cells were included in the analysis to serve as negative control since they lack FcγR expression and do not bind ICs. Using whole blood instead of isolated cell populations in this experimental setup, native leukocyte frequencies remained intact and therefore allowed for competition for IC binding between cells, mimicking physiological conditions.

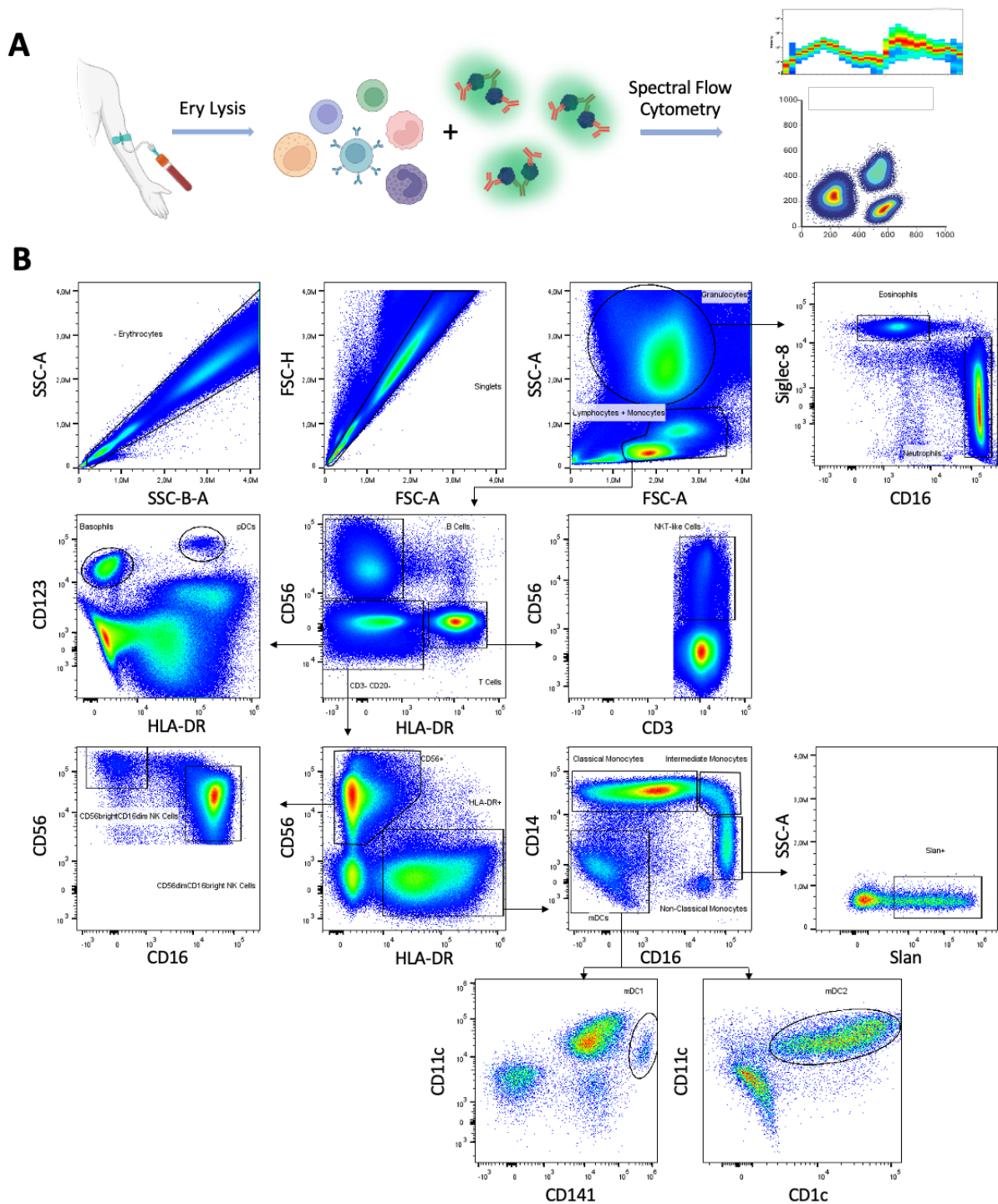


Figure 8. IC binding to peripheral blood leukocytes. **A** Schematic illustration of experimental setup. Fluorescently labelled IC were incubated with leukocytes obtained from whole blood after erythrocyte lysis. IC bound to different cell types was analysed via spectral flow cytometry. **B** Gating strategy to identify all FcγR-expressing leukocytes from peripheral whole blood. 10×10^6 leukocytes were stained with FACS antibody cocktail and incubated with fluorescently labelled IC after. Indicated cell populations were analysed for fluorescence intensity of bound BSA-11NP-FITC:αNP IgG1 IC.

IgG1 is the most abundant of the four human IgG subclasses and accounts for more than 60% of total IgG in human plasma. Consequently, BSA-11NP-FITC:αNP IgG1 immune complexes were used to further examine IC-binding of leukocytes from whole blood by staining the sample cells with FACS antibodies prior to incubation with the fluorescently labelled ICs. To analyse the 10×10^6 cells acquired, their phenotypes, subset frequencies, and IC-binding

intensities, I used a t-distributed stochastic neighbour embedding (t-SNE) visualization after FACS analysis. This dimensionality reduction technique maps the acquired cells in a 2D space, placing similar cells close to each other, whereas dissimilar cells are positioned further apart. This results in cell clusters, which can then be defined by their correspondent marker expression (Figure 9 A).

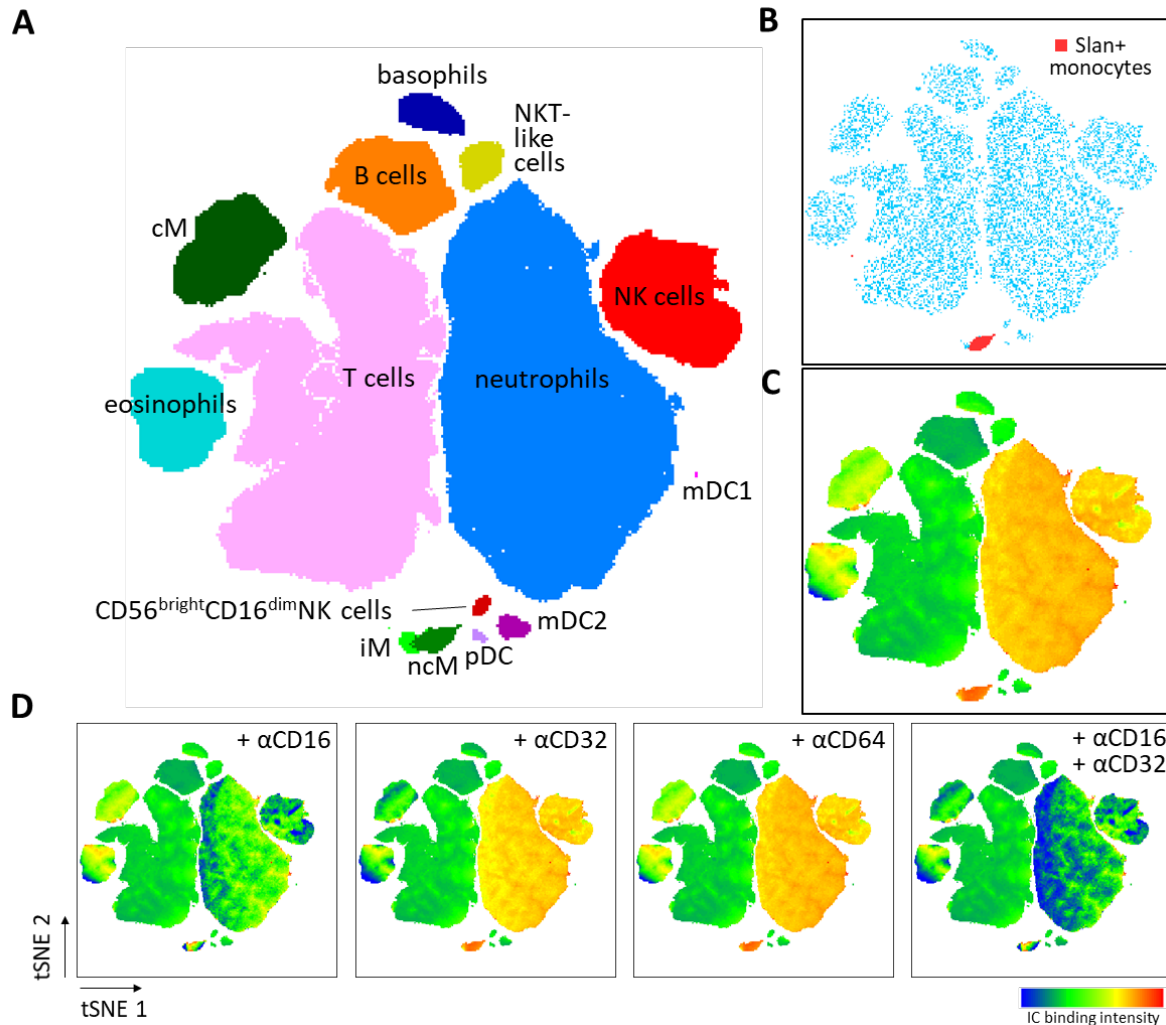


Figure 9: t-SNE visualization of all FcγR-expressing leukocytes from peripheral whole blood and their IC binding capacity. A tSNE plot of 10x106 leukocytes from whole blood after QC gating, identifying cell population clusters. cM = classical monocytes, iM = intermediate monocytes. **B** Identification of slan+ cells within NCM cluster using M-DC8 αslan antibody. **C** Heat map of t-SNE visualization. Color code represents binding intensity of BSA-11NP-FITC:αNP human IgG1 ICs. **D** Heat map of t-SNE visualization showing different IC binding intensities of cell clusters after treatment with different αFcγR blocking antibodies.

The size of the cell clusters represents their relative abundance within the cells acquired. Therefore, neutrophils and T cells are the most frequent cells in the blood of the shown donor, followed by NK cells, B cells, classical monocytes and eosinophils which verifies the correct location of the measured events in this tSNE visualization. The heatmap (Figure 9 C) indicates the individual cells' and cell clusters' binding intensity of the fluorescently labelled ICs. It shows the difference of the mean fluorescence intensity (ΔMFI) of a sample incubated with ICs and a sample incubated with only the fluorescently labelled antigen. Therefore, the IC-specific binding is displayed, and unspecific binding of the antigen is subtracted. Classical

monocytes e.g. showed a high unspecific binding of BSA-11NP-FITC antigen but no increase in signal when incubated with ICs (data not shown). Interestingly, only neutrophils, NK cells and the NCM + intermediate monocyte cluster showed a strong affinity for the ICs used in this experiment. The other cell clusters show neglectable IC binding and showed a similar IC binding intensity to FcγR⁻ T cells. Since defining NCMs and intermediate monocytes is greatly dependent on manual gating during FACS analysis, slan was included as a marker for non-classical monocytes (Figure 9 B). Slan expression colocalized with strong IC binding in the NCM cluster. This finding is relevant since for following experiments investigating interactions between ICs and human NCMs, slan was used as a single marker to isolate the NCMs.

Interestingly, the cell types binding ICs all express FcγRIII (CD16), suggesting a pivotal role of this receptor in IC-binding. To analyse which FcγRs are involved in capturing and binding ICs on the cell surface, cells were incubated with blocking antibodies against FcγRI(CD64), FcγRII(CD32) and FcγRIII (CD16) before incubating with ICs (Figure 9 D). When adding a single blocking antibody, αCD16 showed the greatest reduction of IC binding to neutrophils, NK cells, NCMs and intermediate monocytes, confirming that FcγRIII is the main receptor responsible for IC binding. Blocking FcγRII with an αCD32 antibody, resulted in weak inhibition of IC binding in eosinophils, classical monocytes and neutrophils, whereas blocking FcγRI (CD64) did not show any effect. Consequently, blocking FcγRII and FcγRIII together showed the greatest reduction of IC binding.

3.2 The Role of Non-Classical Monocytes in IC-induced Inflammation in Mice

The previous findings that NCMs showed exceptionally strong binding of ICs, led me to investigate their biological relevance in IC-induced inflammation. Therefore, I chose the well-established IC-induced disease mouse model, the reverse passive arthus (RPA) reaction. This model allowed to further investigate and validate the importance of previous *in vitro* findings in an *in vivo* setting. During the RPA reaction, ICs form locally in the skin, causing inflammation including edema, haemorrhage and immune cell infiltration. This is achieved by injecting BSA as antigen intravenously (i.v.) right after a subcutaneous (s.c.) injection of polyclonal αBSA-rabbit IgG (Figure 13 A). Usage of polyclonal BSA-specific IgG induces inflammation via local formation of large IC lattice structures with low solubility, impeding the removal of these ICs. The IC depositions in the skin are then recognized by FcγR-expressing leukocytes that become activated and induce inflammation. To now decipher the role of NCMs in this model for IC-induced inflammation, the RPA reaction in Nr4a1^{se-/-} mice, which lack NCMs was compared to the reaction occurring in WT mice. To first validate the efficiency of the Nr4a1 super-enhancer subdomain knockout regarding loss of NCMs, cell composition of blood and spleen of Nr4a1^{se-/-} mice were compared to WT mice using FACS (Figure 10, Figure 11).

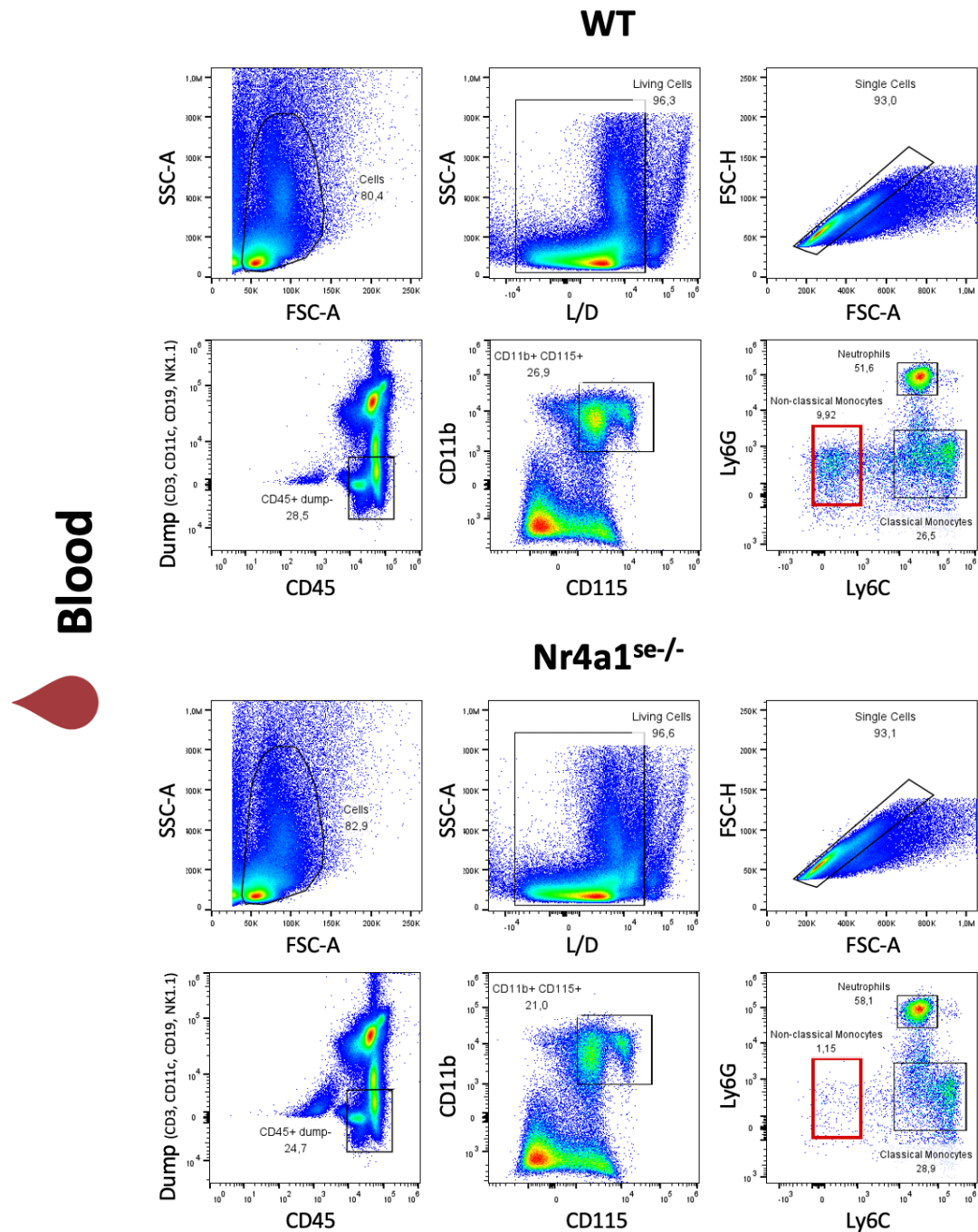


Figure 10. Nr4a1^{se/-} mice show loss of NCMs in peripheral blood. Frequency of NCMs was determined by the shown gating strategy. Non-classical monocytes were defined as living, single cell, CD45+dump-CD11b+CD115+Ly6G-Ly6C^{low} cells (red box). The upper panel shows WT peripheral blood and the bottom panel blood of Nr4a1^{se/-} mice.

FACS analysis of peripheral blood and spleen could confirm that deletion of Nr4a1 super-enhancer subdomain resulted in great reduction of NCMs but could not verify a complete loss of these cells. In peripheral blood, the frequency of NCMs was reduced by 88% from 9.92% to 1.15% (Figure 11, red boxes). A loss of non-classical monocytes could also be observed in the spleen of Nr4a1^{se/-} mice. The frequency of these cells went from 15.3% in WT mice to 3.12% in Nr4a1^{se/-} mice.

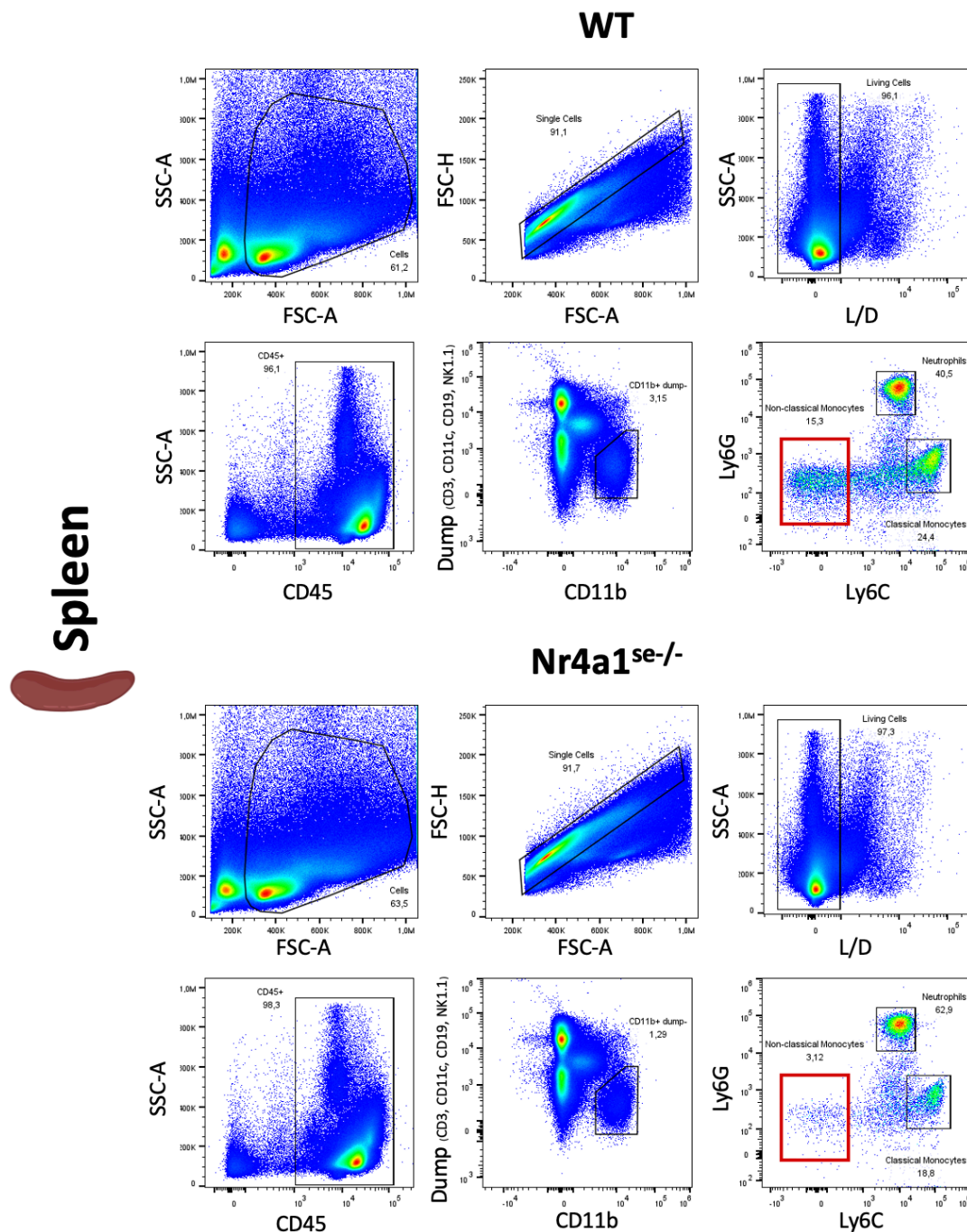


Figure 11. Nr4a1^{se-/-} mice show loss of non-classical monocytes in spleen. Frequency of non-classical monocytes was determined by the shown gating strategy. Non-classical monocytes were defined as living, single cell, CD45⁺CD115⁺Ly6G^{low} cells (red box). The upper panel shows WT splenocytes and the bottom panel splenocytes of Nr4a1^{se-/-} mice.

To further understand a potential involvement of NCMs in the RPA reaction, the expression levels of FcγRIV, the murine functional orthologue of human FcγRIII, were investigated and compared between neutrophils, classical monocytes and NCMs from peripheral blood and spleen (Figure 12). Splenic and peripheral blood cells showed a very similar expression pattern of FcγRIV. NCMs showed the highest FcγRIV expression, being over 10-fold higher than FcγRIV expression on classical monocytes and also surpassing expression on neutrophils. This indicates an important role of these cells in IC-mediated and FcγRIV-dependent inflammation.

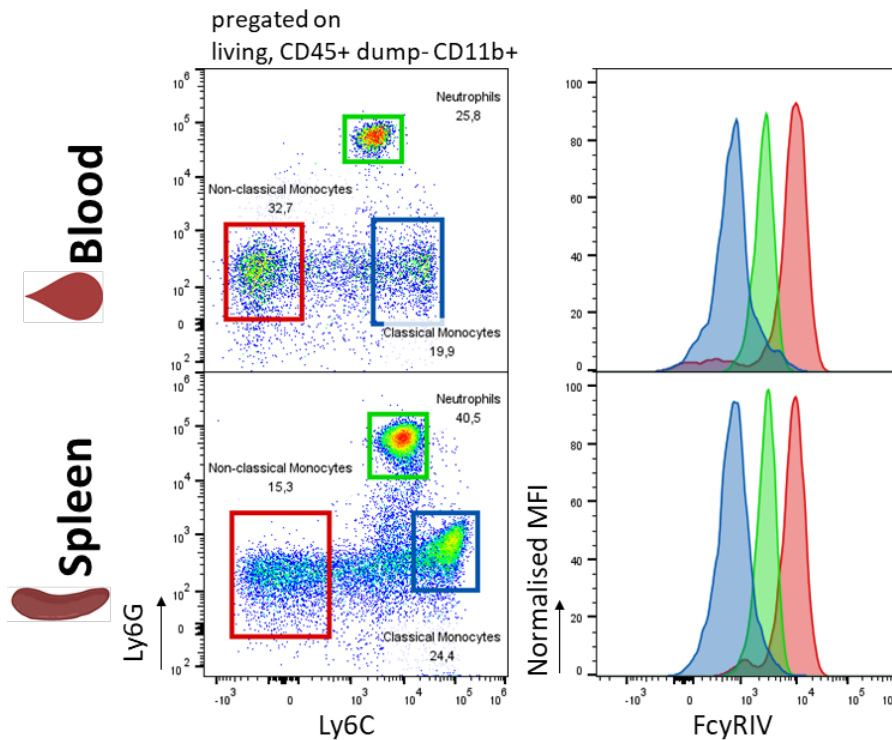


Figure 12. Comparison of FcγRIV expression on neutrophils, classical monocytes and non-classical monocytes in mouse peripheral blood and spleen. Cells were pregated on living, CD45+ dump-CD11b+ events. Colour of histogram peaks corresponds to colours of gates of cell populations.

Having confirmed a strong reduction of NMCs in $Nr4a1^{se/-}$ mice and a strong expression of FcγRIV on these cells, I now investigated the role of NCMs in IC-induced inflammation by comparing the severity of the RPA reaction between WT and $Nr4a1^{se/-}$. To quantify the severity of the reaction, 1% Evans Blue was added to the BSA antigen injected i.v.. Therefore, any haemorrhage and vascular damage could be quantified by extravasation of the dye into the skin (Figure 13 B, solid arrow). To account for any vessel damage occurring by the intradermal injections themselves, a background control was included within each animal. A polyclonal unspecific rabbit IgG was injected s.c. into the back skin (dotted arrow) next to the injection site of the antigen-specific α BSA rabbit IgG. This injection did not lead to IC formation and therefore no inflammation occurred at this injection site. The injection still resulted in minimal dye leakage into the skin (dotted arrow). The RPA reaction could now be confirmed visually, since a comparably large amount of Evans Blue dye leaked into the skin when antigen-specific α BSA rabbit IgG was injected and IC could form, compared to the background control (solid arrow vs. dotted arrow). When the RPA reaction was compared between 4 WT and 4 $Nr4a1^{se/-}$ mice, no difference in the amount of extravasated Evans Blue could be detected (Figure 13 B, D). Another parameter used to determine the severity of the IC-induced inflammation was edema. It was quantified by the weight of 8 mm skin biopsy punches from the injection sites. As expected, edema caused an increase in weight of the skin biopsy punches in WT animals when antigen-specific antibody was injected to form ICs (Figure 13 C) and the skin punch weight changed from $5.6 \text{ mg} \pm 2.3 \text{ mg}$ for isotype control to $33.9 \text{ mg} \pm 8.8 \text{ mg}$ for α BSA-antibody. A very similar increase in edema was measured in NCM-deficient $Nr4a1^{se/-}$ mice with an increase from $6.9 \text{ mg} \pm 2.7 \text{ mg}$ to $34.0 \text{ mg} \pm 8.4 \text{ mg}$. Also, the quantification of extravasated Evans Blue by formamide extraction from skin punch biopsies and subsequent photometric assessment could not reveal differences between WT and $Nr4a1^{se/-}$ animals (Figure 13 D). In WT animals the amount of extravasated Evans Blue was 225

ng \pm 144 ng at the site of isotype control injection and increased to 4377 ng \pm 1123 ng for α BSA injection. In $Nr4a1^{se/-}$ the RPA reaction led to 3494 ng \pm 641 ng, which did not significantly differ from the reaction in WT mice. Taken together, the comparison of the RPA reaction in WT- and $Nr4a1^{se/-}$ mice to investigate the role of NCMs in IC-induced inflammation resulted in no detectable differences. Therefore, NCMs do not appear to play a major role in the cutaneous RPA reaction.

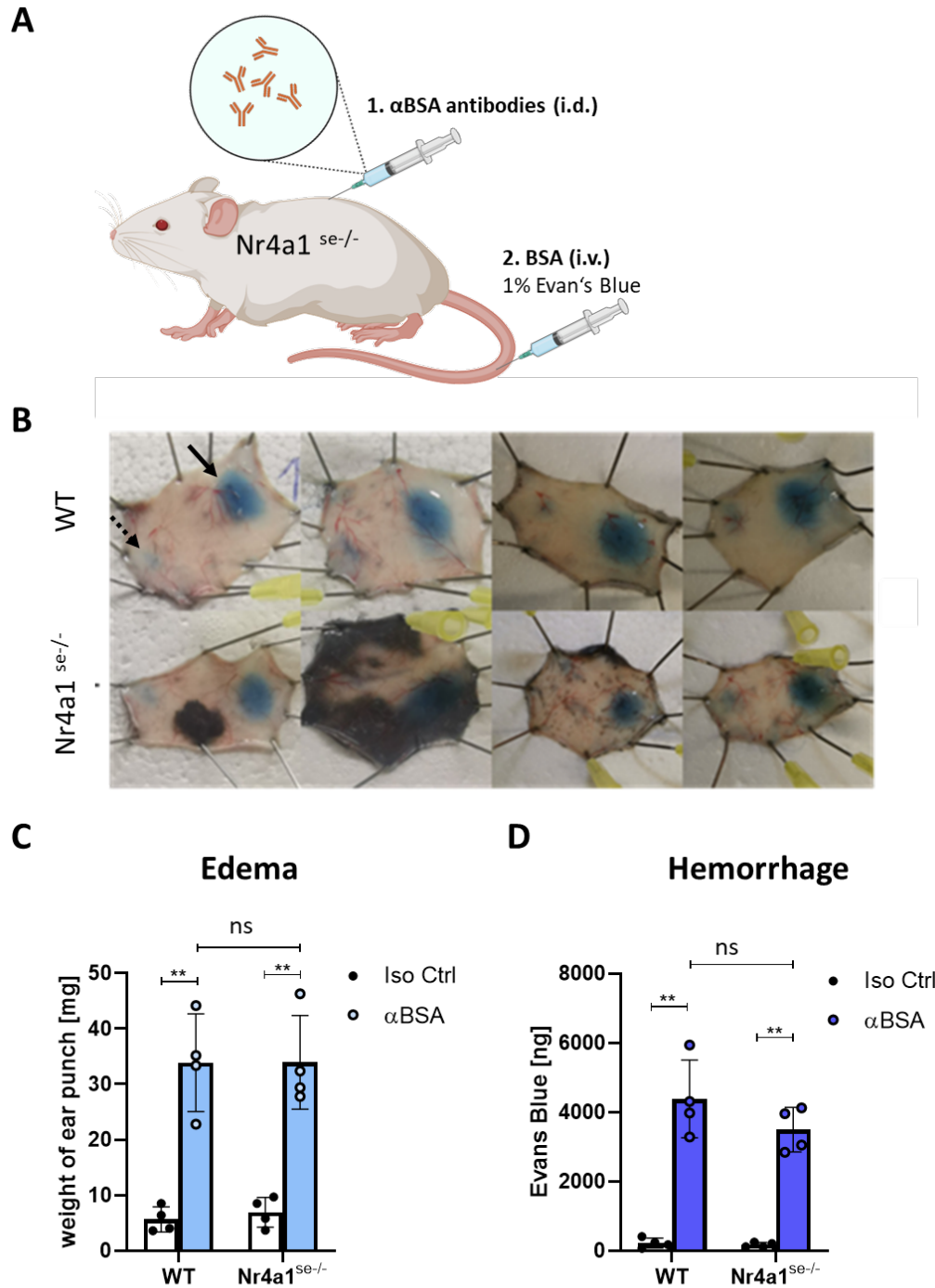


Figure 13. RPA reaction model in $Nr4a1^{se/-}$ mice does not show different course of inflammation compared to WT mice.
A Schematic illustration of cutaneous RPA reaction. Created with BioRender.com. **B** Mounted back skin of mice 4h after induction of RPA reaction. Solid arrow indicates BSA-specific injection site and dotted area site of isotype ctrl injection. **C** Comparison of single 8mm skin biopsy punch weight from respective injection sites to quantify the edema. Every data point

represents weight of one skin punch from one mouse. **D** Quantification of haemorrhage by comparing amount of extravasated Evans Blue after formamide extraction. Significant differences were tested by student's t-test. Means of columns were compared. (**** $p < 0.0001$; *** $p < 0.001$; ** $p < 0.01$; * $p < 0.05$). Error bars indicate SD.

Having excluded a prominent role of NCMs in the RPA reaction, I further investigated whether they show any involvement in this IC-induced inflammation model at all. To do so, WT NCMs were adoptively transferred into $Fc\gamma R^{-/-}$ prior to initiating the RPA reaction (Figure 14 A). $Fc\gamma R^{-/-}$ mice are deficient of all $Fc\gamma R$ s and therefore cannot recognize any ICs formed during the RPA reaction, which inhibits the initiation of the inflammatory cascade. This leads to no detectable RPA reaction in $Fc\gamma R^{-/-}$ mice. Using this negative background, I adoptively transferred $Fc\gamma R$ -competent NCMs from WT mice into $Fc\gamma R^{-/-}$ animals. This ensured that the only potential source of recognizing ICs to initiate an inflammation are the transferred WT NCMs.

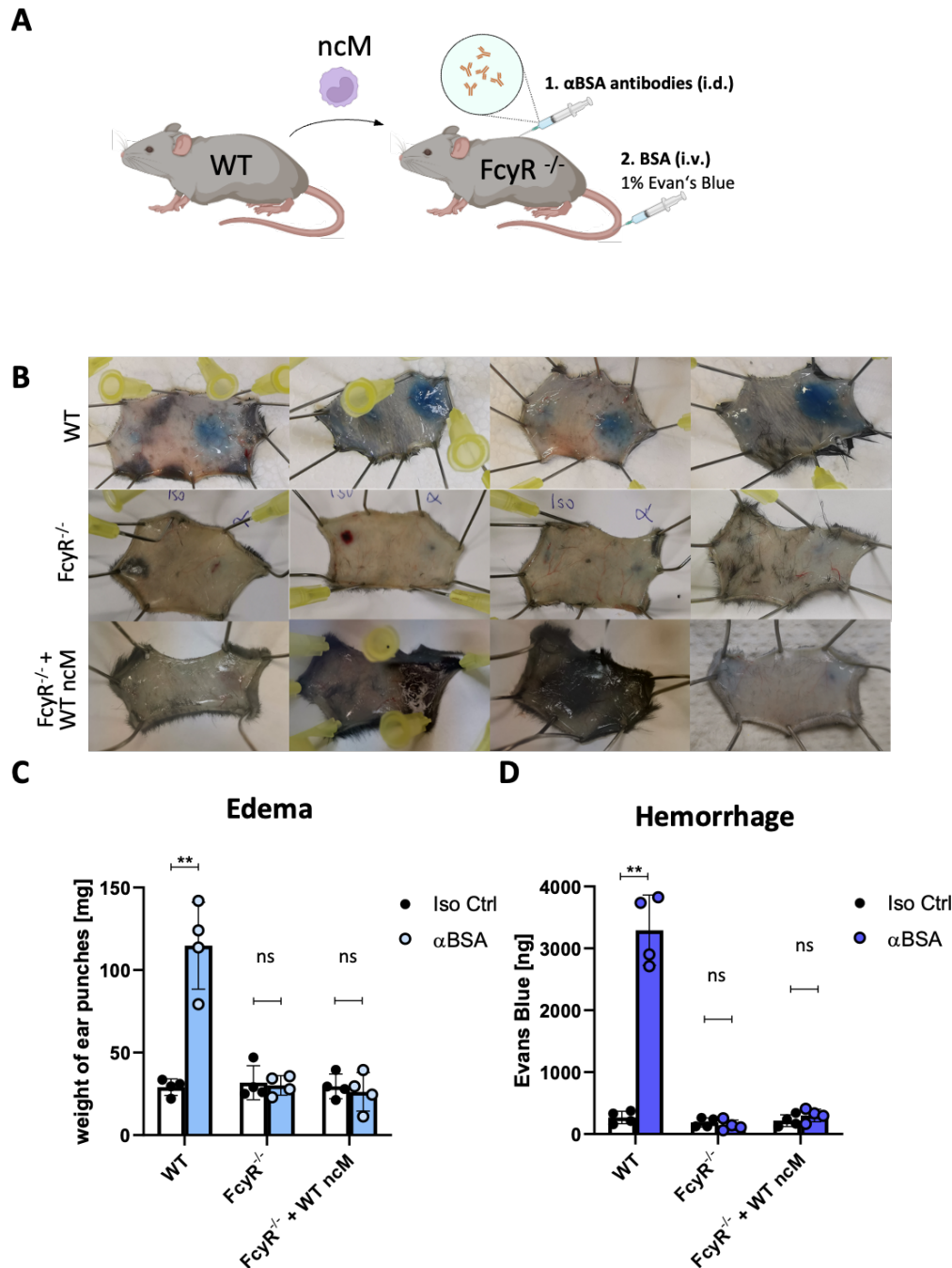


Figure 14. Adoptive transfer of WT non-classical monocytes into FcγR^{-/-} mice could not rescue WT RPA reaction phenotype.
A Schematic illustration of RPA reaction in FcγR^{-/-} mice after receiving 2x10⁵ of WT NCMs. Created with BioRender.com. **B** Mounted back skin of mice 4h after induction of RPA reaction. **C** Comparison of weight of 3x8mm skin biopsy punches from respective injection sites to quantify edema. Every data point represents weight of three skin punches from one mouse. **D** Quantification of haemorrhage by comparing amount of extravasated Evans Blue after formamide extraction from 3 biopsy punches (Ø8mm). Significant differences were tested by student's t-test. Means of columns were compared. (****p<0.0001; ***p<0.001; **p<0.01; *p<0.05). Error bars indicate SD.

In this experimental setting, the RPA reaction was induced in 4 WT mice, 4 FcγR^{-/-} mice and 4 FcγR^{-/-} mice which received adoptive transfer of WT non-classical monocytes prior to the reaction. Similar to the previous experiment, an isotype control was injected next to the antigen-specific antibody to account for any inflammation or vessel leakage due to the injection itself. As expected, the RPA reaction took place in WT animals but not in FcγR^{-/-} mice

(Figure 14 B, top row and middle row). The edema and haemorrhage (Figure 14 C,D) confirmed an IC-dependent- (since there is no edema or haemorrhage in the isotype controls) and FcγR-dependent inflammation (since there is no edema or haemorrhage in the FcγR^{-/-} mice). The adoptive transfer of FcγR⁺ WT NCMs could not rescue the WT RPA reaction phenotype since no differences between FcγR^{-/-} and FcγR^{-/-} + adoptively transferred cells regarding Evans Blue leakage into the skin or edema could be observed. Therefore, no involvement of NCMs in the cutaneous RPA reaction could be detected.

To further elucidate an involvement of these cells in IC-mediated inflammation, I decided to investigate whether peritoneally-induced ICs, instead of cutaneous ICs, could resolve differences in inflammatory responses between WT and Nr4a1^{se/-} mice. Therefore, the peritoneal RPA reaction model was used. Similar to the cutaneous reaction, ICs are generated by injecting BSA as antigen *i.v.* and αBSA rabbit IgG as correspondent antibody *i.p.* (Figure 15 A). 2h after the injections, I analysed whether differences in the composition of the peritoneal immune cell infiltrate occurred between WT and Nr4a1^{se/-} mice by analysing the peritoneal lavage via FACS. Intriguingly, no difference in either infiltrating neutrophil-, classical monocyte or non-classical monocyte frequency was observed between injection of isotype control or αBSA antibody. Nevertheless, a strong increase in CD45⁺ leukocytes could be determined (Figure 15 C), which was caused by the infiltration of dump⁺ cells, meaning either CD3⁺, CD19⁺ or NK1.1⁺ T cells, B cells or NK cells (Figure 15 B). Additionally, no difference in either CD45⁺ leukocyte-, neutrophil-, classical monocyte- or NCM frequency could be observed between WT and Nr4a1^{se/-} animals after the peritoneal RPA reaction. The fact that the same fraction of cells in the peritoneal lavage were dump⁺CD11b⁺Ly6G⁻Ly6C⁻ NCMs when comparing WT and Nr4a1^{se/-} mice, could hint towards a Nr4a1-independent route of NCM development, but 2h of incubation seems implausibly short.

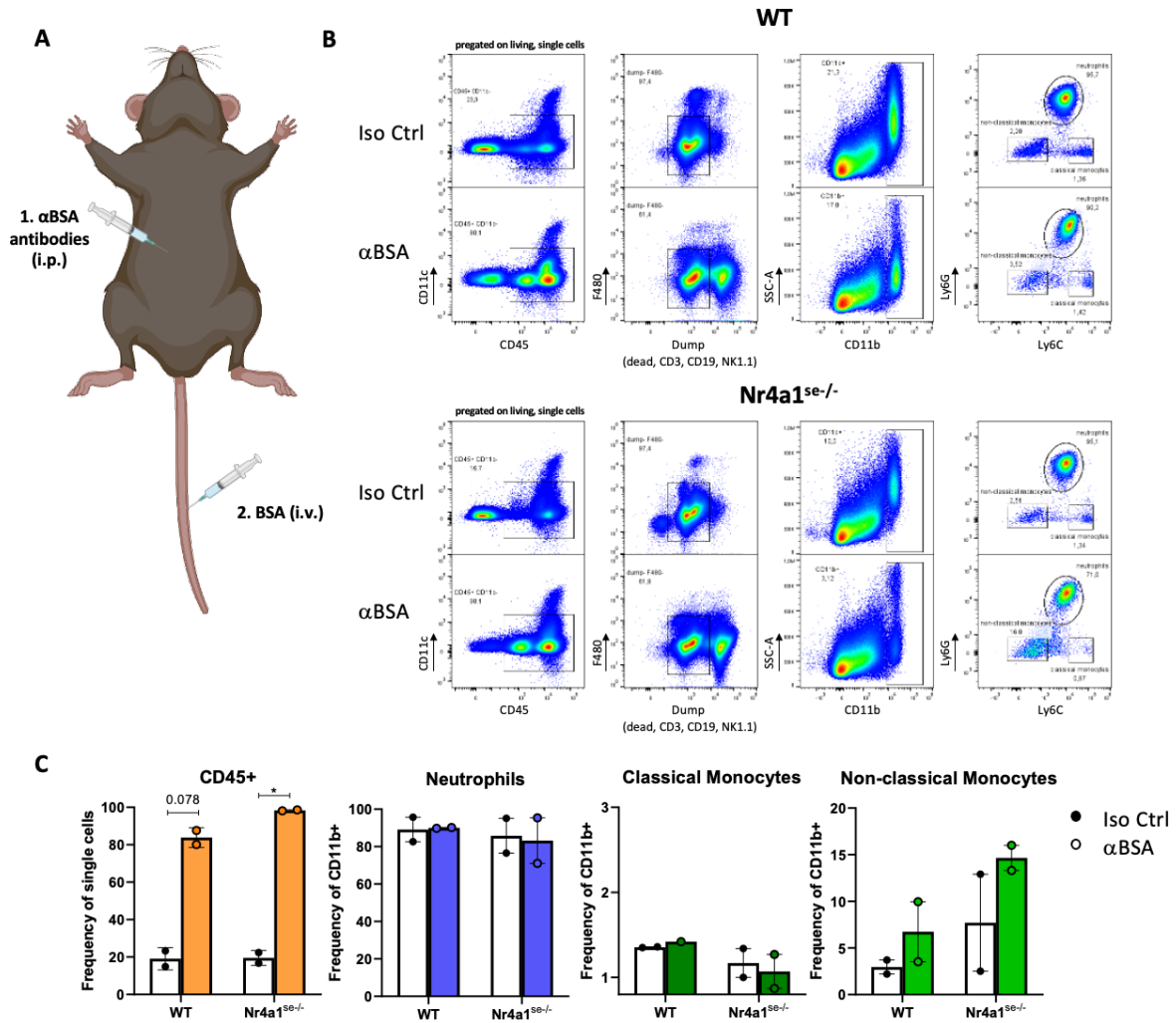


Figure 15. Peritoneal RPA reaction does not show differences between WT and Nr4a1^{se-/-} mice. **A** Schematic illustration of peritoneal RPA reaction. Antibodies were injected i.p. and BSA antigen was injected i.v. right after. Created with BioRender.com. **B** Gating strategy and FACS plots of representative WT and Nr4a1^{se-/-} mice, which received either isotype control or α BSA antibody. Notably, the amount of dump⁺ cells increased in animal, which received α BSA antibody compared to isotype control. **C** Quantification of immune cells and -subsets in peritoneal lavage after RPA reaction or isotype control. 2 mice were used per group. Significant differences were tested by student's t-test. Means of columns were compared. (*p < 0.05). Error bars indicate SD.

3.3 Non-Classical Monocyte-specific Responses to IC-Binding

So far, it was observed that human NCMs show a very high affinity for ICs, but that their murine counterparts do not play a major role in IC-induced inflammation in the RPA reaction. Given that about two thirds of all NCMs *in vivo* constantly adhere to the endothelium and that they express the largest variety and high numbers of Fc γ Rs, their behaviour on immobilized ICs was closely investigated. Immobilized ICs are used as a stimulus for Fc γ R-crosslinking and subsequent cellular responses¹⁰⁹. The major finding in these experiments was, that human (but not murine) NCMs migrate on immobilized IC. Upon this finding, a major part of this project was built.

To activate different leukocytes via Fc γ R-crosslinking, the ICs were immobilized by seeding onto a spatially confined surface prior to seeding the cells. Initially, these experiments were performed under an applied flow, to investigate whether the previously observed affinities

for ICs are strong enough to capture leukocytes out of the blood flow by letting them pass above IC-coated surfaces. While leukocytes were captured with different efficiencies⁷⁷, only SlanMo initiated a migratory response when interacting with immobilized IC. When compared to other CD16-expressing cells like NK cells or neutrophils, there was an eminent difference of SlanMo to the other cells (Figure 17 A). During the adhesion process on immobilized ICs, SlanMo changed their morphology, flattened, elongated shape and formed a broad lamellipodium at their leading edge (Figure 16) Within minutes they started to migrate on the IC lawn and continued to persist in this migration for several hours.

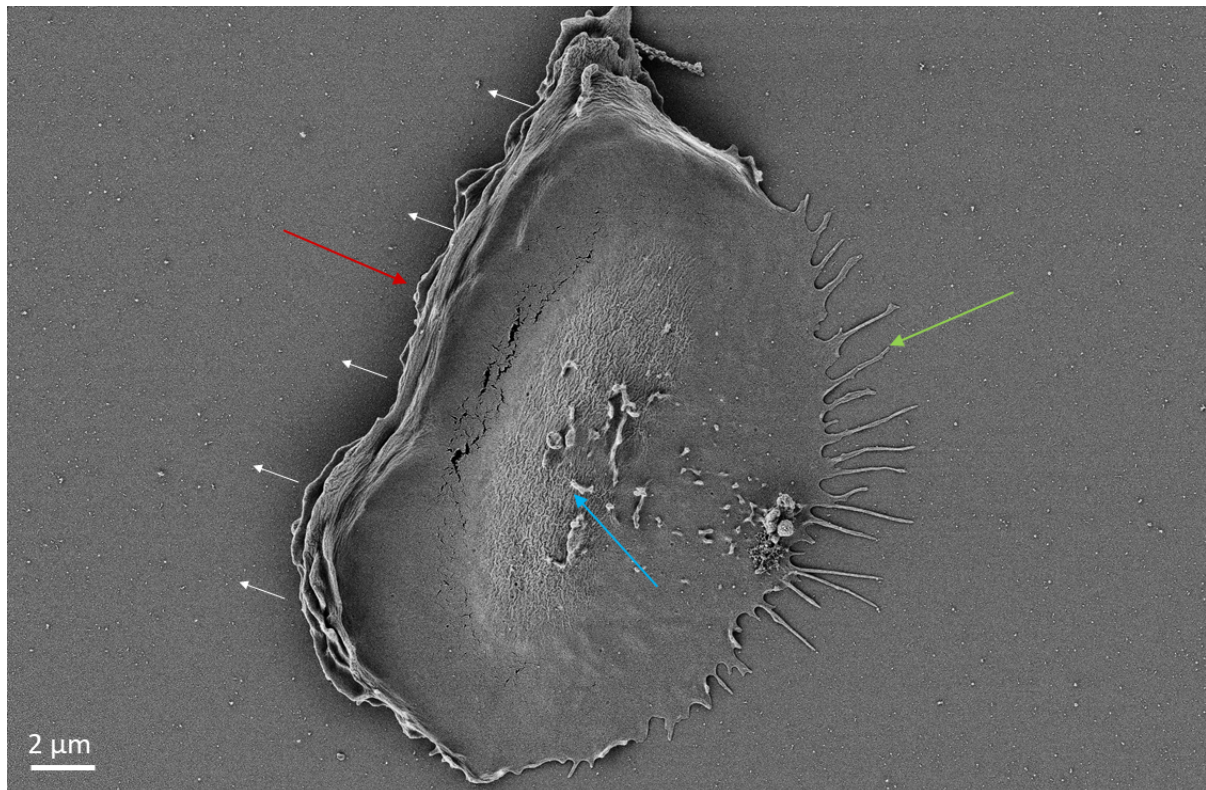


Figure 16. SlanMo change into very distinct migratory morphology. When seeded onto immobilized ICs, SlanMo form cell body (blue arrow), lamellipodium at leading edge (red arrow) and retraction fibers at cell rear (green arrow). White arrows indicate direction of migration. Image kindly provided Stephanie Oehrl.

When compared to other cells like NK cells and neutrophils, this migration phenomenon is unique to SlanMo. Even though minor differences are seen in NK cell and neutrophil behaviour between being seeded on a surface coated with solely antigen or ICs, none of the cells start to exhibit a haptotactic migration. A minor difference between antigen coated and IC-coated surfaces is observed, as a fraction of NK cells as well as of neutrophils became adherent on ICs but not on the antigen coated surface. However, when seeding SlanMo nearly 80% of the cells became adherent and initiated a migratory response (Figure 17 C).

After observing the CD16-dependend binding of ICs to SlanMo (see 3.1), it was investigated whether the migratory response to immobilized ICs is also induced via CD16. In order to do so, CD16 was blocked with an α CD16 antibody prior to seeding the cells onto the IC coated surface. SlanMo with blocked CD16 did not adhere or migrate on ICs (Figure 17 B, right). SlanMo from the same donor were seeded onto immobilized ICs without blocking CD16 as

control (Figure 17 B, left). Here again, SlanMo displayed their unique migration behaviour including adherence, change in morphology and directional migration.

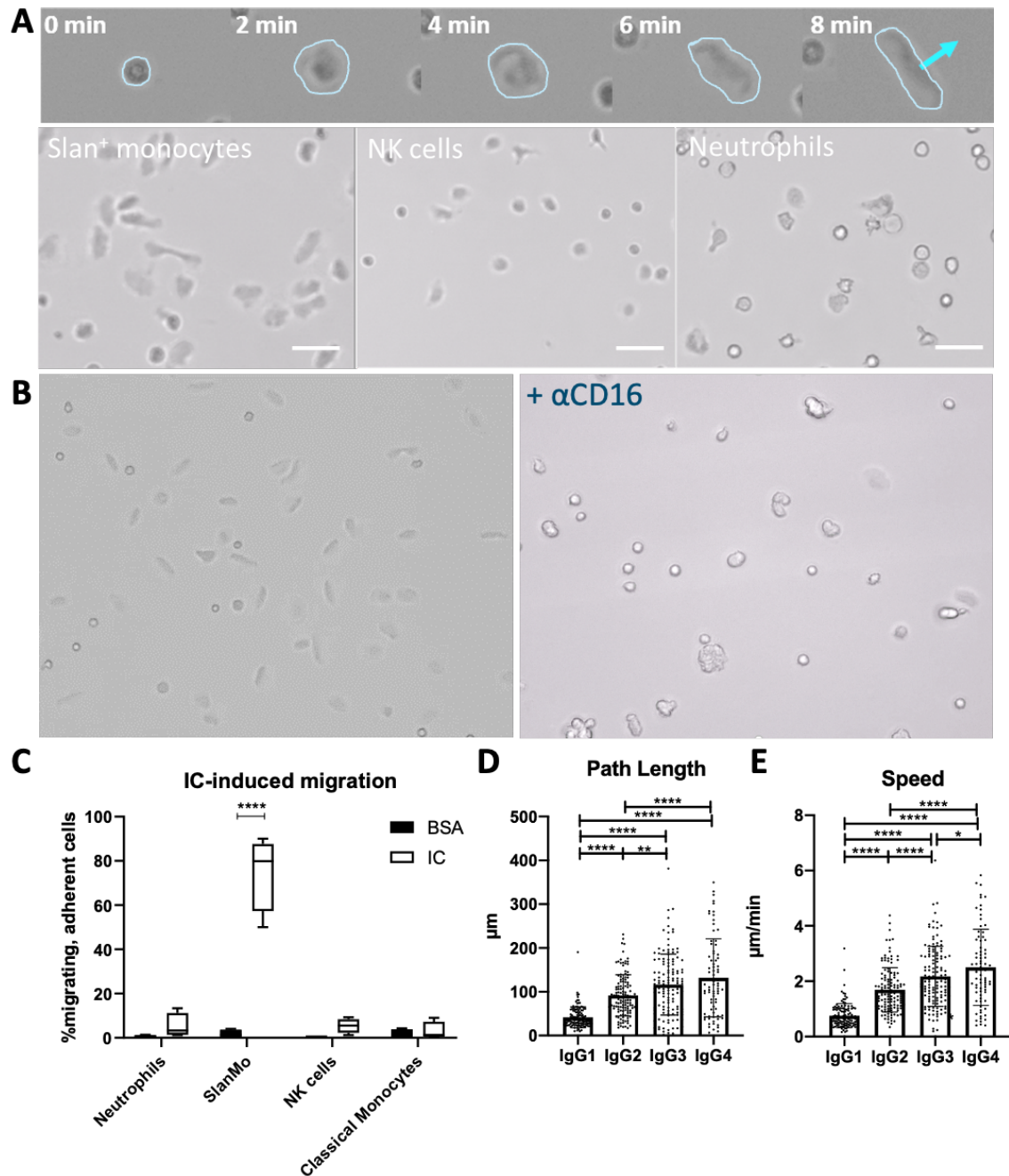


Figure 17. SlanMo migrate on immobilized IC. **A** Timelapse images showing the same SlanMo over 8 min after seeding on an IC-coated surface. The cell first adheres to the surface, flattens, becomes elongated and starts migrating (blue arrow). Images below show SlanMo, NK cells and neutrophils seeded on ICs after 30min incubation. SlanMo become adherent and elongated, whereas only very few NK cells and neutrophils become adherent but do not migrate. Scale bar is 25 μm. **B** IC-induced migration in SlanMo is inhibited by blocking CD16. Left: image of SlanMo on immobilized ICs after 30min, 37°C. Right: SlanMo, pretreated with 10 μg/mL αCD16 blocking antibody, on immobilized ICs after 30min, 37°C. **C** Box plot comparing neutrophil-, SlanMo-, NK cell- and classical monocytes behaviour on antigen- (BSA-6FITC-) and IC-(BSA-6FITC:αFITC rabbit IgG-) coated plastic. Only SlanMo migrate on immobilized ICs. **D, E** Comparison of migration path length (**D**) and migration speed (**E**) of SlanMo seeded on either human IgG1-, IgG2-, IgG3- or IgG4 coating. Results were pooled from 3 donors and 30-50 cells per donor were tracked. Means of columns were compared. (****p<0.0001; ***p<0.001; **p<0.01; *p<0.05). Error bars indicate SD.

First, migration experiments on ICs were performed on BSA-FITC:αFITC rabbit IgG immune complexes. To validate whether this could be a phenomenon of biological relevance, human IgGs were also tested on whether they could induce a migratory response in SlanMo. Pilot experiments revealed that immobilized IgG induces a migration in SlanMo, similar to immobilized ICs. Therefore, SlanMo were seeded onto hIgG1-, hIgG2-, hIgG3 or hIgG4- coated surfaces and their migration was tracked over the course of 1h. Being isolated from human plasma and not recombinantly produced, these IgG subclasses enabled an investigation of interactions of SlanMo with IgGs possessing a human glycosylation pattern. SlanMo exhibited adhesion and migration responses to all four human IgG subclasses, while demonstrating distinct differences in the response magnitude. The observed migrated distance (path length) was the lowest on IgG1 with $41.7\mu\text{m} \pm 23.5\mu\text{m}$ and highest on IgG4 with $131.2\mu\text{m} \pm 89.6\mu\text{m}$. Path length of tracked SlanMo on human IgG2 and IgG3 were in between with $91.8\mu\text{m} \pm 46.2\mu\text{m}$ and $116.6\mu\text{m} \pm 69.9\mu\text{m}$, respectively. Accordingly, the migration speed of the tracked SlanMo differed on different IgG subclasses with $\text{IgG4} > \text{IgG3} > \text{IgG2} > \text{IgG1}$. The respective speeds were $0.8\mu\text{m}/\text{min} \pm 0.4\mu\text{m}/\text{min}$, $1.7\mu\text{m}/\text{min} \pm 0.8\mu\text{m}/\text{min}$, $2.2\mu\text{m}/\text{min} \pm 1.1\mu\text{m}/\text{min}$ and $2.5\mu\text{m}/\text{min} \pm 1.2\mu\text{m}/\text{min}$.

To exclude the possibility that SlanMo are activated by ICs via CD16 crosslinking but other secreted chemotactic factors then induce the migration process, a spot assay was performed. It was hypothesized that ICs crosslink CD16 on the SlanMo's surface, inducing a signalling cascade, directly leading to cytoskeletal rearrangement and subsequent migration in cis. A different hypothesis would be, that SlanMo are activated by immobilized ICs via crosslinking CD16, which leads to a secretion of chemokines that act in an autocrine and paracrine manner in trans to induce migration in the IC-activated and in nearby cells. To decipher the mode of action, a surface was coated with antigen (HSA-1.5FITC, $2\mu\text{g}/\text{mL}$) and subsequently a defined area of previously coated surface was coated with fluorescently labelled antibody (αFITC, $6,6\mu\text{g}/\text{mL}$) using a silicone micro-insert (Ibidi). With this approach, a surface was created which directly neighbours IC- and antigen coating (Figure 18 A). If SlanMo were activated to secrete migration-inducing factors, neighbouring cells on the antigen coated side would start to migrate as soluble factors could diffuse across the surface. Time-lapse imaging of SlanMo seeded on the prepared surface revealed, that SlanMo only adhered and migrated on the IC-coated side of the surface (Figure 18 B). The tracks indicate the migration paths of the correspondent cells over 1h. On the antigen-coated side, a minor fraction of cells adhered to the surface but did not migrate. However, on the antigen + antibody coated side (red), $72.8\% \pm 3.8\%$ of cells were adherent and migrating. The experiment was performed 3 times with 3 different donors. A crossing of the antigen – IC line was not observed in migrating SlanMo, as can be seen by the tracked cells. As soon as migrating SlanMo reached the edge of the IC-coated side, they changed direction and did not continue to migrate on the antigen-coated surface. This experiment concludes that ICs are directly responsible for the adherence, the initiation of the migration but also crucial for the maintenance of the migration process. It also showed that the induction of migration by ICs is a primary and direct effect, since a potential

secondary effect involving secretion of chemokines would induce cell migration in SlanMo on the antigen-coated surface. This was not observed.

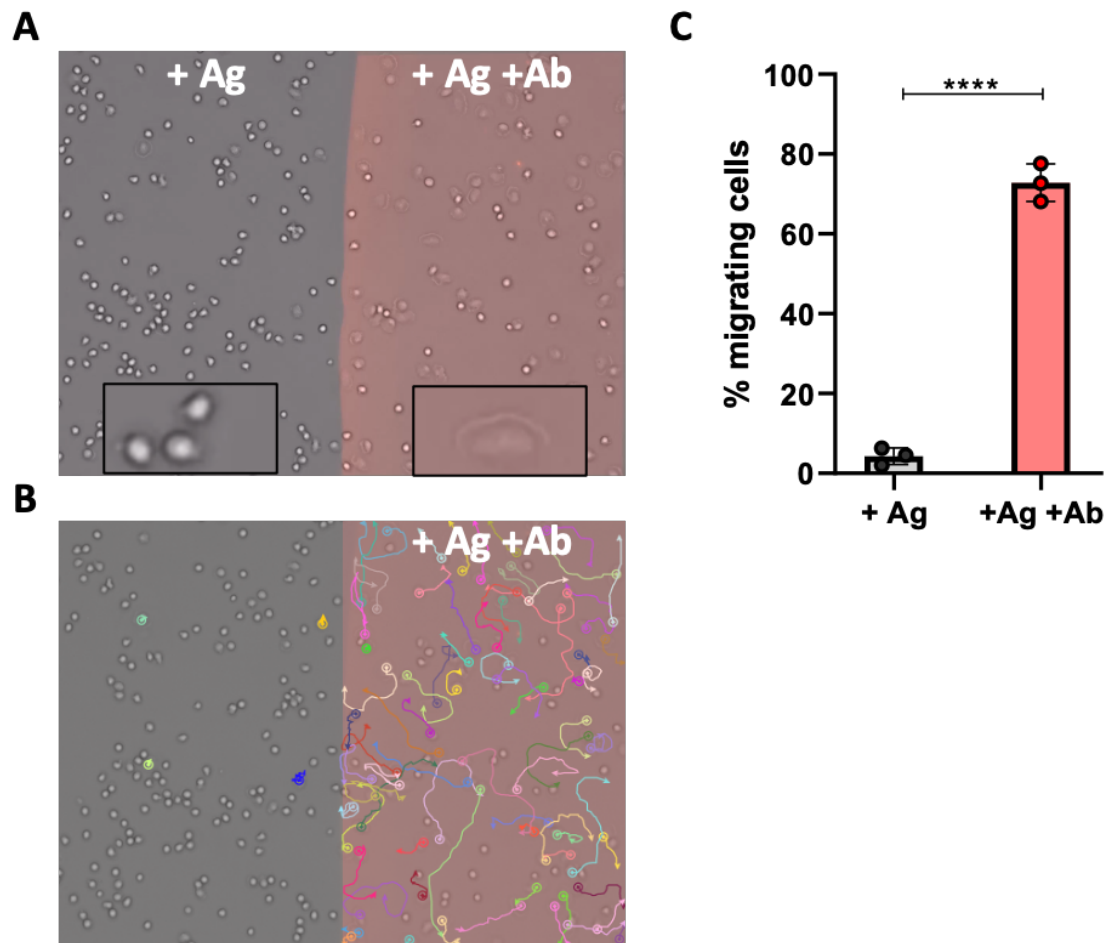


Figure 18 : Immobilized ICs are crucial for adhesion, initiation and maintaining migration. **A** Image of timelapse from spot assay, where one half of the surface is coated with antigen (left side) and other half with antigen + antibody (right side). Antibody component of ICs is fluorescently labelled (red). Seeded SlanMo only migrate on antigen + antibody but not on antigen only. **B** Overlay of migration tracks over all migrating cells from A. **C** Bar plot comparing fraction of migrating cells between antigen coating and antigen+antibody coating. A and B show representative images from 3 experiments performed with 3 different donors. Significant differences were tested by student's t-test. Means of columns were compared. (***p<0.0001; ***p<0.001; **p<0.01; *p<0.05).

The observed migration occurs on a uniformly coated immobilized substrate and lacks directional cues, therefore it is referred to as haptokinesis. Further assessing a potential biological relevance of this *in vitro* finding, I investigated whether the IC-induced migration in SlanMo can occur in a directed manner following a gradient of immune complexes. This haptotaxis would indicate that SlanMo are capable of migrating towards inflammatory sites, e.g. wounds or local viral infections, where ICs are formed by antibodies recognizing their cognate bacterial- or viral antigen. From these sites of IC formation, a gradient of ICs could form through the vasculature or tissue due to diffusion. In this scenario, IC-dependent haptotaxis would characterize SlanMo as first responders to IC-induced inflammation, as they would uniquely migrate to the inflammation site independently of complement or chemokine signals, unlike other cells. To investigate IC-induced migration of SlanMo on an immobilized IC gradient, I collaborated with Prof. A. Cavalcanti-Adam's group from Max Planck Institute for

Medical Research. Using a UV-based photo micropatterning system, an IC-gradient could be generated on an otherwise passivated glass surface. First, a glass surface was pre-treated with O₂ plasma to ensure a clean and reactive surface by introducing functional groups like hydroxyl (-OH) groups. The pre-treated glass was then passivated by a PEG coating (Figure 19 A). This passivation prohibited protein adhesion or cell interaction with the glass surface through steric hindrance and the absence of functional groups. Furthermore, a physical aqueous barrier was created due to the hydrophilicity of PEG, which additionally impeded protein or cell interactions with the glass surface. After passivation, a UV-sensitive photoinitiator was added to the surface, allowing spatially defined removal of the PEG layer. Upon UV illumination, the photoinitiator (PLPP) was activated and generated free radicals that broke down chemical bonds within the PEG layer. Therefore, PEG was selectively removed in illuminated areas, allowing for precise and controlled patterning by focusing the UV light in specific patterns. PEG remained intact in non-illuminated areas. After patterning the PEGylated glass surface, proteins (ICs in this case) were added to the surface and only adsorbed to the PEG-free glass. The IC coating thus mimicked the UV illumination pattern, allowing subsequently seeded cells to adhere only to the adsorbed ICs. To pattern a gradient, the intensity of the UV illumination was gradually changed and lead to only partial removal of PEG in areas with low UV intensity and increasing removal of PEG with increasing UV laser intensity, creating a gradient.

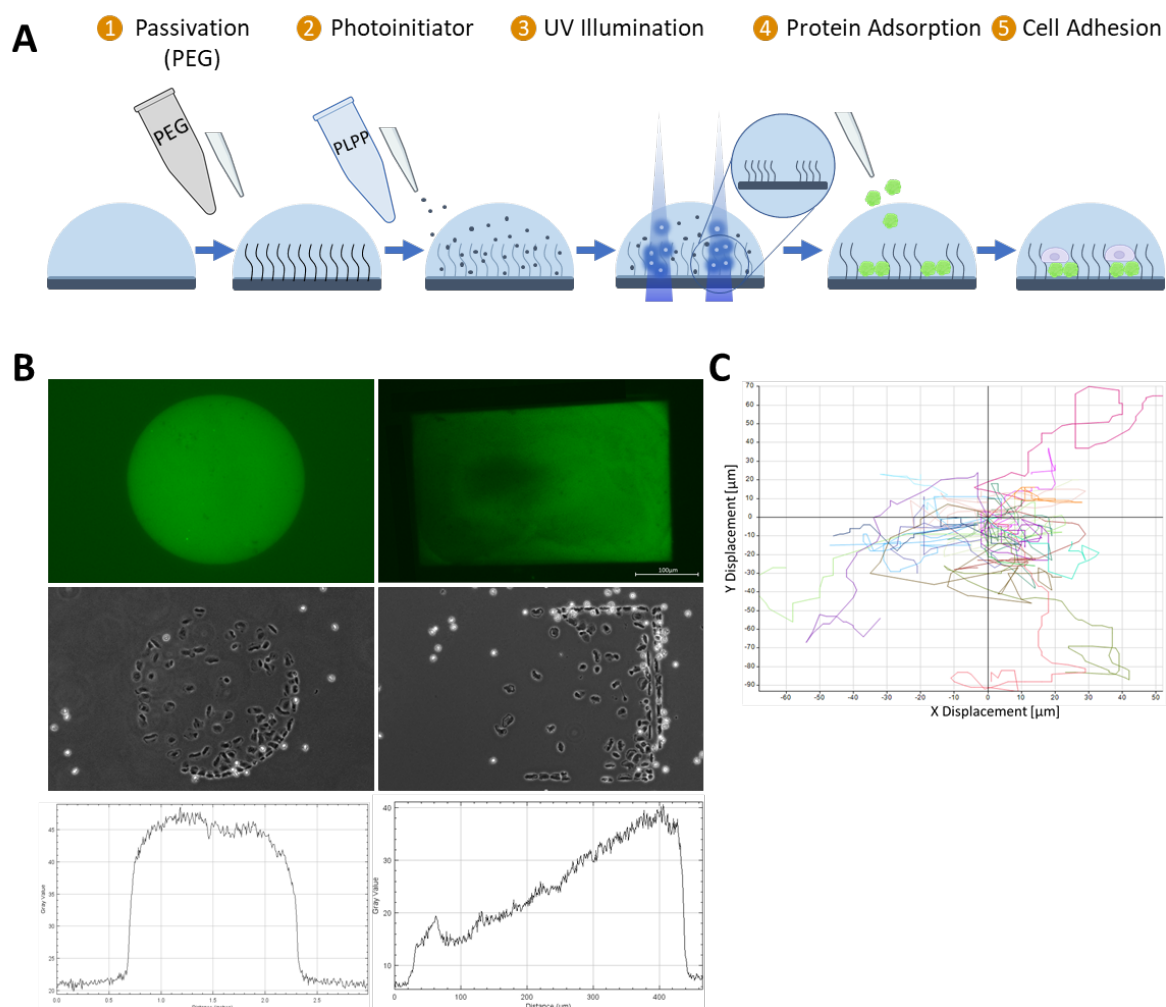


Figure 19. UV-based photo micropatterning system allows generation of immobilized IC gradients. **A** Schematic illustration of UV-based photo micropatterning method. After passivating a surface using PEG, photoinitiator (PLPP) is added. UV illumination enables micropatterning by selectively removing PEG on illuminated areas of surface, allowing protein to adhere. Seeded cells can adhere to protein but not to PEGylated areas. Created with BioRender.com **B** Top: Fluorescence image of a 200 μm micropatterned spot (left) and gradient area (right). Surface was micropatterned with fluorescently labelled IC (green). Middle: Brightfield images of same areas after seeding SlanMo. Cells only attach and migrate on micropatterned area. Bottom: Fluorescence intensity profile through top images. Uniform fluorescence and IC adsorption (left) and gradient fluorescence (right). **C** Orientation plot showing migration paths of SlanMo after seeding on immobilized IC gradient. SlanMo migrated for 2h.

In first pilot experiments, the quality of the patterning, the SlanMo adhesion to the patterned ICs and the IC-induced migration on the treated surface were assessed. A \varnothing 300 μm spot was patterned and coated with fluorescently labelled ICs (Figure 19 B, top left). To ensure reliable IC coating to the illuminated areas, a line profile analysis was performed using ImageJ. A line was drawn across the fluorescent image, and the corresponding fluorescence intensity values were measured along this line to evaluate the distribution and uniformity of the fluorescence signal (Figure 19 B, bottom left) and therefore of the adsorbed ICs. The line profile showed a homogeneous fluorescence signal across the patterned area, verifying a uniform patterning. Seeded SlanMo adhered to the illuminated surface due to the presence of ICs and migrated (Figure 19 B, middle left) but did not adhere to the non-illuminated, passivated glass surface. To pattern a gradient, a gradient UV-illumination mask was created in the photopatterning software Leonardo. The created gradient consisted of a 300 x 400 μm rectangle in which the

UV laser intensity ranged from 30% (left side) to 100% (right side) with a linear gradient in between (Figure 19 B, top right). The linear gradient patterning could be confirmed by the line profile analysis (Figure 19 B, bottom right). Seeded SlanMo again only adhered to the illuminated area with an enrichment of adherent cells at the high end of the gradient (Figure 19 B, middle right). After seeding, cells were tracked for 4h. No directed migration towards high IC concentrations was detected but rather random migration of SlanMo (Figure 19 C). Therefore, an IC-induced haptotaxis implying a gradient-sensitive and directed migration towards high concentrations of IC could not be confirmed in this experimental setting.

The previous experiment was performed to better understand the biological relevance of the IC-induced migration of SlanMo. Since NCMs have been identified as “vascular housekeepers”⁵⁹, clearing the endothelium from apoptotic cells, metastatic tumor cells, and particles, it was proposed that they may also internalize ICs, since they pose a potential threat to the endothelium. Endocytosis of these ICs would support the current notion of non-classical monocytes being responsible for maintaining vascular homeostasis. This would also suggest a dual role for SlanMo in both maintaining vascular homeostasis and responding to inflammatory stimuli. To test, whether SlanMo migrating on immobilized ICs are endocytosing ICs, the pH sensitive fluorescent label pHrodo was conjugated to the antibody portion of the ICs used to coat the plastic surface (Figure 20 A, B). The pH-sensitive dye only becomes fluorescent under low pH-conditions as present in the lysosome. The successful antibody labelling was first tested by coupling the antibody to beads, and incubating SlanMo with the opsonized beads. After 1h, cells were analysed under a fluorescent microscope, and it could be confirmed that all phagocytosed beads became fluorescent (data not shown). No fluorescence signal was detected outside of cells. The validated, pH-sensitive antibodies were now used to generate ICs for coating channels of an Ibidi 6 channel μ -slide. After washing away unbound ICs, purified SlanMo were seeded onto the IC coating and incubated for 1h at 37°C. After incubation, cells were fixated using 4% PFA and analysed under a fluorescence microscope. Cells had to be fixated to prevent phototoxicity effects from damaging cells with potentially endocytosed ICs. It could be confirmed that migrating SlanMo indeed internalized immobilized ICs, as SlanMo with a migrating phenotype became red fluorescent (Figure 20 C).

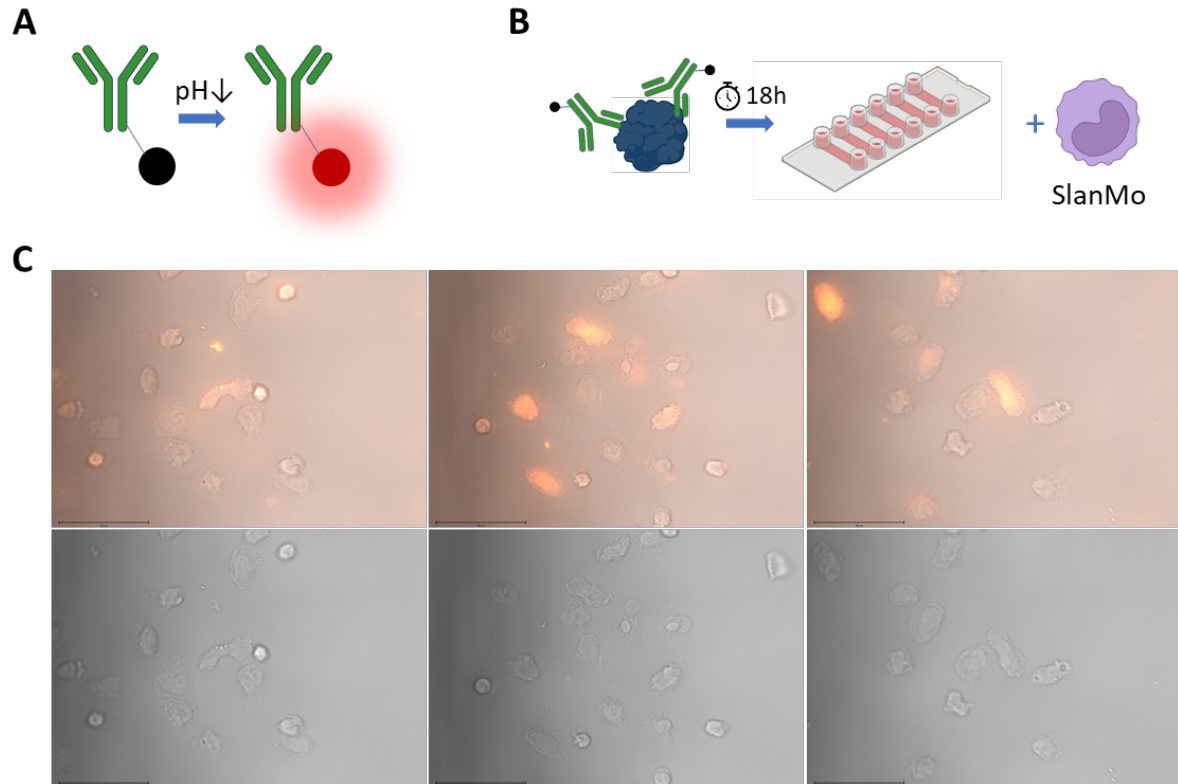


Figure 20. SlanMo internalize immobilised ICs during IC-induced migration. **A** Schematic illustration of conjugation of pH-sensitive pHrodo dye to α FITC rabbit IgG. **B** Schematic illustration of pHrodo-conjugated IC-coating of Ibidi 6 channel μ -slide and seeding of SlanMo. A and B were created with BioRender.com **C** Brightfield microscopic images of SlanMo migrating on ICs (bottom row) and overlay of brightfield and fluorescent image. Red fluorescence indicates phagocytosed ICs. Scale bar 50 μ m.

Briefly summarizing findings so far, human SlanMo bind ICs with high affinity, migrate on surfaces coated with immobilized ICs, and endocytose ICs during migration. However, I could not observe a chemotactic or haptotactic migration of SlanMo towards ICs, meaning a directed migration towards higher IC concentrations. Experiments using immobilized IC gradients did not reveal an enrichment of SlanMo at higher IC concentrations, leading me to investigate whether this response might be elicited by soluble ICs instead. To test this, I utilized a ChemoTx neuroprobe transmigration chamber, which separates the cells and the chemoattractant containing receiver well by a framed PVC membrane. In this transmigration assay, cell medium with the according volume of added PBS was used as negative control, to distinguish directed migration from random, chemokinetic migration. As positive controls, either fractalkine or C5a were used at 10 ng/mL. In this setting, SlanMo transmigrated in response to an IC gradient but not toward monomeric antibody or antigen of the corresponding concentration (Figure 21 A). $9.2\% \pm 1.2\%$ of seeded cells transmigrated toward ICs, whereas only $2.7\% \pm 0.3\%$ migrated towards antigen only, $2.7\% \pm 0.3\%$ towards monomeric antibody, and $2.9\% \pm 0.2\%$ towards cell medium, supplemented with PBS (negative control). SlanMo were viable and motile as $14.9\% \pm 7.4\%$ of SlanMo transmigrated towards C5a.

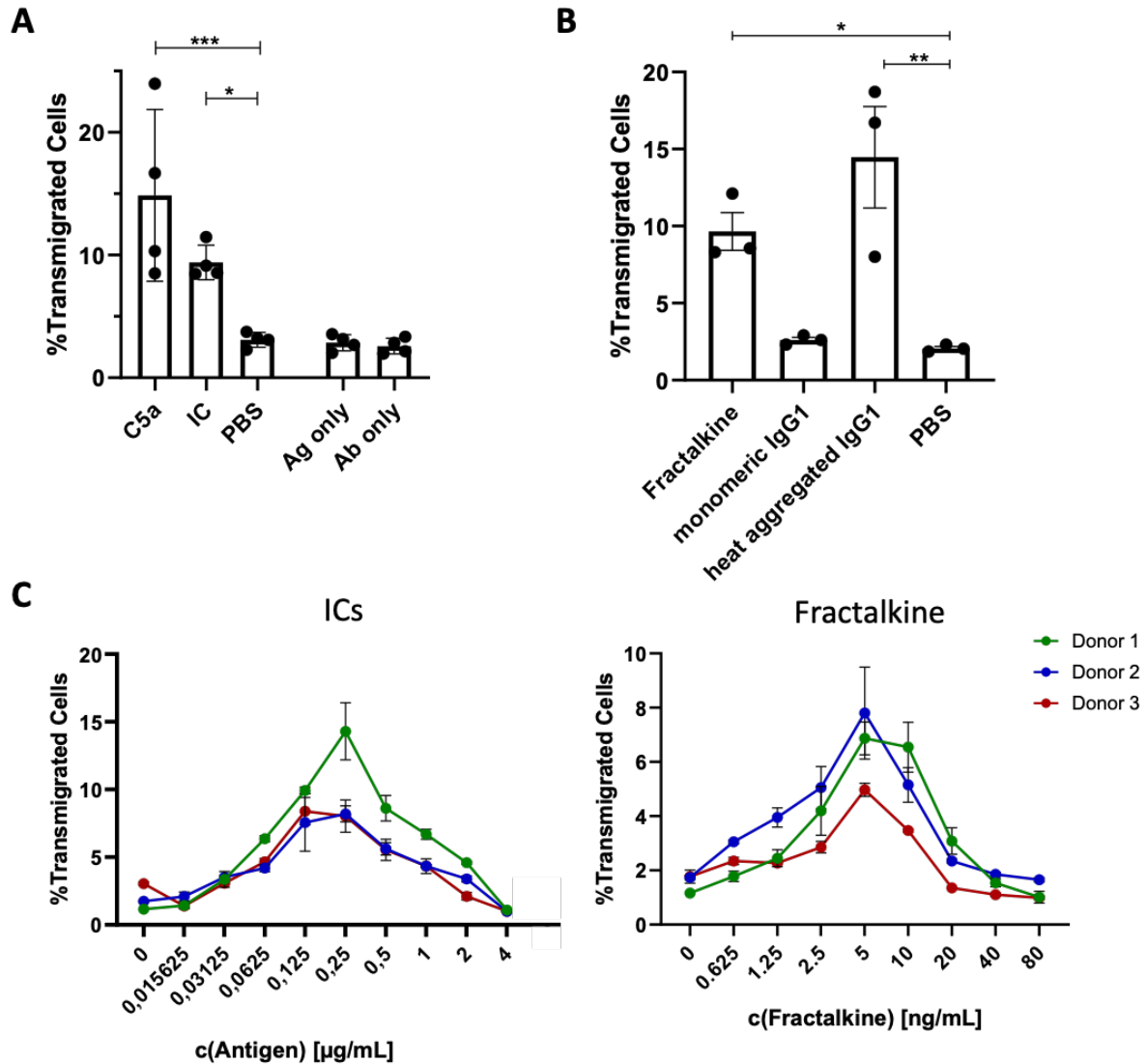


Figure 21. SlanMo transmigrate towards ICs. Bar graphs show fraction of seeded SlanMo that transmigrated into receiver bottom well. **A** C5a was used as positive control at 10 ng/mL. ICs consisted of 1 μL of 1 mg/mL BSA-6-FITC (Ag) and 6.4 μL of 1 mg/mL αFITC rabbit IgG (Ab) diluted to 2 mL with PBS. Final Ag concentration was 0.5 μg/mL and final Ab concentration 3.2 μg/mL. Ag only and Ab only contain same antigen and antibody concentrations as respective components in IC. 4 independent experiments were performed with different donors. Technical replicates were used in each experiment and mean of 4 experiments ± SEM is shown. **B** Fractalkine was used as positive control at 10 ng/mL. Purified IgG1 (100 μg/mL) from human serum was either used untreated (monomeric) or incubated at 65°C for 1h to generate immune complexes (heat-aggregated IgG1). Significant differences were tested by Dunnett's 1-way ANOVA. Mean of each column was compared with the mean of control column (PBS) (**p<0.001; *p<0.01; *p<0.05). **C** ICs induce a concentration-dependent transmigration in SlanMo. C(antigen) corresponds to 6,4*c(antibody), so IC at 0.25μg ag/mL contain 1.6 μg ab/mL. Fractalkine induced transmigration shows characteristic bell-shaped dose-response effect.

Following the observation that SlanMo transmigrate toward ICs containing rabbit IgG, I examined whether they would exhibit a similar response to ICs formed *from* aggregated human IgG. Therefore, human IgG1 isolated from plasma was either directly placed in the receiver well as a chemoattractant or heat-aggregated before use. Fractalkine was used as a positive control and PBS as chemokinetic control to obtain background transmigration activity. With this approach, it could be confirmed that SlanMo transmigrate toward aggregated IgG, mimicking ICs but not toward monomeric IgG at the same concentration as 14.5% ± 3.2% of seeded SlanMo transmigrated toward heat-aggregated IgG1 but only 2.6% ± 0.5% toward

monomeric IgG1 (Figure 21 B). Similarly, to monomeric IgG1, $2.1\% \pm 0.3\%$ transmigrated toward PBS, whereas $9.7\% \pm 2.2\%$ responded to fractalkine. To determine the range of concentrations at which ICs exert a chemotactic activity on SlanMo, ICs were serially diluted and added to the receiver wells. For comparison, fractalkine was also serially diluted and chemotactic properties of the dilutions were examined (Figure 21 C). Data from three different donors revealed similar trends, with some variations in extent. The serial dilution of ICs showed a maximal induction of transmigration at $0.125 - 0.25 \mu\text{g ag/mL}$. The lowest concentration at which a transmigration could be observed was 15.625 ng ag/mL , and the highest concentration $2 \mu\text{g ag/mL}$. For fractalkine, the concentration resulting in the highest rate of transmigration was 5 ng/mL , with transmigration observed across a concentration range from $0.625 \text{ ng/mL} - 20 \text{ ng/mL}$. Strikingly, both serial dilutions showed a bell-shaped dose-response curve highlighting similarities in chemoattractant properties of ICs and fractalkine in *SlanMo*.

The monocyte-IC interaction that is best described in literature is phagocytosis. This cellular process includes dynamic probing, phagocytic cup formation, pseudopod extension and engulfment, followed by further digestion and degradation of the phagocytosed protein. Many of these steps, i.e. pseudopod extension and engulfment are driven by reorganization of the cytoskeleton, mostly actin filaments. This led to the hypothesis, that the observed transmigration might be a result of *SlanMo* passively passing through the membrane pores during phagocytosis of ICs. This could occur by *SlanMo* probing for ICs beneath the membrane they are seeded onto, and passively squeezing through the membrane pores facilitated by the membrane- and actin rearrangement during phagocytosis of IC. To investigate this hypothesis, the gradient of ICs in the neuroprobe chamber was altered and the number of *SlanMo* migrating to the receiver wells was compared to different IC gradients. As a comparison, the same experiment was performed with C5a as chemoattractant. The chemoattractant gradient used so far, resulted from passive diffusion through the membrane pores after adding ICs, C5a or fractalkine to the receiver wells. To examine whether phagocytosis of ICs leads to the enrichment of *SlanMo* in the receiver well, the gradient was either reversed by adding ICs or C5a only to the cell droplet sitting on top of the membrane or the gradient was neutralized by adding the same concentration of ICs or C5a to the receiver well and the cell droplet (Figure 22 A). If the previous transmigration results are caused by cytoskeletal rearrangement during phagocytosis and subsequent falling through the pores, the altered gradients should result in similar transmigration rates. But if the results are due to active, directed and chemotactic mechanisms, they should be reduced or diminished if the intended gradient is neutralized or reversed.

As expected, for C5a the alterations of the chemokine gradient resulted in great differences regarding the transmigration of *SlanMo* toward the receiver well (Figure 22 D). When C5a was added to only the receiver well (bottom) $75.9\% \pm 24.8$ of *SlanMo* transmigrated. But when the gradient was neutralized (bottom + top) or reversed (top) only $26.9\% \pm 23.6$ or $0.5\% \pm 0.1$ respectively transmigrated. The fraction of transmigrated cells was measured via FACS, by counting the seeded cells first and then counting the cells contained in the receiver well after

2h of transmigration (Figure 22 D). To directly visualize the transmigrated cells, microscopy images were taken from the receiver wells after transmigration (Figure 22 B). The microscopic images validated a high cell number in the receiver well for the condition with C5a only added to the receiver well and decreasing numbers of cells for neutralizing and reversing the gradient.

For ICs, similar results could be observed. When added to the receiver well, ICs induced a trans migratory response in $13.6\% \pm 6.1\%$ of the seeded SlanMo (Figure 22 C). When the gradient was neutralized, still $4.4\% \pm 1.0\%$ of SlanMo transmigrated and under reversed gradient conditions, only $1.9\% \pm 1.5\%$ of cells were found in the receiver well. The microscopy images (Figure 22 B) also showed a higher count of SlanMo in the receiver well when ICs were added to the bottom only. The cell counts were lower than for C5a as chemoattractant but importantly, followed the same trend regarding the neutralized and the reversed gradient. This complies with IC-induced transmigration being a directed migration toward ICs and not a bystander effect of phagocytosis.

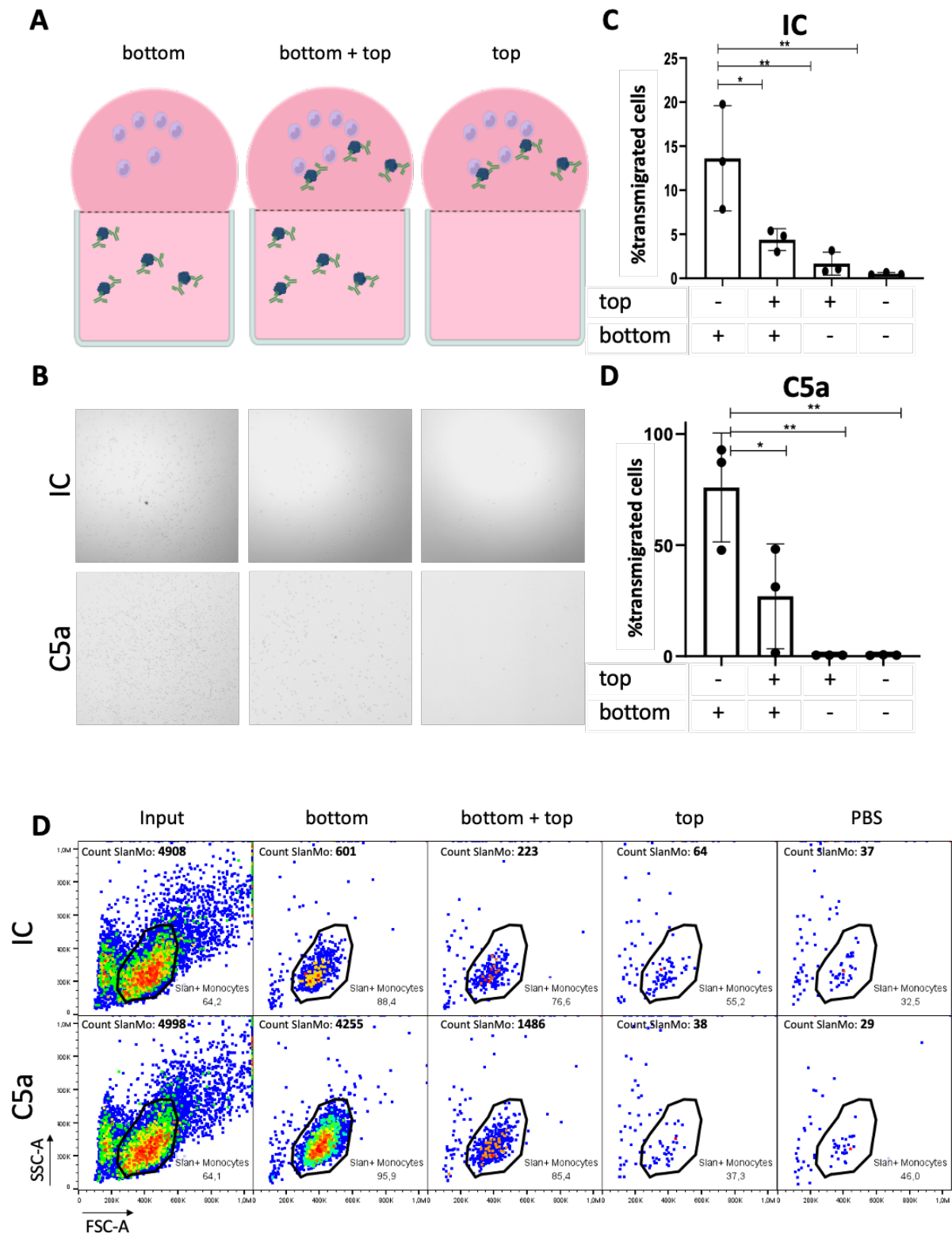


Figure 22. SlanMo transmigrate toward ICs in a gradient-dependent manner. **A** Schematic illustration of experimental setup. Either ICs or C5a were used as chemoattractant and offered in receiver well (bottom), in receiver well and seeded cell droplet on top of membrane (bottom + top) or only in cell droplet but not in receiver well (top) at. C5a was added at 10 ng/mL and IC at 0.5 μ g ag/mL and xx μ g ab/mL. Created with BioRender.com **B** Microscopy images of receiver wells after 2h of transmigration. In the presence of ICs or C5a, most cells transmigrated into the receiver wells when the chemoattractant was added exclusively to the lower chamber (left images). Fewer cells transmigrated when the chemoattractant was evenly distributed across both sides of the membrane (middle images), and minimal transmigration occurred under a reversed gradient, with the chemoattractant applied only to the cell droplet (right images). **C** Quantification of transmigrated cells in response to ICs under different distribution conditions. Percentages of transmigrated cells are shown for: chemoattractant

added only to bottom well (+/-), to top and bottom wells (+/+), to the top well only (-/+), and absent from both wells (-/-). **D** Quantification of transmigrated cells in response to C5a, comparing different gradient settings. Significant differences were tested by Dunnett's 1-way ANOVA. Mean of each column was compared with the mean of control column (-/-). Error bars represent SD. (**p<0.001; *p<0.01; *p<0.05). **E** FACS dot plots showing gating and cell count of either seeded cells (Input, left images) or the contents of the receiver wells for differently altered chemoattractant gradients. Cell count is shown at top within each dot plot. Gate label indicates the fraction of events within the gate.

After ensuring that the observed IC-induced transmigration of SlanMo is truly caused by directed migration toward ICs, further experiments were conducted to gain deeper mechanistic insights into this process. Previous experiments showed that the strong IC binding of SlanMo is exerted by CD16 and that additionally the IC-induced haptokinesis is CD16-mediated. Therefore, it was examined whether the IC-induced transmigration of SlanMo is also driven via CD16. To investigate which FcγRs are involved in detecting, binding and transmigrating toward ICs, blocking antibodies against FcγRI, FcγRII and FcγRIII were used. Before seeding SlanMo on top of the neuroprobe membrane, they were incubated with the according blocking antibody, washed and then exposed to the IC gradient. Blocking antibodies against FcγRI and FcγRII did not show significant differences to untreated SlanMo and still a 4.0 ± 0.4 - and 4.2 ± 1.0 -fold increase in transmigration when compared to background control (Figure 23 A). Untreated SlanMo transmigrated with a transmigration index of 4.9 ± 0.9 toward ICs. When treated with αCD16 blocking antibody prior to transmigration, only a 1.6 ± 0.6 -fold increase in transmigration compared to the background control could be observed, clearly demonstrating that CD16 signalling is necessary for SlanMo to transmigrate toward ICs.

All known chemokine receptors belong to a large protein family called G protein-coupled receptors (GPCR). Upon binding of a chemokine ligand to the receptor, the associated inactive G protein binds to the receptor intracellularly and becomes activated. This activation initiates a signalling cascade, leading to the chemotactic response of the cell. FcγR-mediated signalling on the other hand, involves several kinases including e.g. the tyrosine- protein kinases Lyn and Syk. Through binding of a multivalent ligand (such as an immune complex), several CD16 molecules come into proximity to each other, leading to phosphorylation of their ITAM domains via kinases. This further transduces the signal initiated by IC-binding, ultimately resulting in different cellular processes. Now assuming that the observed transmigration is CD16-dependent, it should not be affected by disturbing any of the chemokine receptor- or GPCR signalling. Therefore, the transmigration experiment using the neuroprobe chamber was repeated in order to investigate the influence of pertussis toxin (ptx), a well described inhibitor of the GPCR-signalling pathway, on the IC-induced transmigration of SlanMo. In this experiment, ptx-treated SlanMo transmigrated significantly worse toward fractalkine, compared to untreated SlanMo (Figure 23 B). Figure 23 A and B show the quantification of transmigration rate as transmigration index. This metric is a ratio between transmigrated cells of experimental conditions and transmigrated cells of the control condition. This provides a normalized value indicating the extent of migration induced by the stimulus, with a transmigration index of 1 meaning no effect. It was chosen in this case because the results obtained by three different donors showed very similar trends but differences in magnitude, reflecting donor variability in this experiment.

The transmigration index for SlanMo transmigrating toward fractalkine was 7.4 ± 2.1 and decreased to 2.9 ± 0.8 when SlanMo were pretreated with ptx. When transmigrating toward ICs, an inhibitory effect of ptx could not be observed as the transmigration index for SlanMo transmigration toward ICs was 4.1 ± 0.6 and changed to 4.6 ± 0.7 for ptx-treated SlanMo. These findings further confirm that the migration toward ICs is driven by CD16 signalling.

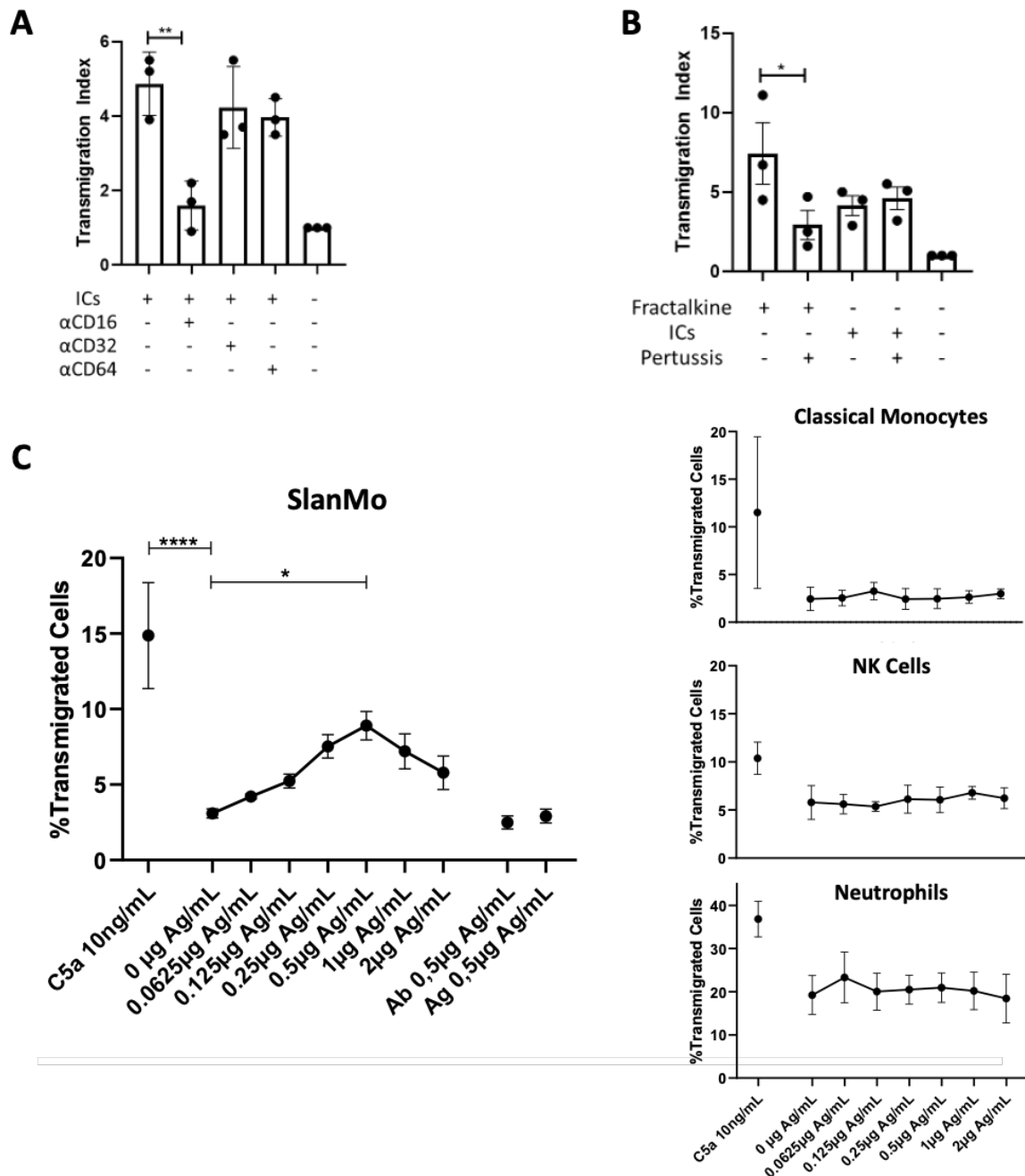


Figure 23. IC-induced transmigration of SlanMo is CD16-dependent, GPCR-independent and occurs only in SlanMo but not in classical monocytes, neutrophils or NK cells. **A** Quantification of SlanMo transmigrating toward ICs with or without blocking Fc γ RI, Fc γ RII or Fc γ RIII using 10 μ g/mL blocking antibody. **B** Comparison of transmigration of SlanMo toward ICs or fractalkine when SlanMo are treated with Pertussis toxin before seeding. **C** Transmigration of SlanMo toward serial dilutions of ICs compared to transmigration of classical monocytes, NK cells and neutrophils to same concentrations of ICs. 4 experiments with 4 different donors were pooled and mean \pm SEM are shown. Significant differences were tested by Dunnett's 1-way ANOVA. Mean of each column was compared with the mean of control column (-/-/-) for **A** (-/-/-) for **B** and 0 μ g ag/mL for **C**, (***) p <0.001; (**) p <0.01; (*) p <0.05).

After thoroughly investigating the IC-induced transmigration in SlanMo, I sought out to examine whether this could also be observed in other CD16-expressing cells, i.e. neutrophils and NK cells and in classical monocytes as this is a precursor cell, closely related to NCMs. To ensure a thorough investigation of whether ICs could induce a trans migratory response in these other cell types, ICs were serially diluted and a wide range of IC concentrations was tested. Additionally, 4 donors were used for this experiment and the 4 cell types were isolated from each donor. For SlanMo a significant difference was measured between background transmigration at 0 $\mu\text{g ag/mL}$ and transmigration at 0.5 $\mu\text{g ag/mL}$. $6\% \pm 0.1\%$ of SlanMo transmigrated without any stimulus and $8.9\% \pm 0.8\%$ were captured in the receiver well using 0.5 $\mu\text{g ag/mL}$ IC. Noticeably, a bell-shaped dose response curve was observed using SlanMo. The other three cell types, namely classical monocytes, NK cells and neutrophils did not show any significant differences between background transmigration and transmigration induced by any IC concentration. Interestingly, classical monocytes and NK cells showed similar background transmigration activity as SlanMo, with $2.5\% \pm 1.2\%$ for classical monocytes and $5.8\% \pm 1.7\%$ for NK cells compared to $2.6\% \pm 0.1\%$ for SlanMo. Neutrophils on the other hand, showed a background transmigration of $18.9\% \pm 4.1\%$.

3.4 Transcriptomic Analysis of IC-induced Migration in SlanMo

So far, many unique properties of SlanMo interacting with ICs have been examined and discovered in this work. I could show that SlanMo bind ICs with a strong affinity, SlanMo uniquely migrate on immobilized ICs and transmigrate toward ICs. These findings strongly suggest a crucial role of these cells in recognizing and responding to ICs in a biological or potentially pathogenic setting. However, these results remain findings from *in vitro* experiments and are therefore only of limited predictive value when it comes to defining their role in any IC-related biological process. The use of mouse models of immune complex-induced inflammation, such as the RPA reaction, was the first logical attempt to confirm the previous findings in a biological, *in vivo* setting. Unfortunately, no conclusive results regarding the biological relevance of non-classical monocyte-IC interactions could be obtained. Therefore, it was decided to perform transcriptomic analysis of human SlanMo next. The aim of the transcriptome analysis of human SlanMo migrating on immobilized ICs, was to first identify a gene signature of IC-induced migration in SlanMo and second to investigate whether this gene signature could be found in any biological processes or diseases. This approach allows for the exploration of a potential involvement of SlanMo in immune complex-related processes and may help link the *in vitro* findings to broader *in vivo* mechanisms.

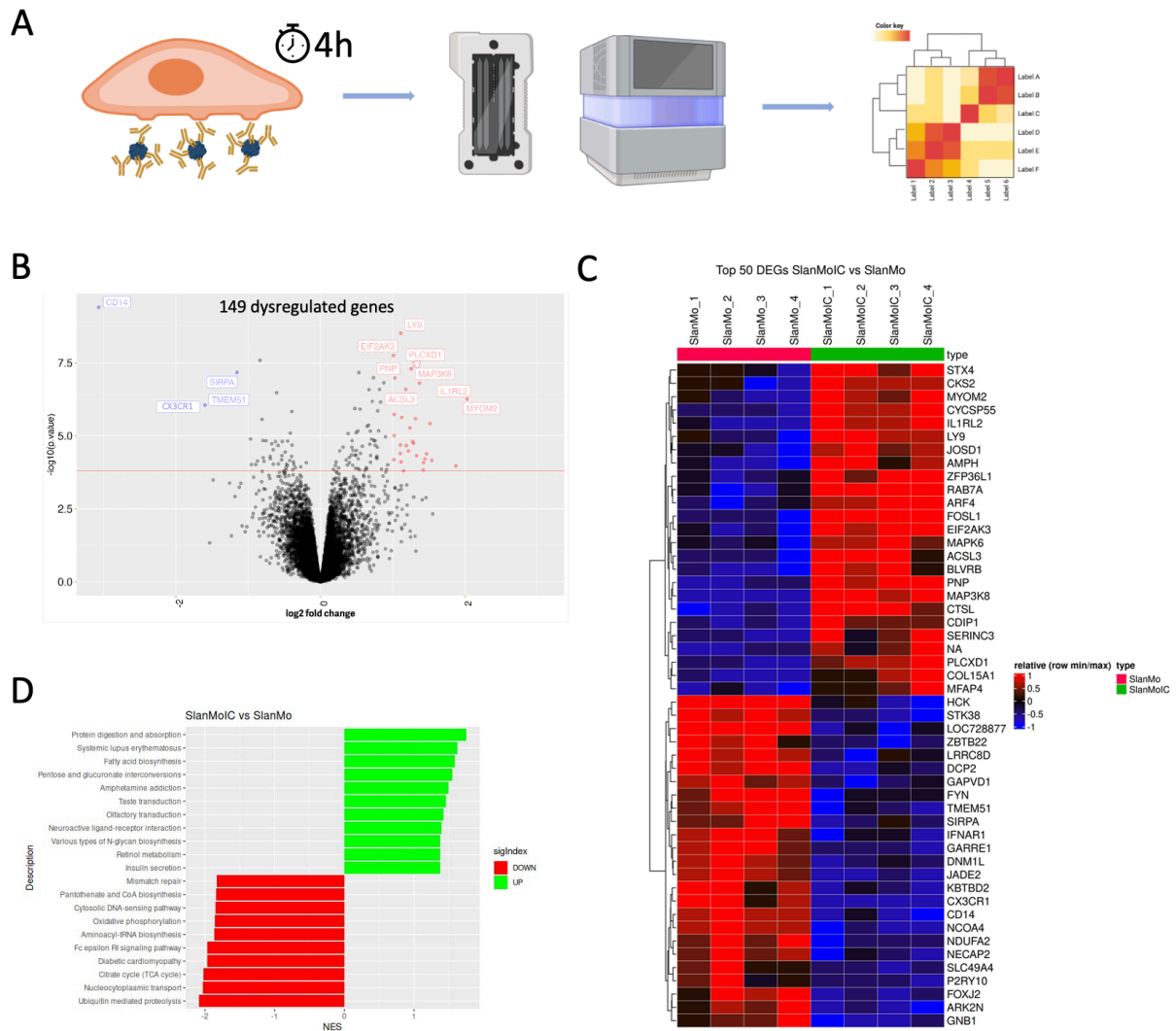


Figure 24. Transcriptomic analysis of IC-induced migration of Slan+ non-classical monocytes. **A** Schematic illustration of experimental setup. SlanMo were seeded on IC-coated surface, incubated for 4h, 37°C and compared to SlanMo seeded on an uncoated surface using Illumina bulk RNA-sequencing. Created with BioRender.com. **B** Volcano plot showing 149 significantly dysregulated genes of SlanMoIC group. **C** Heat map showing 50 most dysregulated genes (25 most up- and 25 most downregulated genes) ranked by q-value. **D** GSEA analysis showing 10 most up- and 10 most downregulated KEGG pathways comparing SlanMoIC and SlanMo groups.

To obtain the transcriptome of IC-induced migration in SlanMo, SlanMo were isolated and seeded on immobilized ICs for 4 hours (Figure 24 A). This short-term stimulation was chosen to capture early transcriptional changes induced by ICs. Illumina sequencing was then performed, and subsequent differential gene expression analysis identified genes significantly altered in IC-stimulated SlanMo (referred to as SlanMoIC) compared to control SlanMo without IC exposure (referred to as SlanMo). Importantly, 6 different conditions were run and sequenced in parallel. To identify a gene signature specifically induced by ICs, an LPS stimulation of the same cell type was included as a broad inflammatory stimulus (referred to as SlanMoLPS). This allowed for the differentiation of an IC-specific gene signature from a general inflammatory response in SlanMo. In addition to these different conditions in SlanMo, classical monocytes were treated and analysed in the same manner (referred to as CD14, CD14IC and CD14LPS). With CD14+ classical monocytes, a different cell type closely related to SlanMo was included to delineate a SlanMo-specific gene signature response to ICs. The

planning and execution of the experiment, up to obtaining the raw and unprocessed list of the assessed genes, was performed by a former PhD student Hao Zhang.

Differential gene expression (DGE) analysis was performed to identify significant transcriptional shifts in SlanMoIC compared to SlanMo, revealing 149 differentially expressed genes (DEGs) (adjusted p-value < 0.05). Of these 149 DEGs, 54 genes were significantly down regulated, and 95 genes were significantly upregulated. Visualizing significantly dysregulated genes with a high fold change in expression compared to the SlanMo group (Figure 24 B) identified interesting genes involved in many different cellular and biological processes. CD14 expression was greatly reduced in SlanMoIC (0.12 fold change, log₂ fold change = -3.07) to only 12.4% of the initial expression level. CD14 acts as a pattern recognition receptor that recognizes LPS from gram- bacteria, helping monocytes to recognize and respond to invading pathogens. Another receptor, CX3C motif chemokine receptor 1 (CX3CR1) was downregulated to 31.2% (log₂ fold change = -1.69) of the control level of SlanMo. This receptor is also called fractalkine receptor and mainly involved in the recruitment of leukocytes via chemotaxis. Upregulated genes included MYOM2 (4.1-fold, log₂ fold change = 2.03); IL1RL2 (3.2-fold, log₂ fold change = 1.67); LY9 (2.2-fold, log₂ fold change = 1.11); and EIFAK3 (2-fold, log₂ fold change = 1.01). IL1RL2 encodes a decoy interleukin 1 receptor. Interestingly, soluble IL1RL2 has been identified as a marker, distinguishing active from inactive SLE, with higher expression in inactive disease patients¹¹⁰. The Ly9 protein (CD229), among other functions, was identified as an inhibitory receptor crucial in preventing autoimmunity, as Ly9-deficient mice developed features of systemic autoimmunity, e.g. anti-nuclear antibodies¹¹¹. EIF2AK3 belongs to a kinase family and plays a crucial role in cellular stress response¹¹². It is involved in reducing global translation and therefore conserving cellular resources during stress responses.

The volcano plot shown in Figure 24 B, shows a summary of 4 biological replicates performed for the SlanMoIC against SlanMo conditions. To visualize a more detailed expression pattern of each donor, a heat map representation of the differential gene expression analysis was chosen, too (Figure 24 C). It shows the top 50 dysregulated genes, by including the 25 most up- and 25 most down regulated genes ranked according to t-value, a measure of statistical significance. Further significantly dysregulated genes could be identified this way. An interesting gene candidate upregulated in SlanMoIC is Cathepsin L (CTSL). It is 2.5-fold upregulated and involved in lysosomal protein degradation. Furthermore, it was shown in mice lacking cathepsins, that they are crucial in the degradation of ICs, internalized by FcγRs of APCs (Driessen et al., 2001). Other upregulated genes that are of potential interest are RAB7A and AMPH. RAB7A encodes for Rab7a, a small GTPase that is involved in cell migration, lysosomal biogenesis and late endocytic pathways (Margiotta et al., 2017) (Guerra & Bucci, 2019). Lysosomal biogenesis refers to the process of lysosome assembly and is involved in protein digestion and recycling, whereas late endocytic pathways correspond to protein trafficking to late endosomes and lysosomes for degradation. The gene product of another gene, AMPH is amphiphsin which was shown to be essential for phagocytosis by mediating actin polymerization (Yamada et al., 2007).

To better interpret the biological significance of these DEGs a gene set enrichment analysis (GSEA) was performed (Figure 24 D). While DGE analysis identifies single dysregulated genes between two experimental conditions, GSEA provides a broader context by highlighting entire biological pathways or gene sets affected by the change in conditions (migration on ICs in this case). The 2 biological processes with the highest normalized enrichment score (NES) were “protein digestion and absorption” and “systemic lupus erythematosus”, which nicely related to prior findings, as the previously defined DEGs e.g. CTSL, RAB7A, IL1RL2 and LY9 are genes related to phagocytosis, protein digestion, autoimmunity and SLE. Furthermore, SlanMo migrating on ICs have already been shown to internalize ICs during this process (Figure 20).

Since SLE is a model disease for IC-mediated inflammation, a closer investigation of the SLE gene set enrichment of IC-induced migration in SlanMo was performed. The Kyoto Encyclopedia of Genes and Genomes (KEGG) SLE gene set is a list of 139 genes, which are defined to be involved in SLE. KEGG is a database that organizes genes into pathways based on their known biological functions and was used as resource to analyse which pathways are impacted in the experimental condition SlanMoIC. An enrichment of the SLE gene set could be confirmed among the significantly upregulated genes of all DEGs in SlanMoIC (Figure 25 A). The enrichment analysis first ranks all DEGs according to significance and fold change, meaning that significantly upregulated genes stand on top of the list and significantly down regulated genes are at the bottom of the list. This ranked gene list is now placed horizontally and the position of each gene of the tested gene set (SLE gene set) is marked as a black bar on the ranked gene list, resulting in a bar code pattern. The red line represents the enrichment score (ES), which reflects how the genes in the SLE gene set are distributed among the ranked list of all genes in the dataset (Figure 25 A, left image). The peak in the enrichment score near the top of the ranked gene list (left side) suggests that genes in this set are enriched among the upregulated genes of the SlanMoIC analysis. Key statistics of this analysis include the False Discovery Rate (FDR) and the Normalized Enrichment Score (NES). The FDR is 0.013 for this analysis, indicating that this result is statistically significant, when adjusted according to multiple testing. The NES is normalized to account for differences in gene set size and allows comparison between different gene sets. The NES of 1.6 in this data set indicates a moderate positive enrichment of the SLE gene set in the DEGs of SlanMoIC. The heat map in Figure 25 A shows the dysregulation of the leading edge genes contributing most to the SLE gene set enrichment in SlanMoIC. In GSEA, leading edge genes are a subset of genes that, within the enriched gene set, contribute most to the enrichment score. They are positioned at the peak of the enrichment curve (red line) and in the context of this study, represent those most strongly associated with the SLE phenotype. Interestingly, among the 45 upregulated leading edge genes strongly contributing to the positive enrichment of the SLE gene set, are many histone- and HLA genes, i.e. H2AC20, H2BC8, H3C10, HLA-DRB5 and HLA-DQA2. Also, TNF is upregulated in SlanMoIC and nicely links SlanMo-IC interactions with SLE disease since engagement of immobilized ICs induces the production of TNF α in SlanMo⁷⁷ and increased levels of TNF- α have been found to be associated with disease severity in SLE patients.

comparing leading edge gene expression of SLE enrichment between all experimental groups. SlanMoIC group (green box) shows negatively enriched cluster and positively enriched cluster.

To ensure that the positive enrichment of the SLE gene set in SlanMoIC is truly specific to SlanMo as well as to IC, the leading edge gene expression fold change was compared to the conditions SlanMoLPS, CD14, CD14IC and CD14LPS. The SlanMoIC signature of the first 10 leading edge genes being downregulated and the other 45 genes being upregulated (Figure 25 C, green box) is unique to SlanMoIC. The genes UBE21, KLHL9 and UBE2M are similarly downregulated in SlanMoLPS but the other leading edge genes do not differ from SlanMo control group. Interestingly, TNF expression is lowest in CD14 control group and CD14IC, hinting towards the lack of IC-recognizing FcγRIII in classical monocytes. Correspondingly, the expression of the 55 leading edge genes is very similar between CD14 and CD14IC, confirming that ICs might not be able to activate classical monocytes.

In addition to “Systemic Lupus Erythematosus”, the KEGG pathway “Protein digestion and absorption” showed the highest NES during GSEA (Figure 24 D). Therefore, the enrichment analysis and the leading edge genes were closely investigated (Figure 25 B). With an NES = 1.68 the gene set is moderately enriched but the FDR = 0.015 indicates a highly significant finding. Interestingly, among the 29 leading edge genes are 11 collagen α chains (COL6A3, COL4A1, COL11A1, COL9A3, COL22A1, COL11A2, COL2A1, COL26A1, COL9A1, COL18A1, COL15A1). Furthermore, 7 leading edge genes encode different proteases and peptidases (CTRB2, MEP1B, PGA3, CPB2, CPA1, CPA3, CTRB1) which aligns with the hypothesis, that these cells are endocytosing, digesting and therefore removing ICs during their migration process.

To further confirm that the SLE gene set enrichment as well as the protein digestion and absorption gene set are unique to SlanMoIC, the NES and FDR of SlanMoIC, SlanMoLPS, CD14IC and CD14LPS for these gene sets were investigated and plotted using a bubble plot visualization (Figure 25 D). This visualization shows that regarding SLE and protein digestion and absorption pathways, SlanMoIC is the only condition for which FDR < 0.05 and NES > 1. This means that only SlanMoIC shows a significant, positive enrichment for these two KEGG pathways. Toll-like receptor signalling pathway, NF-kappa B signalling pathway and legionellosis were included for better understanding of the performed analyses. Notably, the CD14IC condition only shows FDR > 0.5 for all mentioned gene sets, meaning that there is a chance > 50% that the shown NES are random. This further aligns with the notion that SlanMo, but not CD14⁺ classical monocytes are capable of recognizing and responding to ICs. Toll-like receptor signalling pathway shows a NES > 1 and an FDR < 0.05 for both LPS conditions, namely SlanMoLPS and CD14LPS. This finding is supported by the fact that LPS binds to toll-like receptor 4 and further triggers pro-inflammatory responses. NF- κ B signalling pathway and legionellosis are also significantly and positively enriched in both LPS containing conditions. NF- κ B plays a key role in regulating the immune response to infection and therefore associates with a cellular response to LPS. Also, legionellosis, which is caused by gram negative bacteria containing LPS in their outer cell membrane resembles a biological process of which involved genes can be expected to be enriched in SlanMo and classical monocytes treated with LPS.

Summarizing the key findings of the transcriptomic analysis of IC-induced migration in SlanMo, 149 genes are significantly dysregulated in SlanMoIC, of which several are involved in phagocytosis, protein degradation and autoimmunity. Furthermore, GSEA revealed a positive enrichment of the KEGG gene sets for protein degradation and absorption together with SLE only in SlanMoIC but not in SlanMoLPS, CD14IC or CD14LPS. These findings suggest a strong link between IC-induced migration and protein degradation as well as autoimmunity.

4. Discussion

The aim of my thesis was to elucidate the mechanisms behind IC-induced migration in SlanMo. Investigating the unique responses of SlanMo to ICs, I could reveal novel insights into their migratory behaviour, phagocytic capabilities, and transcriptional adaptations. These findings add to our understanding of NCM function and their roles in vascular homeostasis and IC-mediated diseases such as SLE. This discussion now aims to position these findings within the broader context of the current scientific understanding. This will be done in the first two sections “NCMs in intravascular immunity” and “NCMs in SLE”. The following sections will critically evaluate individual findings, address potential limitations and alternative interpretations.

4.1 NCMs in Intravascular Immunity

The immune system provides an essential defense against invading pathogens and must function in many different tissues and parts of the body. To evade immune responses, bacteria and viruses have evolved many strategies, including their dispersion and escape via spreading into various tissues through the blood circulation. It is therefore crucial that blood vessels are patrolled by immune cells to continuously protect the host. The findings presented in this thesis contribute to the understanding of NCMs' role in this intravascular immunity.

In a hallmark study in 2007, Auffray et al.¹⁵ established that NCMs exhibit a patrolling behaviour on the endothelium, even in the absence of inflammation. Since then, several other studies have further investigated NCM function in the vasculature. Importantly, the vasculature has been identified as their niche, as NCMs constantly receive survival signals through their patrolling activity and by scavenging components from the endothelium⁶². Exemplary studies could show that during their patrolling, NCMs also remove potentially harmful agents from the vasculature by internalizing them while migrating and even continue to migrate while carrying their cargo. In a mouse model of vascular necrosis, NCMs could be observed phagocytosing cellular debris, suggesting a safe disposal of potentially harmful damage-associated molecular patterns, such as histones and DNA fragments⁴⁸. Moreover, real-time in vivo imaging has shown that patrolling NCMs remove amyloid beta (A β) deposits from vein endothelium via internalization after being attracted to A β ⁺ vessels and crawling onto A β -aggregates¹¹³. In another study, it was observed that NCMs patrolling the lung vasculature, engulf metastatic tumor cells, proceed to migrate on the endothelium and therefore prevent spreading of cancer cells throughout the vasculature⁶⁴. The findings in this thesis, that NCMs migrate on immobilized ICs and internalize them during migration adds on to their importance in intravascular immunity and aligns with the previous findings. Additionally, their gene expression changes investigated in section 3.4 reveal a downregulation of pro-inflammatory mediators. Thereby, key results of this work have shown that NCMs are removing potentially harmful ICs from the vasculature during migration while promoting an anti-inflammatory immune response, a finding that aligns with and supports the current scientific understanding of NCMs as scavengers maintaining endothelial homeostasis.

In this thesis, the haptotaxis of SlanMo, the prototypical NCM in the human immune system, has been thoroughly investigated. Interestingly, haptotaxis has recently been described as a key effector function of in the vasculature, where platelets perform haptotaxis safeguarding inflamed blood vessels^{114,115}. Similar to the findings regarding IC-induced migration of SlanMo in this thesis, platelets show a patrolling behaviour after adhesion and spreading on immobilized fibrin. This process is associated with a characteristic change in platelet morphology, where spreading platelets initially exhibit a flat, adherent, 'fried-egg-like' morphology before polarizing by extending one side of the lamellipodium while simultaneously retracting the rear end. This process of changing to adherent morphology and polarization is also observed in SlanMo seeded onto ICs. Parallel to SlanMo migrating only on immobilized ICs but not on other substrates, platelets adhere to and initiate migration only on immobilized fibrin. Furthermore, platelets sense and migrate along gradients of fibrin, which *in vivo* helps to limit damage associated with inflammation. In particular, platelets can migrate along this gradient to detect and seal holes in the vasculature caused by transmigrating leukocytes¹¹⁶. These findings suggest that haptotaxis is a conserved migratory mechanism potentially special to the vasculature to maintain vessel integrity. In this work, haptotaxis of SlanMo could not be observed *in vitro* and was not investigated *in vivo*. Limitations of the *in vitro* studies are discussed in section 4.4.

In my thesis, the observed directed transmigration toward ICs could be a result of either chemotaxis or haptotaxis. As most chemokines bind substrates of the extracellular matrix (ECM), such as sulfated sugars of the glycosaminoglycan family¹⁴, it is reasonable to assume that immobilization and therefore haptotaxis plays a critical role *in vivo*. Indeed, up to date there are three examples in which the phase of functional chemokine gradient distribution has been directly examined *in vivo*, revealing immobilized but not soluble chemokine patterns. For example, Schwarz *et al.* investigated CCL21 distribution in the dermal interstitium of explanted mouse ears and observed tissue-immobilized CCL21 gradients, with concentrations diminishing progressively with increasing distance from the lymphatic vessels, the primary source of CCL21²⁷. Sarris *et al.* used a zebrafish model and established proof that CXCL8 forms tissue-bound gradients *in vivo*, by binding to proteoglycan structures such as heparan sulfate¹¹⁷. Findings from Weber *et al.* support the notion of tissue- or proteoglycan-bound chemokines *in vivo* by showing that interstitial CCL21 is immobilized to heparan sulfate¹¹⁸. These studies verified that chemokines most likely occur in an immobilized form in the ECM of tissues. Similarly, protein binding proteoglycans, glycoproteins and heparan sulfate are integral components of the endothelial glycocalyx. The endothelial glycocalyx is a complex, membrane bound layer of proteins and carbohydrates covering the whole niche of NCMs - the vasculature¹¹⁹. Even though no direct reports of the glycocalyx directly binding ICs exist, it has been shown that single components of it, such as heparan sulfate, could remove and bind CR1-bound ICs from erythrocytes. Therefore, the endothelial glycocalyx could indeed be a scaffold for IC deposition and provide a surface for NCM migration *in vivo*. Alongside resident macrophages, which clear large insoluble IC structures from the bloodstream, and

erythrocytes, which bind and remove small ICs, patrolling NCMs could be responsible for removal of ICs bound to the vasculature via the glycocalyx.

In parallel, with the potential role of NCMs clearing ICs bound to the vasculature, emerging studies on the dynamics of chemokine gradients *in vivo* provide a new perspective on the complex interplay between immobilized and soluble chemokines. Established by Schumann *et al.* and Alanko *et al.*^{120,121}, immobilized chemokines can be cleaved off from a surface to form soluble chemokines. Additionally, the migrating cells actively shape and modulate gradients of soluble chemokines by internalization of receptor-bound chemokines. They are therefore locally depleting the environment of the chemokine and acting as a “sink”, creating a local gradient. Another layer of complexity is added by Aronin *et al.*, showing that stable gradients fail to induce persistent directional migration and instead a temporally rising chemokine concentration is needed for long-range myeloid cell migration¹²². Taken together, these findings reveal a dynamic interplay between immobilized and soluble chemokines, where the cleavage of immobilized chemokines into their soluble form and the active internalization of receptor-bound chemokines by migrating cells collectively shape the chemokine landscape. This dynamic process establishes localized gradients that guide collective immune cell migration with high precision. Furthermore, the studies show that the gradients locally generated by internalization of chemokines, can be used as guidance cues for other cells, i.e. T cells¹²¹. Also, since the gradients are created by cells which are depleting their environment of the chemokine, the shaping of the gradient is greatly influenced by cell density and can become a self-enforcing mechanism. Such mechanisms emphasize the active role of migrating cells not only as responders but also as modulators of their chemotactic environment, shaping the collective migration of immune cells. The additional requirement of temporal dynamics in chemokine concentrations for persistent myeloid cell migration greatly emphasizes the complexity and challenges of investigating haptotactic and chemotactic properties of ICs.

Even though it could not fully be resolved whether haptotaxis or chemotaxis are underlying mechanisms, it was clearly observed that ICs attract SlanMo in a gradient-dependent manner. This can be considered as alternative, less inflammatory route to the current notion, that ICs activate the endothelium via upregulation of adhesion molecules and chemokines, e.g. during SLE¹²³. This also has potential implications for translational research. Understanding the mechanisms by which NCMs interact with ICs provides a foundation for developing targeted therapies aimed at modulating their activity. For example, enhancing the IC-clearing capacity of NCMs while suppressing their pro-inflammatory responses could exploit their unique migratory response and represent a novel therapeutic strategy for IC-mediated diseases. In addition, the migration of SlanMo on ICs and their distinct transcriptional signature could be used as potential biomarker for IC-mediated disease activity.

Translating these insights into therapeutic strategies requires to address major challenges in research. The following sections evaluate key individual findings and address limitations of the methods used. This can help to design future experiments to further investigate the role of NCMs in IC-mediated disease. A primary example of technical challenges is the usage of ICs in

current research. It requires a collective agreement on critical factors, such as glycosylation, size, solubility and the reliance on rabbit IgG, which should be replaced with human IgG for improved translational relevance.

4.2 NCMs in SLE

GSEA of SlanMo migrating on immobilized ICs revealed a significant enrichment of the SLE gene set. Even though numerous studies have shown an involvement of NCMs in SLE, a defined pathophysiological role of NCMs remains unclear. Theories on monocyte involvement in SLE can be broadly categorized into two classes: defective monocytes and activated monocytes in SLE¹²⁴. Defective clearance and phagocytic function of monocytes represents the hallmark of the “defective monocyte” model in SLE. Older theories, which were formulated in the 1980’s suggest that defective phagocytosis leads to the accumulation of apoptotic debris¹²⁵⁻¹²⁸. This debris is an important source of autoantigens with the potential to trigger severe autoimmune reactions as observed in SLE. Furthermore, the defective clearance of ICs can lead to the activation of FcγR-expressing cells and induce severe tissue damage. Recent studies on the other hand suggest an active role of monocytes in SLE, with NCMs displaying an activated, inflammatory phenotype¹²⁹ and causing tissue inflammation⁴⁹. Recently, it has been shown that there is an expansion of NCMs expressing slan in SLE patients, which is associated with lupus nephritis¹³⁰. Additionally, our group has shown that SlanMo are recruited by deposited ICs, accumulate in the kidney of lupus nephritis patients, and are activated by ICs to produce proinflammatory cytokines such as TNFα, IL-6 and CXCL2⁷⁷. Transcriptomic analysis of NCMs of SLE patients identified <1100 DEGs in NCMs and that among all monocyte subsets, they exhibit the largest amount of DEGs¹²⁹. This suggests an extensive reprogramming of especially NCMs in SLE. The proinflammatory and disease-driving activity of monocytes in SLE is further underlined by the outcome of a pilot clinical study conducted in 18 SLE patients. The aim of the study was to investigate the effects of selective removal of monocytes (and granulocytes) from patients with active SLE¹³¹. The selective removal of these cells was associated with a significant clinical improvement in these patients, without any adverse effects. This study further points toward an active role of monocytes in SLE and does not support the “defective monocyte” model.

Our transcriptomic analysis of SlanMo migration on ICs suggests a rather protective role of NCMs in SLE. The experimental setting of SlanMo migrating on ICs can be placed in a progressed disease state, where extensive IC deposits have already formed and attracted SlanMo as shown in Olaru et al.⁷⁷. Our results show a downregulation of proinflammatory cytokine receptors (CD14, IFNAR1, CX3CR1), and an upregulation of genes involved in the clearance and endocytosis of ICs (CTSL, RAB7A, ARF4). Additionally, genes inhibiting endocytosis were significantly downregulated (NECAP-2, SIRPα), indicating enhanced capabilities to remove ICs. Ly-9, a cell surface receptor which has recently been shown to reinforce tolerance and to protect from autoantibody responses¹¹¹ was also among the 25 most upregulated genes in SlanMo migrating on ICs. These findings indicate an anti-inflammatory role for NCMs as the downregulation of proinflammatory cytokine receptors

decreases their responsiveness and capability to induce inflammation. They also suggest a contribution to the resolution and healing from SLE by endocytosing and removing harmful ICs from the vasculature.

Transcriptomic and proteomic profiling of NCMs in lupus patients revealed increased proinflammatory cytokine production and type-I interferon signalling¹²⁹. These results seem to contradict our results at first but could also highlight important dynamic changes of the role of NCMs during SLE initiation, progression and remission. In general, studies regarding the role and the abundance of NCMs in lupus come to very different conclusions. Some studies find a decreased number of NCMs in SLE patients¹³²⁻¹³⁴, whereas other studies correlate increased numbers of NCMs with SLE^{79,130}. Additionally, studies show age-related differences regarding the role of NCMs in SLE, as Peckham et al. found higher percentages of pro-inflammatory CD16+ monocyte subsets in adult-onset lupus compared to juvenile-onset patients¹³⁵. Moreover, gene expression patterns of NCMs in SLE patients were shown to vary based on disease activity, interferon levels, and medication use¹³⁶. These results from cited studies emphasize the complexity of the investigation of NCM involvement in SLE but also highlight NCMs importance in SLE.

4.3 Challenges and Advances in Usage of Human IgG ICs

The ICs used in this study mainly bound to the CD16-expressing leukocytes neutrophils, NK cells, NCMs and intermediate monocytes. While the superior binding of hIgG1 and hIgG3 by FcγRs is consistent with many studies and current scientific understanding⁹⁵, the poor binding of ICs to the other FcγR-expressing cells, such as different DC subsets, classical monocytes, eosinophils and B cells was unexpected. Hellman *et al.* show an efficient binding and uptake of ICs by classical monocytes and myeloid DCs, reaching >30% of cells with internalized ICs under certain conditions¹³⁷. The ICs used in the cited study were formed by incubating α-ovalbumin (OA) polyclonal rabbit IgG and fluorescently labelled OA. By using polyclonal antibodies, very large ICs which form lattice structures are used. This greatly differs to my experiments, in which small, soluble ICs were generated by using monoclonal antibodies and pretested stoichiometric concentrations. It is highly likely, that the differences in IC size led to different binding properties. This is supported by Lux *et al.*¹³⁸, who utilize ICs consisting of a hapten labelled antigen and a hapten-specific human IgG subclass-antibody and vary the size of the ICs by using antigens with different hapten loading ratios. They verify that IC binding to FcγRs increases with IC size. Taking this into consideration, it is reasonable to assume that the smaller ICs used in this study, facilitate interaction with cells that have a high affinity for ICs but might be too small to be bound by cells with weaker affinity, i.a. classical monocytes.

Almost all studies investigating the biological activity of ICs have traditionally used polyclonal rabbit IgG to generate these complexes. It can be inferred that inherent differences in the amino acid sequence¹³⁹, glycosylation¹⁴⁰, and aggregation properties¹⁴¹ between rabbit and human IgGs lead to differences in their binding to FcγRs. Nonetheless, current understanding of IC binding and activation of leukocytes, as well as animal models used to investigate IC-mediated disease, is based on findings generated using polyclonal rabbit IgG. Consequently,

the use of ICs formed with human IgGs may lead to results that differ from those reported in earlier studies using rabbit IgG. This shift is not unexpected, and the introduction of human IgGs in the study of IC-cell interaction should rather be seen as a significant advancement.

The experiments in this work do not capture the influence of Fc- and FcγR-glycosylation on IC binding, even though they have been shown to directly participate and modulate IgG binding to FcγRs^{142,143}. This drawback is currently not addressed in any studies investigating IC-mediated disease and could be addressed by either directly purifying ICs from SLE patients or isolation of total IgG and subsequent incubation with nuclear antigen, i.a. Sm/RNP to generate lupus-like ICs with a human Fc glycosylation pattern as done by Bonegio *et al.*¹⁴⁴.

The experimental setup in this thesis still bears several strong advantages over other studies investigating IC binding to cells or FcγRs. Here, ICs containing human IgGs were used to investigate the binding to human leukocytes in whole blood. Additionally, this setup considers binding of ICs to whole cells and is not limited to single FcγRs. Paired with simultaneous binding to all FcγR-expressing leukocytes and allowing competition for IC binding under physiological cell composition, results in a greater predictive value when it comes to translation of these findings to pathological settings and treatments. Up to date, there is no study combining the use of human IgG ICs in a whole cell-based approach, since studies so far used either rabbit IgG ICs or investigated binding to single FcγRs recombinantly expressed on cell lines^{95-97,145-147}.

4.4 IC-induced Migration of SlanMo

The most crucial finding of this work is that ICs attract SlanMo in a way that is comparable to chemokines. In a transmigration assay, SlanMo uniquely transmigrated toward ICs in a gradient-dependent manner, meaning that they transmigrated to higher concentrations of ICs. After observing that immobilized ICs induce a haptokinetic response in SlanMo, it was hypothesized that via passive diffusion and adsorption, an immobilized gradient forms on top of the membrane in the transmigration assay. It is important to mention that the experiments performed, could not unravel whether the observed directed transmigration is due to a gradient of immobilized or soluble ICs. The generation of an immobilized IC gradient by UV-based photo micropatterning was performed to investigate this phenomenon, but a directed migration toward higher concentration of ICs on an immobilized gradient could not be observed in SlanMo. The designed gradient was of a linear profile with unknown concentrations of immobilized ICs. However, several IC concentrations were tested for the coating of the activated surface. Additionally, IC-induced migration on immobilized ICs was observed on concentrations spanning a 1000-fold dilution range. Therefore, it is unlikely that the lack of directed migration is due to insufficient IC concentration. However, a potential bottleneck in the investigation of a SlanMo haptotaxis on immobilized ICs is the steepness and the profile of the gradient. In vivo, a gradient is established as molecules diffuse away from a source (e.g. a secreting cell) into surrounding tissues. It is rarely linear but typically follows an exponential profile. This results from the combined effect of diffusion according to Fick's law¹⁴⁸ and the enzymatic digestion and binding as the molecule diffuses across the tissue.

Schwarz *et al.* have conclusively demonstrated that haptotaxis strongly depends on the gradient shape²⁷. They showed that DCs migrate along an exponential, *in vivo*-like gradient but not along a linear gradient of immobilized CCL21. In this thesis, only linear gradients were tested for the induction of a haptotaxis in SlanMo. Unfortunately, these linear gradients poorly recapitulate *in vivo* characteristics of chemokine gradient and are not sufficient to properly investigate whether SlanMo perform haptotaxis on ICs. Since the detection of a concentration difference across the cell's diameter is a prerequisite for directed cell migration^{20,149}, exponential gradients provide a more physiologically relevant environment than linear gradients. Further experiments utilizing immobilized exponential gradients generated with the photo micropatterning technique could help to validate and extend these findings. Unfortunately, these experiments could not be performed as part of this thesis due to the relocation of the necessary equipment to Bayreuth. Future work will be crucial in further exploring and fully addressing whether immobilized ICs can induce a directed migration in SlanMo.

Another suggestion for improvement involves the used micropatterning technique and the utilization of a subtractive gradient. In this work, the surface is partially freed of a continuous inherent PEG layer to enable ICs to adsorb to the glass surface. After gradient patterning, PEG residues remain inside the IC gradient and potentially interfere with SlanMo migration. An additive gradient would be better suited as used in Schwarz *et al.*²⁷. Here, the authors print a gradient of biotin-FITC directly onto a glass surface using a UV beam. The photobleached FITC is activated and binds to the glass surface, creating a biotin patterning copy of the UV mask that was used. The printed biotin gradient is then used as template to create an immobilized chemokine gradient by chemokine-streptavidin addition. This allows for the generation of a gradient without potential interference of inert PEG residues.

Nevertheless, the observed enrichment of SlanMo at higher IC concentrations in transmigration assays remains significant and has important implications for biological processes, regardless of whether the mechanism is chemotactic or haptotactic. Additionally, the exertion of chemotactic properties of ICs on SlanMo indicates a completely new mechanism of cell recruitment to sites of inflammation.

Interestingly, older publications have already mentioned a chemotactic effect of antigen-antibody complexes. Stephen Boyden, the name giver to the Boyden chamber transmigration assay described a transmigration of rabbit granulocytes toward rabbit immune complexes when incubated with medium containing fresh serum but not heat-treated serum¹⁵⁰. This observation likely reflects the ability of ICs to fix early complement proteins from the fresh rabbit serum, thereby initiating the complement cascade and leading to the release of strong chemotaxins, such as C5a and C3a. The ICs would then solely have served as a scaffold to allow the initiation of the complement cascade. A few years later, another group reported about chemotactic effects of ICs and showed that small, soluble antigen-antibody complexes from guinea pigs exert strong chemotactic effects on guinea pig leukocytes despite the lack of strong complement fixation¹⁵¹. However, after generating ICs by incubating antibody and

antigen, they allowed the ICs to react with fresh guinea pig serum which could still potentially lead to a release of C5a and a distortion of the results. Findings generated in this thesis accounted for such potential bystander effects of C5a by using ptx to block any GPCR-dependent effector functions in the transmigration assay, since the C5a receptor belongs to the GPCR family. Furthermore, to address the possibility of migration being driven by secreted factors from IC-activated SlanMo, an experimental setup was designed in which SlanMo migrating on immobilized ICs could potentially activate neighbouring cells, that were not in contact with ICs. This ensured that any migration observed was not due to secondary effects mediated by secreted factors (Figure 18).

Experiments performed in this thesis, clearly indicated that binding of ICs to CD16 on SlanMo is crucial to induce (trans)migration. It is not clear, how IC binding can lead to cell migration in SlanMo. To identify how the activation of FcγRIIIa can lead to cell migration, the signalling pathways of CD16 and of CX3CR1 can be compared. After ligand binding, FcγRIII primarily signals via ITAM domains and the Src-family kinases Lyn and Syk, whereas CX3CR1 signalling occurs through its heterotrimeric G protein complex. The following intracellular signalling then shows great overlap as for example studies demonstrated that Syk, a kinase crucial in FcγR-signalling, is also required for CX3CL1-mediated actin polymerization and chemotaxis¹⁵². Main signalling pathways of CX3CR1 which lead to cell migration and chemotaxis involve PI3K and PLCγ¹⁵³. Those same proteins also play a crucial role in FcγR signal transduction since their activity is increased upon FcγR cross-linking and their function is essential for FcγR-mediated processes, such as phagocytosis¹⁵⁴. Similarly, PLCγ activation occurs after activation of both receptors and leads to the production of diacylglycerol and IP3, which promote calcium mobilization and PKC activation, key steps in cytoskeletal reorganization and cell movement^{155,156}. Furthermore, both signalling pathways require Rac1 and RhoA, which are critical regulators of actin dynamics. This shared reliance on cytoskeletal remodeling highlights the functional overlap between FcγRIII and CX3CR1 signaling in driving migration but does not fully explain how CD16 activation via immobilized ICs can lead to cell migration. Phosphoproteomic analysis of IC-induced migration in SlanMo was performed to unravel the intracellular signalling cascades leading to cell migration. However, due to the complexity of the dataset and the scope of this thesis, a comprehensive analysis could not be completed, and the results are not further discussed here.

4.5 Transcriptomic Analysis

The transcriptome analysis of SlanMo migrating on immobilized ICs revealed many interesting genes that were either significantly down- or upregulated, compared to resting SlanMo. Additionally, classical monocytes showed very little transcriptomic adaptations to ICs, highlighting a potential specialization of SlanMo in IC clearance mechanisms. Among the 25 most downregulated genes was SIRPA. It encodes the transmembrane protein SIRPα which is mainly expressed by myeloid cells¹⁵⁷. This inhibitory receptor contains ITIM domains and additional tyrosine residues in its cytoplasmic region which act as further ITIMs^{158,159}. Downstream signalling of SIRPα involves the recruitment of the phosphatases SHP-1 and SHP-

2, leading to outcomes similar to inhibitory FcγRIIb signalling in B cells. Recently, Morrissey *et al.* could show that SIRPα is a highly efficient suppressor of FcγR-dependent phagocytosis¹⁶⁰. They showed that inactive SIRPα, meaning SIRPα which is not bound by its ligand CD47, is spatially excluded from phagocytosis whereas in the presence of CD47, SIRPα remains at the phagocytic cup. Furthermore, the presence of SIRPα at the phagocytic cup is sufficient to inhibit the engulfment and phagocytosis of silica beads, acting by preventing integrin activation. Additionally, NECAP2 is significantly downregulated and among the 25 most downregulated genes. NECAP proteins negatively regulate clathrin-mediated endocytosis, promoting a closed and inactive conformation of the clathrin complex^{161,162}. In the context of IC-induced migration of SlanMo, this can promote the FcγR-dependent internalization of ICs, since small aggregates such as the ICs used in this study are internalized via clathrin-dependent endocytosis¹⁶³. Only large particulate complexes binding FcγRs, e.g. opsonized cells, lead to a clathrin-independent internalization. Therefore, NECAP2 and SIRPα are examples for suppressive proteins which are downregulated during IC-induced migration of SlanMo- leading to enhanced internalization of ICs.

The other two most downregulated genes in the SlanMoIC group were CD14 and CX3CR1, which encode the receptors for LPS and fractalkine, respectively. Interestingly, both genes are used as markers to distinguish classical monocytes and NCMs and CD14 is only weakly expressed on the SlanMo used in this study. The ligands LPS and fractalkine are both indicators of inflammation. The activation of their respective receptors triggers many pro-inflammatory responses, including cytokine release^{164,165}, activation of the pro-inflammatory transcription factor NF-κB, and the activation of TLRs¹⁶⁶. Moreover, the downregulation of IFNAR1, a subunit of the type-1 interferon receptor, further contributes to the reduced sensitivity of SlanMo to pro-inflammatory signals when migrating on ICs. Additionally, fractalkine acts as a chemokine, guiding SlanMo to sites of inflammation via CX3CR1. Taken together, the downregulation of these pro-inflammatory receptors upon IC-induced migration likely reduces the responsiveness of SlanMo to these potent stimuli and helps to retain them at the site of IC deposition. The suppression of pro-inflammatory responses by downregulation of receptors may be a compensatory mechanism to reduce inflammation during IC-clearance, aligning with the generally accepted anti-inflammatory nature of NCMs. Combined with the downregulation of the endocytosis-inhibiting molecules SIRPα and NECAP2, SlanMo are retained at the site of IC deposition, with the brakes on IC-uptake removed. This could allow for efficient local engagement and removal of ICs while minimizing systemic inflammatory responses.

Strikingly, genes involved in endocytosis are also found among the 25 most upregulated genes. RAB7A for example, a member of the Rab family of membrane proteins, participates in multiple cellular processes, including endosomal sorting, phagocytosis, and the maturation of endosomes^{167,168}. Furthermore, RAB7A is a key regulator for the generation of lysosomes and the fusion of endosomes with lysosomes¹⁶⁹. Deficiency of RAB7A leads to defective lysosomes which do not further fuse with endosomes, impairing the degradation machinery of endocytosed molecules, such as ICs. Also, amphiphysin, a protein encoded by the upregulated

gene AMPH is important during endocytosis. It serves as an adaptor protein, linking the clathrin coat of endosomes to dynamin, a protein which is responsible for the fission of vesicles from the plasma membrane during endocytosis¹⁷⁰. The disruption of amphiphysin-dynamin interactions through recombinantly engineered amphiphysin, inhibited vesicle endocytosis at the stage prior to pinching off vesicles from the plasma membrane, the process exerted by dynamin¹⁷¹. Next to the upregulated genes AMPH and RAB7A, ARF4 is significantly upregulated in SlanMo migrating on ICs. During endocytosis, ARF4 regulated endosome morphology and endosome-endosome fusion^{172,173}. Additionally, the cathepsin L-encoding gene CTSL is upregulated 2.5-fold in the SlanMoIC group. This cysteine protease is contained in lysosomes and therefore plays a major role in the degradation of proteins after endocytosis and subsequent endosome-lysosome fusion^{174,175}. Taken together, the transcriptional adaptations show a coordinated downregulation of inhibitory genes and upregulation of key players in endocytosis as well as a downregulation of pro-inflammatory mediators. This transcriptional program in SlanMo migrating on ICs points to an enhanced capacity for IC uptake and IC degradation.

In conclusion, this thesis provides valuable insights into the role of NCMs in IC-mediated diseases, highlighting their unique migratory behaviour and potential involvement in the removal of ICs from the vasculature. Addressing the technical challenges discussed, such as the use of human IgG and immobilized IC gradient characteristics, will enable a more precise understanding of NCMs' role in IC-mediated disease. These findings can be used for future investigations aimed at developing targeted therapies for autoimmune diseases such as SLE and inflammatory diseases caused by ICs.

5. References

- 1 Thomas, G. D. *et al.* Deleting an Nr4a1 Super-Enhancer Subdomain Ablates Ly6C(low) Monocytes while Preserving Macrophage Gene Function. *Immunity* **45**, 975-987 (2016). <https://doi.org/10.1016/j.immuni.2016.10.011>
- 2 Thucydides. The plague in Athens. Thucydides. The history of the Peloponnesian War. Translated by Thomas Hobbes. *N C Med J* **41**, 230-232 (1980).
- 3 van Furth, R. *et al.* The mononuclear phagocyte system: a new classification of macrophages, monocytes, and their precursor cells. *Bull World Health Organ* **46**, 845-852 (1972).
- 4 Frank, M. M., Joiner, K. & Hammer, C. The function of antibody and complement in the lysis of bacteria. *Rev Infect Dis* **9 Suppl 5**, S537-545 (1987). https://doi.org/10.1093/clinids/9.supplement_5.s537
- 5 Tschopp, J., Masson, D. & Stanley, K. K. Structural/functional similarity between proteins involved in complement- and cytotoxic T-lymphocyte-mediated cytolysis. *Nature* **322**, 831-834 (1986). <https://doi.org/10.1038/322831a0>
- 6 Snyderman, R., Shin, H. S. & Hausman, M. H. A chemotactic factor for mononuclear leukocytes. *Proc Soc Exp Biol Med* **138**, 387-390 (1971). <https://doi.org/10.3181/00379727-138-35903>
- 7 Hampton, H. R. & Chtanova, T. Lymphatic Migration of Immune Cells. *Front Immunol* **10**, 1168 (2019). <https://doi.org/10.3389/fimmu.2019.01168>
- 8 Sallusto, F. & Lanzavecchia, A. Mobilizing dendritic cells for tolerance, priming, and chronic inflammation. *J Exp Med* **189**, 611-614 (1999). <https://doi.org/10.1084/jem.189.4.611>
- 9 Shi, C. & Pamer, E. G. Monocyte recruitment during infection and inflammation. *Nat Rev Immunol* **11**, 762-774 (2011). <https://doi.org/10.1038/nri3070>
- 10 Badolato, R. Defects of leukocyte migration in primary immunodeficiencies. *Eur J Immunol* **43**, 1436-1440 (2013). <https://doi.org/10.1002/eji.201243155>
- 11 Mrass, P. & Weninger, W. Immune cell migration as a means to control immune privilege: lessons from the CNS and tumors. *Immunol Rev* **213**, 195-212 (2006). <https://doi.org/10.1111/j.1600-065X.2006.00433.x>
- 12 Renkawitz, J., Donnadieu, E. & Moreau, H. D. Editorial: Immune Cell Migration in Health and Disease. *Front Immunol* **13**, 897626 (2022). <https://doi.org/10.3389/fimmu.2022.897626>
- 13 Keller, H. U. *et al.* A proposal for the definition of terms related to locomotion of leucocytes and other cells. *Clin Exp Immunol* **27**, 377-380 (1977).
- 14 Rot, A. & von Andrian, U. H. Chemokines in innate and adaptive host defense: basic chemokinese grammar for immune cells. *Annu Rev Immunol* **22**, 891-928 (2004). <https://doi.org/10.1146/annurev.immunol.22.012703.104543>
- 15 Auffray, C. *et al.* Monitoring of blood vessels and tissues by a population of monocytes with patrolling behavior. *Science* **317**, 666-670 (2007). <https://doi.org/10.1126/science.1142883>
- 16 Moreno-Canadas, R., Luque-Martin, L. & Arroyo, A. G. Intravascular Crawling of Patrolling Monocytes: A Levy-Like Motility for Unique Search Functions? *Front Immunol* **12**, 730835 (2021). <https://doi.org/10.3389/fimmu.2021.730835>
- 17 Thomas, G., Tacke, R., Hedrick, C. C. & Hanna, R. N. Nonclassical patrolling monocyte function in the vasculature. *Arterioscler Thromb Vasc Biol* **35**, 1306-1316 (2015). <https://doi.org/10.1161/ATVBAHA.114.304650>

- 18 Amselem, G., Theves, M., Bae, A., Beta, C. & Bodenschatz, E. Control parameter description of eukaryotic chemotaxis. *Phys Rev Lett* **109**, 108103 (2012). <https://doi.org/10.1103/PhysRevLett.109.108103>
- 19 Bialek, W. & Setayeshgar, S. Physical limits to biochemical signaling. *Proc Natl Acad Sci U S A* **102**, 10040-10045 (2005). <https://doi.org/10.1073/pnas.0504321102>
- 20 Rappel, W. J. & Levine, H. Receptor noise limitations on chemotactic sensing. *Proc Natl Acad Sci U S A* **105**, 19270-19275 (2008). <https://doi.org/10.1073/pnas.0804702105>
- 21 Li Jeon, N. *et al.* Neutrophil chemotaxis in linear and complex gradients of interleukin-8 formed in a microfabricated device. *Nat Biotechnol* **20**, 826-830 (2002). <https://doi.org/10.1038/nbt712>
- 22 Kunkel, S. L., Standiford, T., Kasahara, K. & Strieter, R. M. Interleukin-8 (IL-8): the major neutrophil chemotactic factor in the lung. *Exp Lung Res* **17**, 17-23 (1991). <https://doi.org/10.3109/01902149109063278>
- 23 Hammond, M. E. *et al.* IL-8 induces neutrophil chemotaxis predominantly via type I IL-8 receptors. *J Immunol* **155**, 1428-1433 (1995).
- 24 Shields, J. M. & Haston, W. S. Behaviour of neutrophil leucocytes in uniform concentrations of chemotactic factors: contraction waves, cell polarity and persistence. *J Cell Sci* **74**, 75-93 (1985). <https://doi.org/10.1242/jcs.74.1.75>
- 25 Feng, D., Nagy, J. A., Pyne, K., Dvorak, H. F. & Dvorak, A. M. Neutrophils emigrate from venules by a transendothelial cell pathway in response to FMLP. *J Exp Med* **187**, 903-915 (1998). <https://doi.org/10.1084/jem.187.6.903>
- 26 Luther, S. A. *et al.* Differing activities of homeostatic chemokines CCL19, CCL21, and CXCL12 in lymphocyte and dendritic cell recruitment and lymphoid neogenesis. *J Immunol* **169**, 424-433 (2002). <https://doi.org/10.4049/jimmunol.169.1.424>
- 27 Schwarz, J. *et al.* Dendritic Cells Interpret Haptotactic Chemokine Gradients in a Manner Governed by Signal-to-Noise Ratio and Dependent on GRK6. *Curr Biol* **27**, 1314-1325 (2017). <https://doi.org/10.1016/j.cub.2017.04.004>
- 28 Tiberio, L. *et al.* Chemokine and chemotactic signals in dendritic cell migration. *Cell Mol Immunol* **15**, 346-352 (2018). <https://doi.org/10.1038/s41423-018-0005-3>
- 29 Tran, V. D. & Kumar, S. Transduction of cell and matrix geometric cues by the actin cytoskeleton. *Curr Opin Cell Biol* **68**, 64-71 (2021). <https://doi.org/10.1016/j.ceb.2020.08.016>
- 30 Bordeleau, F., Tang, L. N. & Reinhart-King, C. A. Topographical guidance of 3D tumor cell migration at an interface of collagen densities. *Phys Biol* **10**, 065004 (2013). <https://doi.org/10.1088/1478-3975/10/6/065004>
- 31 SenGupta, S., Parent, C. A. & Bear, J. E. The principles of directed cell migration. *Nat Rev Mol Cell Biol* **22**, 529-547 (2021). <https://doi.org/10.1038/s41580-021-00366-6>
- 32 Sheetz, M. P., Felsenfeld, D. P. & Galbraith, C. G. Cell migration: regulation of force on extracellular-matrix-integrin complexes. *Trends Cell Biol* **8**, 51-54 (1998). [https://doi.org/10.1016/s0962-8924\(98\)80005-6](https://doi.org/10.1016/s0962-8924(98)80005-6)
- 33 Renkawitz, J. & Sixt, M. Mechanisms of force generation and force transmission during interstitial leukocyte migration. *EMBO Rep* **11**, 744-750 (2010). <https://doi.org/10.1038/embo.2010.147>
- 34 Pollard, T. D. & Borisy, G. G. Cellular motility driven by assembly and disassembly of actin filaments. *Cell* **112**, 453-465 (2003). [https://doi.org/10.1016/s0092-8674\(03\)00120-x](https://doi.org/10.1016/s0092-8674(03)00120-x)

- 35 Mseka, T. & Cramer, L. P. Actin depolymerization-based force retracts the cell rear in polarizing and migrating cells. *Curr Biol* **21**, 2085-2091 (2011). <https://doi.org/10.1016/j.cub.2011.11.006>
- 36 Abercrombie, M., Heaysman, J. E. & Pegrum, S. M. The locomotion of fibroblasts in culture. IV. Electron microscopy of the leading lamella. *Exp Cell Res* **67**, 359-367 (1971). [https://doi.org/10.1016/0014-4827\(71\)90420-4](https://doi.org/10.1016/0014-4827(71)90420-4)
- 37 King, S. J. *et al.* Lamellipodia are crucial for haptotactic sensing and response. *J Cell Sci* **129**, 2329-2342 (2016). <https://doi.org/10.1242/jcs.184507>
- 38 Ridley, A. J. *et al.* Cell migration: integrating signals from front to back. *Science* **302**, 1704-1709 (2003). <https://doi.org/10.1126/science.1092053>
- 39 Scarpa, E. & Mayor, R. Collective cell migration in development. *J Cell Biol* **212**, 143-155 (2016). <https://doi.org/10.1083/jcb.201508047>
- 40 Yamazaki, D., Kurisu, S. & Takenawa, T. Regulation of cancer cell motility through actin reorganization. *Cancer Sci* **96**, 379-386 (2005). <https://doi.org/10.1111/j.1349-7006.2005.00062.x>
- 41 Renkawitz, J. *et al.* Nuclear positioning facilitates amoeboid migration along the path of least resistance. *Nature* **568**, 546-550 (2019). <https://doi.org/10.1038/s41586-019-1087-5>
- 42 Cohn, Z. A. & Benson, B. The Differentiation of Mononuclear Phagocytes. Morphology, Cytochemistry, and Biochemistry. *J Exp Med* **121**, 153-170 (1965). <https://doi.org/10.1084/jem.121.1.153>
- 43 Leon, B. *et al.* Dendritic cell differentiation potential of mouse monocytes: monocytes represent immediate precursors of CD8- and CD8+ splenic dendritic cells. *Blood* **103**, 2668-2676 (2004). <https://doi.org/10.1182/blood-2003-01-0286>
- 44 Fogg, D. K. *et al.* A clonogenic bone marrow progenitor specific for macrophages and dendritic cells. *Science* **311**, 83-87 (2006). <https://doi.org/10.1126/science.1117729>
- 45 Jakubzick, C. *et al.* Minimal differentiation of classical monocytes as they survey steady-state tissues and transport antigen to lymph nodes. *Immunity* **39**, 599-610 (2013). <https://doi.org/10.1016/j.immuni.2013.08.007>
- 46 Jakubzick, C. V., Randolph, G. J. & Henson, P. M. Monocyte differentiation and antigen-presenting functions. *Nat Rev Immunol* **17**, 349-362 (2017). <https://doi.org/10.1038/nri.2017.28>
- 47 Nahrendorf, M. *et al.* The healing myocardium sequentially mobilizes two monocyte subsets with divergent and complementary functions. *J Exp Med* **204**, 3037-3047 (2007). <https://doi.org/10.1084/jem.20070885>
- 48 Carlin, L. M. *et al.* Nr4a1-dependent Ly6C(low) monocytes monitor endothelial cells and orchestrate their disposal. *Cell* **153**, 362-375 (2013). <https://doi.org/10.1016/j.cell.2013.03.010>
- 49 Mukherjee, R. *et al.* Non-Classical monocytes display inflammatory features: Validation in Sepsis and Systemic Lupus Erythematosus. *Sci Rep* **5**, 13886 (2015). <https://doi.org/10.1038/srep13886>
- 50 Hamers, A. A. J. *et al.* Human Monocyte Heterogeneity as Revealed by High-Dimensional Mass Cytometry. *Arterioscler Thromb Vasc Biol* **39**, 25-36 (2019). <https://doi.org/10.1161/ATVBAHA.118.311022>
- 51 Schakel, K. *et al.* 6-Sulfo LacNAc, a novel carbohydrate modification of PSGL-1, defines an inflammatory type of human dendritic cells. *Immunity* **17**, 289-301 (2002). [https://doi.org/10.1016/s1074-7613\(02\)00393-x](https://doi.org/10.1016/s1074-7613(02)00393-x)

- 52 Tamassia, N. *et al.* The slan antigen identifies the prototypical non-classical CD16(+)-monocytes in human blood. *Front Immunol* **14**, 1287656 (2023). <https://doi.org/10.3389/fimmu.2023.1287656>
- 53 Yona, S. *et al.* Fate mapping reveals origins and dynamics of monocytes and tissue macrophages under homeostasis. *Immunity* **38**, 79-91 (2013). <https://doi.org/10.1016/j.immuni.2012.12.001>
- 54 Patel, A. A. *et al.* The fate and lifespan of human monocyte subsets in steady state and systemic inflammation. *J Exp Med* **214**, 1913-1923 (2017). <https://doi.org/10.1084/jem.20170355>
- 55 Gotsch, U., Jager, U., Dominis, M. & Vestweber, D. Expression of P-selectin on endothelial cells is upregulated by LPS and TNF-alpha in vivo. *Cell Adhes Commun* **2**, 7-14 (1994). <https://doi.org/10.3109/15419069409014198>
- 56 Fan, S. T. & Edgington, T. S. Integrin regulation of leukocyte inflammatory functions. CD11b/CD18 enhancement of the tumor necrosis factor-alpha responses of monocytes. *J Immunol* **150**, 2972-2980 (1993).
- 57 Johnston, B. & Butcher, E. C. Chemokines in rapid leukocyte adhesion triggering and migration. *Semin Immunol* **14**, 83-92 (2002). <https://doi.org/10.1006/smim.2001.0345>
- 58 Laudanna, C., Kim, J. Y., Constantin, G. & Butcher, E. Rapid leukocyte integrin activation by chemokines. *Immunol Rev* **186**, 37-46 (2002). <https://doi.org/10.1034/j.1600-065x.2002.18604.x>
- 59 Buscher, K., Marcovecchio, P., Hedrick, C. C. & Ley, K. Patrolling Mechanics of Non-Classical Monocytes in Vascular Inflammation. *Front Cardiovasc Med* **4**, 80 (2017). <https://doi.org/10.3389/fcvm.2017.00080>
- 60 Sumagin, R., Prizant, H., Lomakina, E., Waugh, R. E. & Sarelius, I. H. LFA-1 and Mac-1 define characteristically different intraluminal crawling and emigration patterns for monocytes and neutrophils in situ. *J Immunol* **185**, 7057-7066 (2010). <https://doi.org/10.4049/jimmunol.1001638>
- 61 Cros, J. *et al.* Human CD14dim monocytes patrol and sense nucleic acids and viruses via TLR7 and TLR8 receptors. *Immunity* **33**, 375-386 (2010). <https://doi.org/10.1016/j.immuni.2010.08.012>
- 62 Thierry, G. R. *et al.* Non-classical monocytes scavenge the growth factor CSF1 from endothelial cells in the peripheral vascular tree to ensure survival and homeostasis. *Immunity* **57**, 2108-2121 e2106 (2024). <https://doi.org/10.1016/j.immuni.2024.07.005>
- 63 Turner-Stokes, T. *et al.* Live Imaging of Monocyte Subsets in Immune Complex-Mediated Glomerulonephritis Reveals Distinct Phenotypes and Effector Functions. *J Am Soc Nephrol* **31**, 2523-2542 (2020). <https://doi.org/10.1681/ASN.2019121326>
- 64 Hanna, R. N. *et al.* Patrolling monocytes control tumor metastasis to the lung. *Science* **350**, 985-990 (2015). <https://doi.org/10.1126/science.aac9407>
- 65 Olingy, C. E. *et al.* Non-classical monocytes are biased progenitors of wound healing macrophages during soft tissue injury. *Sci Rep* **7**, 447 (2017). <https://doi.org/10.1038/s41598-017-00477-1>
- 66 Heidbreder, K. *et al.* Nr4a1-dependent non-classical monocytes are important for macrophage-mediated wound healing in the large intestine. *Front Immunol* **13**, 1040775 (2022). <https://doi.org/10.3389/fimmu.2022.1040775>
- 67 Karasawa, K. *et al.* Vascular-resident CD169-positive monocytes and macrophages control neutrophil accumulation in the kidney with ischemia-reperfusion injury. *J Am Soc Nephrol* **26**, 896-906 (2015). <https://doi.org/10.1681/ASN.2014020195>

- 68 Misharin, A. V. *et al.* Nonclassical Ly6C(-) monocytes drive the development of inflammatory arthritis in mice. *Cell Rep* **9**, 591-604 (2014). <https://doi.org/10.1016/j.celrep.2014.09.032>
- 69 Kawanaka, N. *et al.* CD14+,CD16+ blood monocytes and joint inflammation in rheumatoid arthritis. *Arthritis Rheum* **46**, 2578-2586 (2002). <https://doi.org/10.1002/art.10545>
- 70 Lacerte, P. *et al.* Overexpression of TLR2 and TLR9 on monocyte subsets of active rheumatoid arthritis patients contributes to enhance responsiveness to TLR agonists. *Arthritis Res Ther* **18**, 10 (2016). <https://doi.org/10.1186/s13075-015-0901-1>
- 71 Funderburg, N. T. *et al.* Shared monocyte subset phenotypes in HIV-1 infection and in uninfected subjects with acute coronary syndrome. *Blood* **120**, 4599-4608 (2012). <https://doi.org/10.1182/blood-2012-05-433946>
- 72 Gatti, A., Radrizzani, D., Vigano, P., Mazzone, A. & Brando, B. Decrease of Non-Classical and Intermediate Monocyte Subsets in Severe Acute SARS-CoV-2 Infection. *Cytometry A* **97**, 887-890 (2020). <https://doi.org/10.1002/cyto.a.24188>
- 73 Sanchez-Cerrillo, I. *et al.* COVID-19 severity associates with pulmonary redistribution of CD1c+ DCs and inflammatory transitional and nonclassical monocytes. *J Clin Invest* **130**, 6290-6300 (2020). <https://doi.org/10.1172/JCI140335>
- 74 Chilunda, V. *et al.* Transcriptional Changes in CD16+ Monocytes May Contribute to the Pathogenesis of COVID-19. *Front Immunol* **12**, 665773 (2021). <https://doi.org/10.3389/fimmu.2021.665773>
- 75 Lin, Q. *et al.* FcγRIIb on B Cells and Myeloid Cells Modulates B Cell Activation and Autoantibody Responses via Different but Synergistic Pathways in Lupus-Prone Yaa Mice. *J Immunol* **201**, 3199-3210 (2018). <https://doi.org/10.4049/jimmunol.1701487>
- 76 Kuriakose, J. *et al.* Patrolling monocytes promote the pathogenesis of early lupus-like glomerulonephritis. *J Clin Invest* **129**, 2251-2265 (2019). <https://doi.org/10.1172/JCI125116>
- 77 Olaru, F. *et al.* Intracapillary immune complexes recruit and activate slan-expressing CD16+ monocytes in human lupus nephritis. *JCI Insight* **3** (2018). <https://doi.org/10.1172/jci.insight.96492>
- 78 Hansel, A. *et al.* Human 6-sulfo LacNAc (slan) dendritic cells have molecular and functional features of an important pro-inflammatory cell type in lupus erythematosus. *J Autoimmun* **40**, 1-8 (2013). <https://doi.org/10.1016/j.jaut.2012.07.005>
- 79 Zhu, H. *et al.* CD16(+) Monocyte Subset Was Enriched and Functionally Exacerbated in Driving T-Cell Activation and B-Cell Response in Systemic Lupus Erythematosus. *Front Immunol* **7**, 512 (2016). <https://doi.org/10.3389/fimmu.2016.00512>
- 80 Ankerhold, J. *et al.* Circulating multimeric immune complexes contribute to immunopathology in COVID-19. *Nat Commun* **13**, 5654 (2022). <https://doi.org/10.1038/s41467-022-32867-z>
- 81 Kerntke, C., Nimmerjahn, F. & Biburger, M. There Is (Scientific) Strength in Numbers: A Comprehensive Quantitation of Fc Gamma Receptor Numbers on Human and Murine Peripheral Blood Leukocytes. *Front Immunol* **11**, 118 (2020). <https://doi.org/10.3389/fimmu.2020.00118>
- 82 Dobel, T. *et al.* FcγRIII (CD16) equips immature 6-sulfo LacNAc-expressing dendritic cells (slanDCs) with a unique capacity to handle IgG-complexed antigens. *Blood* **121**, 3609-3618 (2013). <https://doi.org/10.1182/blood-2012-08-447045>

- 83 Kishore, U. & Reid, K. B. C1q: structure, function, and receptors. *Immunopharmacology* **49**, 159-170 (2000). [https://doi.org/10.1016/s0162-3109\(00\)80301-x](https://doi.org/10.1016/s0162-3109(00)80301-x)
- 84 Kenneth Murphy, C. W. in *Janeway's Immunobiology* Ch. 10-20, 430-431 (2017).
- 85 Nash, J. T. *et al.* Immune complex processing in C1q-deficient mice. *Clin Exp Immunol* **123**, 196-202 (2001). <https://doi.org/10.1046/j.1365-2249.2001.01459.x>
- 86 Manderson, A. P., Botto, M. & Walport, M. J. The role of complement in the development of systemic lupus erythematosus. *Annu Rev Immunol* **22**, 431-456 (2004). <https://doi.org/10.1146/annurev.immunol.22.012703.104549>
- 87 Junker, F., Gordon, J. & Qureshi, O. Fc Gamma Receptors and Their Role in Antigen Uptake, Presentation, and T Cell Activation. *Front Immunol* **11**, 1393 (2020). <https://doi.org/10.3389/fimmu.2020.01393>
- 88 Heesters, B. A. *et al.* Endocytosis and recycling of immune complexes by follicular dendritic cells enhances B cell antigen binding and activation. *Immunity* **38**, 1164-1175 (2013). <https://doi.org/10.1016/j.immuni.2013.02.023>
- 89 Wu, Y. *et al.* Immune complex-bearing follicular dendritic cells deliver a late antigenic signal that promotes somatic hypermutation. *J Immunol* **180**, 281-290 (2008). <https://doi.org/10.4049/jimmunol.180.1.281>
- 90 Sylvestre, D. L. & Ravetch, J. V. Fc receptors initiate the Arthus reaction: redefining the inflammatory cascade. *Science* **265**, 1095-1098 (1994). <https://doi.org/10.1126/science.8066448>
- 91 Hazenbos, W. L. *et al.* Impaired IgG-dependent anaphylaxis and Arthus reaction in Fc gamma RIII (CD16) deficient mice. *Immunity* **5**, 181-188 (1996). [https://doi.org/10.1016/s1074-7613\(00\)80494-x](https://doi.org/10.1016/s1074-7613(00)80494-x)
- 92 Nimmerjahn, F. & Ravetch, J. V. Fcgamma receptors as regulators of immune responses. *Nat Rev Immunol* **8**, 34-47 (2008). <https://doi.org/10.1038/nri2206>
- 93 Qiu, W. Q., de Bruin, D., Brownstein, B. H., Pearse, R. & Ravetch, J. V. Organization of the human and mouse low-affinity Fc gamma R genes: duplication and recombination. *Science* **248**, 732-735 (1990). <https://doi.org/10.1126/science.2139735>
- 94 Metes, D. *et al.* Expression of functional CD32 molecules on human NK cells is determined by an allelic polymorphism of the FcgammaRIIC gene. *Blood* **91**, 2369-2380 (1998).
- 95 Bruhns, P. *et al.* Specificity and affinity of human Fcgamma receptors and their polymorphic variants for human IgG subclasses. *Blood* **113**, 3716-3725 (2009). <https://doi.org/10.1182/blood-2008-09-179754>
- 96 Bournazos, S., Wang, T. T. & Ravetch, J. V. The Role and Function of Fcgamma Receptors on Myeloid Cells. *Microbiol Spectr* **4** (2016). <https://doi.org/10.1128/microbiolspec.MCHD-0045-2016>
- 97 Rosales, C. Fcgamma Receptor Heterogeneity in Leukocyte Functional Responses. *Front Immunol* **8**, 280 (2017). <https://doi.org/10.3389/fimmu.2017.00280>
- 98 Collin, M. & Bigley, V. Human dendritic cell subsets: an update. *Immunology* **154**, 3-20 (2018). <https://doi.org/10.1111/imm.12888>
- 99 Lu, J., Ellsworth, J. L., Hamacher, N., Oak, S. W. & Sun, P. D. Crystal structure of Fcgamma receptor I and its implication in high affinity gamma-immunoglobulin binding. *J Biol Chem* **286**, 40608-40613 (2011). <https://doi.org/10.1074/jbc.M111.257550>
- 100 Treffers, L. W. *et al.* FcgammaRIIIb Restricts Antibody-Dependent Destruction of Cancer Cells by Human Neutrophils. *Front Immunol* **9**, 3124 (2018). <https://doi.org/10.3389/fimmu.2018.03124>

- 101 Unkeless, J. C., Shen, Z., Lin, C. W. & DeBeus, E. Function of human Fc gamma RIIA and Fc gamma RIIB. *Semin Immunol* **7**, 37-44 (1995). [https://doi.org/10.1016/1044-5323\(95\)90006-3](https://doi.org/10.1016/1044-5323(95)90006-3)
- 102 Mkaddem, S. B. *et al.* Lyn and Fyn function as molecular switches that control immunoreceptors to direct homeostasis or inflammation. *Nat Commun* **8**, 246 (2017). <https://doi.org/10.1038/s41467-017-00294-0>
- 103 Ben Mkaddem, S., Benhamou, M. & Monteiro, R. C. Understanding Fc Receptor Involvement in Inflammatory Diseases: From Mechanisms to New Therapeutic Tools. *Front Immunol* **10**, 811 (2019). <https://doi.org/10.3389/fimmu.2019.00811>
- 104 Preuss, S. L. *et al.* Immune complex-induced haptokinesis in human non-classical monocytes. *Front Immunol* **14**, 1078241 (2023). <https://doi.org/10.3389/fimmu.2023.1078241>
- 105 Schakel, K. *et al.* A novel dendritic cell population in human blood: one-step immunomagnetic isolation by a specific mAb (M-DC8) and in vitro priming of cytotoxic T lymphocytes. *Eur J Immunol* **28**, 4084-4093 (1998). [https://doi.org/10.1002/\(SICI\)1521-4141\(199812\)28:12<4084::AID-IMMU4084>3.0.CO;2-4](https://doi.org/10.1002/(SICI)1521-4141(199812)28:12<4084::AID-IMMU4084>3.0.CO;2-4)
- 106 *absoluteantibody.com*, <https://absoluteantibody.com/product/anti-hapten-4-hydroxy-3-nitrophenyl-acetyl-np-b1-8/Ab00104-1.1_mouse_igg1/> (
- 107 *MACS Handbook Dendritic Cells*, <<https://www.miltenyibiotec.com/DE-en/support/macs-handbook/human-cells-and-organs/human-cell-types/dendritic-cells-human.html>> (
- 108 Heidkamp, G. F. *et al.* Human lymphoid organ dendritic cell identity is predominantly dictated by ontogeny, not tissue microenvironment. *Sci Immunol* **1** (2016). <https://doi.org/10.1126/sciimmunol.aai7677>
- 109 Marsh, C. B., Wewers, M. D., Tan, L. C. & Rovin, B. H. Fc(gamma) receptor cross-linking induces peripheral blood mononuclear cell monocyte chemoattractant protein-1 expression: role of lymphocyte Fc(gamma)RIII. *J Immunol* **158**, 1078-1084 (1997).
- 110 Italiani, P. *et al.* IL-1 family cytokines and soluble receptors in systemic lupus erythematosus. *Arthritis Res Ther* **20**, 27 (2018). <https://doi.org/10.1186/s13075-018-1525-z>
- 111 de Salort, J., Cuenca, M., Terhorst, C., Engel, P. & Romero, X. Ly9 (CD229) Cell-Surface Receptor is Crucial for the Development of Spontaneous Autoantibody Production to Nuclear Antigens. *Front Immunol* **4**, 225 (2013). <https://doi.org/10.3389/fimmu.2013.00225>
- 112 Wek, R. C., Jiang, H. Y. & Anthony, T. G. Coping with stress: eIF2 kinases and translational control. *Biochem Soc Trans* **34**, 7-11 (2006). <https://doi.org/10.1042/BST20060007>
- 113 Michaud, J. P., Bellavance, M. A., Prefontaine, P. & Rivest, S. Real-time in vivo imaging reveals the ability of monocytes to clear vascular amyloid beta. *Cell Rep* **5**, 646-653 (2013). <https://doi.org/10.1016/j.celrep.2013.10.010>
- 114 Nicolai, L. *et al.* Author Correction: Vascular surveillance by haptotactic blood platelets in inflammation and infection. *Nat Commun* **13**, 4645 (2022). <https://doi.org/10.1038/s41467-022-31310-7>
- 115 Gaertner, F. & Massberg, S. Patrolling the vascular borders: platelets in immunity to infection and cancer. *Nat Rev Immunol* **19**, 747-760 (2019). <https://doi.org/10.1038/s41577-019-0202-z>

- 116 Gros, A. *et al.* Single platelets seal neutrophil-induced vascular breaches via GPVI during immune-complex-mediated inflammation in mice. *Blood* **126**, 1017-1026 (2015). <https://doi.org/10.1182/blood-2014-12-617159>
- 117 Sarris, M. *et al.* Inflammatory chemokines direct and restrict leukocyte migration within live tissues as glycan-bound gradients. *Curr Biol* **22**, 2375-2382 (2012). <https://doi.org/10.1016/j.cub.2012.11.018>
- 118 Weber, M. *et al.* Interstitial dendritic cell guidance by haptotactic chemokine gradients. *Science* **339**, 328-332 (2013). <https://doi.org/10.1126/science.1228456>
- 119 Reitsma, S., Slaaf, D. W., Vink, H., van Zandvoort, M. A. & oude Egbrink, M. G. The endothelial glycocalyx: composition, functions, and visualization. *Pflugers Arch* **454**, 345-359 (2007). <https://doi.org/10.1007/s00424-007-0212-8>
- 120 Schumann, K. *et al.* Immobilized chemokine fields and soluble chemokine gradients cooperatively shape migration patterns of dendritic cells. *Immunity* **32**, 703-713 (2010). <https://doi.org/10.1016/j.immuni.2010.04.017>
- 121 Alanko, J. *et al.* CCR7 acts as both a sensor and a sink for CCL19 to coordinate collective leukocyte migration. *Sci Immunol* **8**, eadc9584 (2023). <https://doi.org/10.1126/sciimmunol.adc9584>
- 122 Petrie Aronin, C. E. *et al.* Migrating Myeloid Cells Sense Temporal Dynamics of Chemoattractant Concentrations. *Immunity* **47**, 862-874 e863 (2017). <https://doi.org/10.1016/j.immuni.2017.10.020>
- 123 Sun, W. *et al.* Immune complexes activate human endothelium involving the cell-signaling HMGB1-RAGE axis in the pathogenesis of lupus vasculitis. *Lab Invest* **93**, 626-638 (2013). <https://doi.org/10.1038/labinvest.2013.61>
- 124 Katsiari, C. G., Liossis, S. N. & Sfrikakis, P. P. The pathophysiologic role of monocytes and macrophages in systemic lupus erythematosus: a reappraisal. *Semin Arthritis Rheum* **39**, 491-503 (2010). <https://doi.org/10.1016/j.semarthrit.2008.11.002>
- 125 Hurst, N. P., Nuki, G. & Wallington, T. Evidence for intrinsic cellular defects of 'complement' receptor-mediated phagocytosis in patients with systemic lupus erythematosus (SLE). *Clin Exp Immunol* **55**, 303-312 (1984).
- 126 Salmon, J. E., Kimberly, R. P., Gibofsky, A. & Fotino, M. Defective mononuclear phagocyte function in systemic lupus erythematosus: dissociation of Fc receptor-ligand binding and internalization. *J Immunol* **133**, 2525-2531 (1984).
- 127 Pablos, J. L. & Gomez-Reino, J. J. Defective phagocytosis in systemic lupus erythematosus. *Eur J Clin Invest* **28**, 864-865 (1998). <https://doi.org/10.1046/j.1365-2362.1998.00261.x>
- 128 Gaip, U. S. *et al.* Clearance deficiency and systemic lupus erythematosus (SLE). *J Autoimmun* **28**, 114-121 (2007). <https://doi.org/10.1016/j.jaut.2007.02.005>
- 129 Stergioti, E. M. *et al.* Transcriptomic and proteomic profiling reveals distinct pathogenic features of peripheral non-classical monocytes in systemic lupus erythematosus. *Clin Immunol* **255**, 109765 (2023). <https://doi.org/10.1016/j.clim.2023.109765>
- 130 Zeisbrich, M., Rzepka, R., Finzel, S., Venhoff, N. & Voll, R. E. Macrophage colony-stimulating factor receptor/CD115(+) non-classical monocytes are expanded in systemic lupus erythematosus and associated with lupus nephritis. *Scand J Rheumatol*, 1-10 (2024). <https://doi.org/10.1080/03009742.2024.2387483>
- 131 Soerensen, H. *et al.* Pilot clinical study of Adacolumn cytapheeresis in patients with systemic lupus erythematosus. *Rheumatol Int* **26**, 409-415 (2006). <https://doi.org/10.1007/s00296-005-0031-1>

- 132 Burbano, C. *et al.* Potential Involvement of Platelet-Derived Microparticles and Microparticles Forming Immune Complexes during Monocyte Activation in Patients with Systemic Lupus Erythematosus. *Front Immunol* **9**, 322 (2018). <https://doi.org/10.3389/fimmu.2018.00322>
- 133 Shirakawa, F., Yamashita, U. & Suzuki, H. Decrease in HLA-DR-positive monocytes in patients with systemic lupus erythematosus (SLE). *J Immunol* **134**, 3560-3562 (1985).
- 134 Barrera Garcia, A. *et al.* Infiltrating CD16(+) Are Associated with a Reduction in Peripheral CD14(+)CD16(++) Monocytes and Severe Forms of Lupus Nephritis. *Autoimmune Dis* **2016**, 9324315 (2016). <https://doi.org/10.1155/2016/9324315>
- 135 Rita A. Moura, F. O.-R., Cláudia Marques, Alexandre Brito, Rui, L. Teixeira, V. R., Raquel Campanilho-Marques, Vítor Teixeira & , M. J. S., Cristina Ponte, Nikita Khmelinski, Joao Eurico Fonseca. CHILDREN WITH EXTENDED OLIGOARTICULAR AND POLYARTICULAR JUVENILE IDIOPATHIC ARTHRITIS HAVE A CYTOKINE PATTERN FAVOURING B CELL ACTIVATION IN CIRCULATION SIMILARLY TO EARLY AND ESTABLISHED RHEUMATOID ARTHRITIS PATIENTS. *Annals of the Rheumatic Diseases* (2019). <https://doi.org/DOI:10.1136/annrheumdis-2019-eular.7201>
- 136 Jin, Z. *et al.* Single-cell gene expression patterns in lupus monocytes independently indicate disease activity, interferon and therapy. *Lupus Sci Med* **4**, e000202 (2017). <https://doi.org/10.1136/lupus-2016-000202>
- 137 Hellman, P., Andersson, L. & Eriksson, H. Ligand surface density is important for efficient capture of immunoglobulin and phosphatidylcholine coated particles by human peripheral dendritic cells. *Cell Immunol* **258**, 123-130 (2009). <https://doi.org/10.1016/j.cellimm.2009.04.001>
- 138 Lux, A., Yu, X., Scanlan, C. N. & Nimmerjahn, F. Impact of immune complex size and glycosylation on IgG binding to human FcγR1s. *J Immunol* **190**, 4315-4323 (2013). <https://doi.org/10.4049/jimmunol.1200501>
- 139 M. Koshland, R. R., S. Dray. Differences in amino acid composition related to allotypic and antibody specificity of rabbit IgG heavy chains. *Immunochemistry* **5**, 471-483 (1968). [https://doi.org/https://doi.org/10.1016/0019-2791\(68\)90183-3](https://doi.org/https://doi.org/10.1016/0019-2791(68)90183-3)
- 140 Raju, T. S., Briggs, J. B., Borge, S. M. & Jones, A. J. Species-specific variation in glycosylation of IgG: evidence for the species-specific sialylation and branch-specific galactosylation and importance for engineering recombinant glycoprotein therapeutics. *Glycobiology* **10**, 477-486 (2000). <https://doi.org/10.1093/glycob/10.5.477>
- 141 Rayner, L. E. *et al.* The solution structure of rabbit IgG accounts for its interactions with the Fc receptor and complement C1q and its conformational stability. *J Mol Biol* **425**, 506-523 (2013). <https://doi.org/10.1016/j.jmb.2012.11.019>
- 142 Vidarsson, G., Dekkers, G. & Rispen, T. IgG subclasses and allotypes: from structure to effector functions. *Front Immunol* **5**, 520 (2014). <https://doi.org/10.3389/fimmu.2014.00520>
- 143 Ferrara, C. *et al.* Unique carbohydrate-carbohydrate interactions are required for high affinity binding between FcγRIII and antibodies lacking core fucose. *Proc Natl Acad Sci U S A* **108**, 12669-12674 (2011). <https://doi.org/10.1073/pnas.1108455108>
- 144 Bonegio, R. G. *et al.* Lupus-Associated Immune Complexes Activate Human Neutrophils in an FcγRIIA-Dependent but TLR-Independent Response. *J Immunol* **202**, 675-683 (2019). <https://doi.org/10.4049/jimmunol.1800300>
- 145 Barrionuevo, P. *et al.* Immune complex-FcγR interaction modulates monocyte/macrophage molecules involved in inflammation and immune response.

- Clin Exp Immunol* **133**, 200-207 (2003). <https://doi.org/10.1046/j.1365-2249.2003.02208.x>
- 146 Hart, S. P., Alexander, K. M. & Dransfield, I. Immune complexes bind preferentially to Fc gamma RIIA (CD32) on apoptotic neutrophils, leading to augmented phagocytosis by macrophages and release of proinflammatory cytokines. *J Immunol* **172**, 1882-1887 (2004). <https://doi.org/10.4049/jimmunol.172.3.1882>
- 147 Tan, Z. C. *et al.* Mixed IgG Fc immune complexes exhibit blended binding profiles and refine FcR affinity estimates. *Cell Rep* **42**, 112734 (2023). <https://doi.org/10.1016/j.celrep.2023.112734>
- 148 Fick, A. On liquid diffusion. *Journal of Membrane Science* **100**, 33 - 38 (1995). [https://doi.org/https://doi.org/10.1016/0376-7388\(94\)00230-V](https://doi.org/https://doi.org/10.1016/0376-7388(94)00230-V)
- 149 Berg, H. C. & Purcell, E. M. Physics of chemoreception. *Biophys J* **20**, 193-219 (1977). [https://doi.org/10.1016/S0006-3495\(77\)85544-6](https://doi.org/10.1016/S0006-3495(77)85544-6)
- 150 Boyden, S. The chemotactic effect of mixtures of antibody and antigen on polymorphonuclear leucocytes. *J Exp Med* **115**, 453-466 (1962). <https://doi.org/10.1084/jem.115.3.453>
- 151 Leung-Tack, J., Maillard, J. & Voisin, G. A. Chemotaxis for polymorphonuclear leucocytes induced by soluble antigen- antibody complexes. *Immunology* **33**, 937-945 (1977).
- 152 Park, H. & Cox, D. Syk regulates multiple signaling pathways leading to CX3CL1 chemotaxis in macrophages. *J Biol Chem* **286**, 14762-14769 (2011). <https://doi.org/10.1074/jbc.M110.185181>
- 153 Szukiewicz, D. CX3CL1 (Fractalkine)-CX3CR1 Axis in Inflammation-Induced Angiogenesis and Tumorigenesis. *Int J Mol Sci* **25** (2024). <https://doi.org/10.3390/ijms25094679>
- 154 Ninomiya, N. *et al.* Involvement of phosphatidylinositol 3-kinase in Fc gamma receptor signaling. *J Biol Chem* **269**, 22732-22737 (1994).
- 155 Sheridan, G. K. & Murphy, K. J. Neuron-glia crosstalk in health and disease: fractalkine and CX3CR1 take centre stage. *Open Biol* **3**, 130181 (2013). <https://doi.org/10.1098/rsob.130181>
- 156 Breton, A. & Descoteaux, A. Protein kinase C-alpha participates in Fc gamma R-mediated phagocytosis in macrophages. *Biochem Biophys Res Commun* **276**, 472-476 (2000). <https://doi.org/10.1006/bbrc.2000.3511>
- 157 Seiffert, M. *et al.* Human signal-regulatory protein is expressed on normal, but not on subsets of leukemic myeloid cells and mediates cellular adhesion involving its counterreceptor CD47. *Blood* **94**, 3633-3643 (1999).
- 158 Lienard, H., Bruhns, P., Malbec, O., Fridman, W. H. & Daeron, M. Signal regulatory proteins negatively regulate immunoreceptor-dependent cell activation. *J Biol Chem* **274**, 32493-32499 (1999). <https://doi.org/10.1074/jbc.274.45.32493>
- 159 Zen, K. *et al.* Inflammation-induced proteolytic processing of the SIRPalpha cytoplasmic ITIM in neutrophils propagates a proinflammatory state. *Nat Commun* **4**, 2436 (2013). <https://doi.org/10.1038/ncomms3436>
- 160 Morrissey, M. A., Kern, N. & Vale, R. D. CD47 Ligation Repositions the Inhibitory Receptor SIRPA to Suppress Integrin Activation and Phagocytosis. *Immunity* **53**, 290-302 e296 (2020). <https://doi.org/10.1016/j.immuni.2020.07.008>
- 161 Beacham, G. M., Partlow, E. A., Lange, J. J. & Hollopeter, G. NECAPs are negative regulators of the AP2 clathrin adaptor complex. *Elife* **7** (2018). <https://doi.org/10.7554/eLife.32242>

- 162 Ritter, B. *et al.* Identification of a family of endocytic proteins that define a new alpha-adaptin ear-binding motif. *EMBO Rep* **4**, 1089-1095 (2003).
<https://doi.org/10.1038/sj.embor.embor7400004>
- 163 Tse, S. M. *et al.* Differential role of actin, clathrin, and dynamin in Fc gamma receptor-mediated endocytosis and phagocytosis. *J Biol Chem* **278**, 3331-3338 (2003).
<https://doi.org/10.1074/jbc.M207966200>
- 164 Dentener, M. A., Bazil, V., Von Asmuth, E. J., Ceska, M. & Buurman, W. A. Involvement of CD14 in lipopolysaccharide-induced tumor necrosis factor-alpha, IL-6 and IL-8 release by human monocytes and alveolar macrophages. *J Immunol* **150**, 2885-2891 (1993).
- 165 Ancuta, P., Wang, J. & Gabuzda, D. CD16+ monocytes produce IL-6, CCL2, and matrix metalloproteinase-9 upon interaction with CX3CL1-expressing endothelial cells. *J Leukoc Biol* **80**, 1156-1164 (2006). <https://doi.org/10.1189/jlb.0206125>
- 166 Zanoni, I. *et al.* CD14 controls the LPS-induced endocytosis of Toll-like receptor 4. *Cell* **147**, 868-880 (2011). <https://doi.org/10.1016/j.cell.2011.09.051>
- 167 Zhang, M., Chen, L., Wang, S. & Wang, T. Rab7: roles in membrane trafficking and disease. *Biosci Rep* **29**, 193-209 (2009). <https://doi.org/10.1042/BSR20090032>
- 168 Hyttinen, J. M., Niittykoski, M., Salminen, A. & Kaarniranta, K. Maturation of autophagosomes and endosomes: a key role for Rab7. *Biochim Biophys Acta* **1833**, 503-510 (2013). <https://doi.org/10.1016/j.bbamcr.2012.11.018>
- 169 Bucci, C., Thomsen, P., Nicoziani, P., McCarthy, J. & van Deurs, B. Rab7: a key to lysosome biogenesis. *Mol Biol Cell* **11**, 467-480 (2000).
<https://doi.org/10.1091/mbc.11.2.467>
- 170 Takei, K., Slepnev, V. I., Haucke, V. & De Camilli, P. Functional partnership between amphiphysin and dynamin in clathrin-mediated endocytosis. *Nat Cell Biol* **1**, 33-39 (1999). <https://doi.org/10.1038/9004>
- 171 Shupliakov, O. *et al.* Synaptic vesicle endocytosis impaired by disruption of dynamin-SH3 domain interactions. *Science* **276**, 259-263 (1997).
<https://doi.org/10.1126/science.276.5310.259>
- 172 Lenhard, J. M., Kahn, R. A. & Stahl, P. D. Evidence for ADP-ribosylation factor (ARF) as a regulator of in vitro endosome-endosome fusion. *J Biol Chem* **267**, 13047-13052 (1992).
- 173 Nakai, W. *et al.* ARF1 and ARF4 regulate recycling endosomal morphology and retrograde transport from endosomes to the Golgi apparatus. *Mol Biol Cell* **24**, 2570-2581 (2013). <https://doi.org/10.1091/mbc.E13-04-0197>
- 174 Repnik, U., Stoka, V., Turk, V. & Turk, B. Lysosomes and lysosomal cathepsins in cell death. *Biochim Biophys Acta* **1824**, 22-33 (2012).
<https://doi.org/10.1016/j.bbapap.2011.08.016>
- 175 Gallwitz, L. *et al.* Cellular depletion of major cathepsin proteases reveals their concerted activities for lysosomal proteolysis. *Cell Mol Life Sci* **81**, 227 (2024).
<https://doi.org/10.1007/s00018-024-05274-4>

6. Acknowledgements

First of all, I want to thank Knut, my supervisor. You gave me the chance to pursue my PhD in your group and always took your time to meet and discuss when needed, even though you have a busy schedule. Thank you for that. You always kept the bigger picture in mind and patiently guided me back to the project when I got lost in dead ends and details.

Next, I want to kindly mention the members of my thesis advisory committee. Prof. Adelheid Cerwenka for the very first words of appreciation during my PhD journey (after the 2nd TAC meeting and 2 years of working on the project, I received a: "First of all, congratulations on your progress! It really paid off to switch from mice to human.") and for helpful insights about FcγR biology and -blocking experiments. Prof. Axel Roers I want to thank for always emphasizing the clinical and translational aspects of the project. Especially, I want to thank Nina for taking the lead as chairwoman of the TAC. You were exceptionally approachable, and your grasp of concepts and stories behind scientific projects is incredibly sharp. Furthermore, I, as PhD student, always felt treated fairly and taken seriously by you.

Thank you to all collaboration partners. Dr. Victoria Levario-Diaz, I Chen and Prof. Dr. Elisabetta Ada Cavalcanti-Adam greatly helped me with generating immobilized IC gradients. Prof. Dr. Petr Chlanda and Liv Zimmermann kindly provided virus like particles. Sadi (Dr. Sadaf Pashapour) provided guidance and help in designing microfluidic channels to generate IC gradients. Carolina De La Torre, you were of incredible help in analyzing Hao's transcriptomic data and in generating figures to visualize the findings.

A big thanks goes to all lab members who made all those lab days a lot funnier. Thank you to Karsten, you are doing a great job in leading the whole lab space and it is inspiring to see, how respectfully you treat and how supportive you are to your PhD students. Thank you to Stefan, who helped me to order countless antibodies and buffy coats and thanks again for always helping out with isolating those SlanMo. Huge thanks goes to my office neighbour Sophi! It made a huge difference on the working atmosphere when you started your PhD. Thanks for the cocktails at your place and your spontaneous joining on many activities throughout the whole time. Now to Luci! Lucas with a "c", it was awesome and a bit contagious to meet such an enthusiastic spirit. I definitely learned to appreciate good memes and good science! Keep it up. To Romy, you are such an honest, funny, and kind person, please just stay as you are.

Here I want to mention my family and friends. Thanks to my parents, who never asked about my PhD project but always listened. I always know that I can count on you and have your unwavering support. Ramis and Tamara, I could not ask for more caring, supportive, funny and honest siblings. You are invaluable to me. Steve, Andi, Kai I am deeply grateful to have such good friends and hope that we can continue to quench our thirst and just have a good time together (Schocken heißt das Spiel!), forever. Another cheers goes to the whole Heidelberg/Darmstadt/BME/La Familia group. Canoeing, skiing, Novemberfest, Putenfest and all the crazy birthdays, parties, PhD defenses, climbing sessions always were pretty grounding, making everything else less serious and foggy. Alica and David, thanks for letting me stop by

at any time and for being gute Gastgeber. I never had to ask for a refill, because it was already there. Harry und Therry, thanks for always being there. Those bouldering-, surfing-, running- (marathon!) sessions, made me feel less spießig and are part of the best memories I have.

Maike, thank you for sharing your life with me. Your quiet strength, selflessness, and empathy have given me a lot to learn from and have helped me in ways I can't fully express. You make everything feel more manageable, just by being you. And Fritz, you little, cheeky, strong-minded bugger. Thanks for entering the stage and resetting all priorities😊.

Last but not least, my biggest thanks goes to Steffi. You are an exceptional person, one of the smartest people I know, and made all the difference during the past three years.